SEPARATION AND DETECTION OF CHEMICAL AND BIOLOGICAL CONTAMINANTS IN FRESH PRODUCE BY PLASMOFLUIDIC DEVICE

A Dissertation

presented to

the Faculty of the Graduate School

at the University of Missouri-Columbia

In Partial Fulfillment

of the Requirements for the Degree

Doctor of Philosophy

---

by

SARA ASGARI

Drs. Mengshi Lin and Jian Lin, Dissertation Supervisors

MAY 2022

The undersigned, appointed by the dean of the Graduate School, have examined the dissertation entitled

SEPARATION AND DETECTION OF CHEMICAL AND BIOLOGICAL CONTAMINANTS IN FRESH PRODUCE BY PLASMOFLUIDIC DEVICE

presented by Sara Asgari,

a candidate for the degree of doctor of philosophy

and hereby certify that, in their opinion, it is worthy of acceptance.

_____

Dr. Mengshi Lin, Food Science

_____

Dr. Azlin Mustapha, Food Science

_____

Dr. Bongkosh Vardhanabhuti, Food Science

_____

Dr. Jian Lin, Mechanical and Aerospace Engineering

_____

Dr. Yi Zhang, Institute of Materials Science, University of Connecticut

ACKNOWLEDGEMENTS

I would like to express my deep and sincere gratitude to my advisors, Drs. Mengshi Lin and Jian Lin. Throughout my time as a Ph.D. student, they have never failed to provide support to me whenever it was needed. Their patience, academic advising, and keen interest in my success allow me to grow as a food scientist.

I am indeed grateful to Drs. Azlin Mustapha, Bongkosh Vardhanabhuti, and Yi Zhang, for kindly serving on my dissertation committee. Their insightful thoughts and constructive feedback really helped me to sharpen the focus of my research.

I would like to express my sincere appreciation to my labmates, Rajiv Dhital, Guangfu Wu, and Kai Wen Choo for their time spent training and assisting me in my research projects.

I would like to thank all my friends at the University of Missouri for their enduring friendship and help over the years, particularly Zhilong Yu, Fouad K. Alsammarrraie, Ezgi Tekin Pulatsu, Akkasubha Kotchabhakdi, Liang Mao, Kairui Zhai, and JungMun Yang. I also want to thank Jennifer Garrett, Misty Brown, and Secley Kennedy, who are devoted and do everything in their power to help bring a problem to closure.

Last but not least, I wish to make a special mention of my family members and express my sincerest appreciation to Mahboubeh Hafezi, Samira Asgari, and Samin Asgari. There are not enough words to describe how fortunate I am to be a daughter or a sister to you. Without your support and encouragement, I couldn't have reached this far.

TABLE OF CONTENTS

LIST OF FIGURES

LIST OF TABLES

SEPARATION AND DETECTION OF CHEMICAL AND BIOLOGICAL CONTAMINANTS IN FRESH PRODUCE BY PLASMOFLUIDIC DEVICE

Sara Asgari

Drs. Mengshi Lin and Jian Lin, Dissertation Supervisors

ABSTRACT

Plasmofluidic platforms are considered powerful approaches for onsite, fast, and reliable detection of chemical and biological contaminants in food products. In this study, two different protocols have been developed to separate and detect pesticides and foodborne pathogens, either individually or simultaneously, in fruits and vegetables. For detection of pesticides, a filter-based optofluidic SERS sensor was developed to detect four pesticides, thiabendazole, thiram, endosulfan, and malathion in strawberries. In this method, gold-silver (core-shell) nanoparticles (Au@AgNPs) were synthesized and used for SERS measurement owing to their multiple pesticides SERS detection ability. On-line filtration, sample-nanoparticles mixing, and SERS detection resulted in a fast and powerful detection and determination method for probing trace amounts of pesticides in strawberries. The results of our research showed that our filter-based optofluidic SERS sensor achieved very low limit of detection (LOD) values of about 55, 44, 88, and 54 μg/Kg for thiabendazole, thiram, endosulfan, and malathion, respectively. For detection of food-borne pathogens, a SERS-based microfluidic immunosensor was designed to detect *Escherichia coli* O157:H7 individually and the mixture of *Escherichia coli* O157:H7, *Salmonella enteritis,* and *Salmonella enterica* subsp. *enterica* in lettuce and packed salad.

The integration of a primary enrichment step with a hydrodynamic flow-focusing microfluidic device and immune SERS-nanoprobes provided a reliable technique for bacterial detection in complex food samples. For individual *E. coli* O157:H7 analysis, our developed SERS-based microfluidic immunosensor reached a LOD of 0.5 CFU/mL in lettuce. In the multiplex assay, the LOD for the bacterial mixture was found to be 10 CFU/ml in both lettuce and packed salad. This project demonstrates and proves the potentiality of plasmofluidic SERS devices to separate and simultaneously detect multiple chemical and biological contaminants in fresh produce.

CHAPTER 1

INTRODUCTION

1.1 Background

Fruits and vegetables largely contribute to a healthy and balanced lifestyle. They are important due to their critical role in human nutrition owing to their high nutrient content, such as vitamins, minerals and dietary fibers (Philippe et al. 2021). According to World Health Organization, low consumption of fruits and vegetables is associated with an increased risk of non-communicable diseases, and is estimated to cause about 9, 11 and 14% of death for stroke, ischemic heart disease, and gastrointestinal cancer, respectively (WHO 2018). Therefore, a daily consumption of at least 400 g, or five portions, of fresh fruits and vegetables is recommended to prevent non-communicable diseases (WHO 2020). However, raw fruits and vegetables are also considered an important source of pesticides and food-borne pathogens. Reportedly, there are more than a thousand various pesticides that are frequently used in agriculture to protect crops from pests, fungi, insects, and weeds. (Philippe et al. 2021). Agricultural crops can also be contaminated by pathogens during growing stages, harvesting, production, washing, cutting, packaging, and distribution (Mir et al. 2018). In conclusion, raw or slightly processed fruits and vegetables can expose human to pesticides and pathogens. As a result, since the consumption of fruits and vegetables increases, people are more prone to health risks associated with pesticides and pathogens.

This highlights the importance of early detection of chemical and biological contaminants in fresh produce to prevent further contamination during the production and processing chains. Therefore, different analytical methods have been developed for the identification and detection of contaminants in food products. Spectrophotometry, voltammetry, chromatography, capillary electrophoresis, chemiluminescence analysis, and flow injection amperometry are the analytical methods that have been suggested to detect pesticides in fruits and vegetables. Although many of these methods show reasonable sensitivity and accuracy, they are usually complicated, expensive, laborious, time and material-consuming. Conventional methods for detection of biological contaminants in foods commonly involve cultivating sample cells, making it time and money consuming (Roda et al. 2012). Rapid and accurate identification of hazardous materials in the field is very important for prompt prevention of their spreading (Quang et al. 2008). Over recent years, lab-on-chip technology has paved the way to develop powerful real-time sensing and measurement devices, offering significant advantages over their macroscopic counterparts (Lin et al. 2016a). The microfluidic analytical platform has been developing rapidly because of its capabilities for safe performance, low-volume and low-energy-consuming, and high-throughput analytics. It has seen a revolution of miniaturized analytical laboratory equipment in different fields including biology, chemistry and the environment (Janasek et al. 2006). However, for detection purposes, a microfluidic device needs to be coupled with a detection technique.

Raman spectroscopy is a spectroscopic method that is used for studying vibrational, rotational, and other states in a molecule system. This method is based on the Raman effect that relies on inelastic scattering of a monochromatic light, usually a laser beam in the visible or near ultraviolet range, by atoms and molecules in the sample (Figure 1.1) (Yang and Ying 2011).

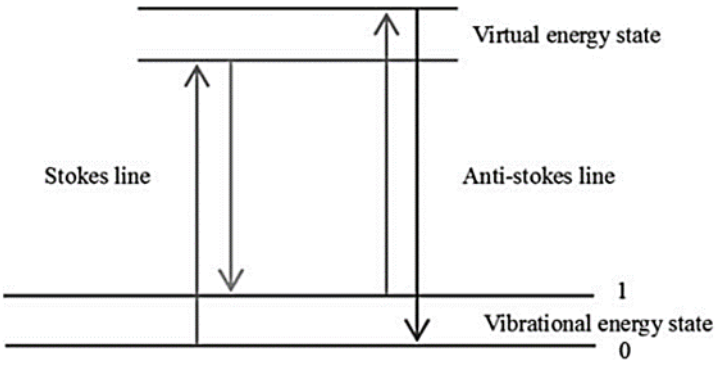

Figure 1.1 Rayleigh and Raman effects (Yang and Ying 2011).

When the incident light interacts with a sample and the electron clouds of the bonds in the sample molecules, the incident photon excites the molecules from a ground state and puts them into a virtual energy state. The return of the molecules to the ground state results in an inelastic scattering, i.e., the energy level of the outcoming scattered photons can either remain the same or be shifted up or down. The scattered radiation with the same energy level as the original radiation is called Rayleigh scattering. However, the small portion of the scattered radiations that have a different energy level than the original radiation is known as Raman scattering, and the energy difference between the laser radiation and scattered radiation is called as Raman shift. If the scattered photon has a lower frequency

than the original photon, it is called the Stokes Raman scattering. While if the scattered photon has a higher frequency than the original photon, it is called anti-Stokes Raman scattering. Raman scattering provides information about the photon modes in a system by representing as spectra. Depending on the scattered photons, various peaks appear in the Raman spectrum, representing vibrational characteristics of the chemical bonds and functional groups of the components in the sample. These peaks undergo changes by the variations in the sample characteristics. Therefore, Raman spectra are fingerprint-like spectra of a substance that can be used for structural and qualitative analysis purposes. However, spontaneous Raman scattering is usually weak, and therefore, various modifications have been developed to improve this technique (Yang and Ying 2011; Parab and Tomar 2012).

Surface-enhanced Raman spectroscopy (SERS) is a modified version of Raman spectroscopy in which Raman scattering is enhanced through nanoscale phenomena by a nanostructured metallic surface. SERS enhancement is facilitated by two widely recognized models; electromagnetic enhancement and chemical enhancement. In electromagnetic enhancement, Raman scattering is enhanced by the excitation of localized surface plasmon resonance (LSPR) on the surface of the nanostructure material, where an intense electromagnetic field is created and is known as hotspots. Metals including gold, silver, titanium, platinum, and copper support surface plasmons. Generally, silver has relatively higher plasmon activity than other metals owing to the high negativity of the

dielectric constant. Roughened metallic surfaces accumulate some plasmons, resulting in the energy radiation and producing high local electromagnetic fields. Multiple factors affect the performance of a roughened metallic surface, such as the size, shape, and gap (Fan et al. 2011). The chemical enhancement mechanism has been proposed as a complementary contribution to electromagnetic enhancement. In the chemical enhancement, the resonances of the system are enhanced by the metal-to-molecule or molecule-to-metal charge transfer, specifically metal-ligand complex formation, charge transfer resonances between metal and molecules, or the transient transfer of hot electrons of the metal into the adsorbed molecules. This mechanism is analyte-specific, i.e., some chemicals do not show SERS enhancement, such as ethanol, whereas some chemicals show large SERS enhancement, including rhodamine 6G (Liu et al. 2019). The ratio between Raman signals from a given number of the molecules in the presence and in the absence of the nanostructured metallic material is known as the SERS enhancement factor, which is highly affected by the size and shape of the nanostructure material and typically varies between 10^6-10^9 (Fan et al. 2011).

Integration of highly sensitive surface-enhanced Raman spectroscopy (SERS) with microfluidics facilitates portable, label-free, non-destructive, highly efficient detection within a well-controlled microsystem. SERS microsystems are capable of precisely detecting target analytes in the order of seconds or fractions of seconds if continuous flow and homogeneous mixing are performed in microfluidic channel. Miniaturization also

leads to lower power consumption and small sample/reagent requirement, resulting in reduced performance costs (Roda et al. 2012). These benefits have made this approach to find growing applications in food safety monitoring aimed for trace chemical and biological detections including pathogens, toxins, heavy metals and pesticide residues in fresh food (Wang et al. 2014). They can be employed for rapid and high-sensitivity detection and diagnosis of solution-based analytes for various applications.

1.2 Objectives

The aims of this study were to fabricate a novel plasmofluidic sensor by coupling a microfluidic channel with SERS to separate and detect multiple chemical and biological contaminants in fresh produce. Specific objectives were to:

(a) Design and fabricate a plasmofluidic sensor to detect contaminants in fresh produce

- ✓ To design and optimize a plasmofluidic sensor by coupling a microfluidic channel and SERS method.
- ✓ To fabricate the plasmofluidic sensor using the standard photolithography and soft lithography.

(b) Devise a protocol to detect and identify multiple pesticides in fruits and vegetables using a plasmofluidic sensor

- ✓ To develop a protocol for simultaneous extraction and detection of pesticides in fresh produce using a plasmofluidic sensor platform.

(c) Devise a protocol to detect and identify multiple food-borne pathogens in fruits and vegetables using a plasmofluidic sensor

- ✓ To develop a protocol for simultaneous extraction and detection of pesticides in fresh produce using a plasmofluidic sensor platform.

CHAPTER 2

LITERATURE REVIEW

2.1 Detection of chemical and biological contaminants using plasmofluidic devices

To address the necessity of in-field analysis of food samples, portable sensing platforms were developed by integration of microfluidic devices with the SERS technique. SERS-based microfluidic devices provide a fast, sensitive, and onsite sample analysis with only a small amount of sample. Such an innovative sensing platform is an efficient approach for sample manipulation and analysis and has been explored over different scenarios.

2.2 Detection of chemical contaminants using plasmofluidic sensor platform

SERS-based microfluidic devices have been widely applied for the detection of chemical contaminants, such as pesticides, heavy metals, mycotoxins, and organic pollutants.

2.2.1 Pesticides

The first SERS-based microfluidic device was designed in an alligator-teeth-shaped microfluidic channel. In this method, a passive micromixer was used to efficiently blend the sample with silver nanoparticles (AgNPs), and the detection limit of methyl parathion was found to be 0.1 ppm (Gweon et al. 2006). Malathion was successfully detected in a SERS-based microfluidic device that was equipped with packed nanoporous silica microspheres, and the SERS laser was focused on the detection area by fiber optic cables to eliminate the need for optical alignment and focusing. The successful detection of 12 ppb of malathion was reported by this study (Yazdi and White 2012a). Later, the same research group achieved simultaneous

detection of 5 ppm methyl parathion, 0.1 ppb malachite green, and 5 ppb thiram within the same optofluidic SERS device by adding a passive micromixer to the system (Yazdi and White 2012b). Coupling SERS-microfluidic devices with AgNPs@basil-seeds resulted in a detection limit of 0.68 ppm melamine in raw milk (Zhou et al. 2016). In another research, a paper-based microfluidic device was coupled with SERS to detect thiram using Au@AgNPs. The limit of detection for thiram in this method was found to be 1.0×10^{-9} mol/L (Zhu et al. 2017).

2.2.2 Heavy metals

The integration of SERS-based microfluidic device with immunoassay resulted in efficient detection of Hg^{2+} in water with a detection limit of 0.45 pg/mL (She et al. 2016). The same ions were successfully detected by a SERS-based droplet microfluidic device coupled with rhodamine B decorated AuNPs, and a detection limit of Hg^{2+} in this method was estimated to be between 100 to 500 ppt (Wang et al. 2009). A zigzag microfluidic device integrated with SERS was used to detect As^{3+} by glutathione/4-mercaptopyridine functionalized AgNPs and the detection limit of 0.67 ppb was achieved for As^{3+} by this method (Qi et al. 2014).

2.2.3 Mycotoxins

A SERS-microfluidic device was used to capture and detect ochratoxin-A. In this study, aptamer was used as the capturing agent, and the conformational changes of an oligonucleotide of the aptamer sequence before and after its interaction with ochratoxin-A molecules were detected by the SERS technique, indicating the presence of ochratoxin-A in the sample. The detection limit of 2.5 μM was achieved for ochratoxin-A in this research (Galarreta et al. 2013).

2.3 Detection of biological contaminants by using SERS-based microfluidic immunosensor

2.3.1 ELISA-based microfluidic sensors

ELISA-based microfluidic is one of the promising techniques to detect microorganisms, mycotoxins, or other biomarkers. In this method, the target molecule is detected by an ELISA test kit inside the microfluidic platform. The detection can be performed by different methods such as colorimetric, Raman, or SERS. In a recent report, the hepatitis B virus was detected by coupling SERS, ELISA, and microfluidics. Jacek Waluk's group developed a method that an ELISA test kit is bonded on a gold slide and attached to the microfluidic channel. The ELISA test kit consists of three layers and diagnosis is performed as these three layers are formed. The first layer is the support layer surface chemically bonded and covered by the target antibodies. The second layer is the virus antigens, which are present in the sample and are now bonded with the antibodies. The third layer is the labeled- antibodies. The Raman label is a complex of a dye and a gold-based SERS signal intensifier (gold nanoflower). The presence of the target antigens is implied by the high-intensity SERS signals (Kamińska et al. 2015a).

2.3.2 Printed microfluidics

Printed microfluidics are another promising analytical microfluidics that has attracted attention recently. The fabrication of these devices starts with designing the microfluidic pattern using particular software, and then the device is made using appropriate printing technique based on the material for fabrication. Dr. Juhong Chen's research team fabricated a biosensor based on electrochemical detection in a flexible, cheap nanoimprinted microfluidic device. The device is fabricated of cheap soft polymer, PET, which has a high potential for commercial mass production. For

detection of *Salmonella*, they conducted an electrochemical assay through on-site production of an electroactive substance that can be measured on a prefabricated electrode inside the microfluidic channel (Chen et al. 2015). Hua-Zhong Yu's group has developed a microfluidic channel plate fabricated using a 3D-printing method and coupled with an indirect competitive ELISA for the detection of aflatoxin B1. For this protocol, the indirect competitive immunoassay is performed on a PDMS microfluidic channel plate bonded on a plastic chip. The results obtained by the ELISA test are read and analyzed by an Android app (developed for this purpose). Accordingly, the presence of aflatoxin B1 is represented by less dark strips, while the absence of aflatoxin B1 is represented by darker strips (Li et al. 2017).

2.3.3 Paper-based microfluidic devices

Paper-based microfluidic devices (μPADs) have gained a lot of attention as analytical tools for the detection of a wide variety of analytes. These devices are promising for wide applications due to the abundance, low cost of paper, fluid-storing, and fluid-wicking capabilities of cellulose and its derivatives (Cate et al. 2015). Charles S. Henry's group developed a paper microfluidic channel sensor to detect β-lactam antibiotics through a colorimetric method. The device consists of reservoirs to measure the pH of the sample and probe the presence of β-lactam antibiotics. The reservoirs for the detection of antibiotics are coated by β-lactamase. The sample is injected through the channel along with the nitrocefin, a chromogenic substrate. β-lactam antibiotics and nitrocefin compete with each other for the reaction with the enzyme. In the presence of β-lactam antibiotics, a yellow color is observed, whereas the color change from yellow to red indicated the reaction between nitrocefin and β-lactamase and, as a result implying the presence of falsified antibiotic in the sample (Boehle et al. 2018).

2.3.4 SERS-based immunosensors

Recently, SERS-based immunosensors have gained increasing attention as a powerful alternative method for clinical and biochemical diagnosis. These techniques are generally operated by (i) SERS-nanoprobes which are consisted of antibodies for anchoring onto the bacterial cells, (ii) SERS reporter molecules or Raman active molecules as the target indicator, and (iii) SERS active substrates to enhance the intensity from the labeled bacteria. The method is superior to conventional immunoassay methods, such as ELISA and fluorescence-based assays, owing to (i) relatively high selectivity of SERS even at very low concentrations for the target analytes and molecules, (ii) less susceptibility of Raman signals to photobleaching, leading to lower detection limits, (iii) possibility of multiplexing by using multiple antibodies against various targets and different Raman reporters, and (iv) narrow Raman signals, facilitating the detection of multiple biomarkers and pathogens. However, inconsistency and reproducibility of SERS signals cause difficulties in quantitative analysis. Coupling of SERS-based immunoassay with a microfluidic channel results in a homogeneous analysis condition, facilitating precise quantitative analysis of the target analytes. Moreover, this sensing platform offers automatic sampling, continuous and multiplex analysis with low sample requirements. SERS-based microfluidic immunosensors have been used to detect various pathogens. Different strategies were developed by each research group to reduce the detection limit.

Integration of SERS-nanoprobes into a microfluidic dielectrophoresis sensor resulted in the detection limit of 70 CFU/mL. However, inefficient liquid from such sensors usually causes incompetent quantitative analysis of bacteria, especially in complex samples. Online enrichment, separation, and detection of *E. coli* O157:H7 in

water were conducted in a nano-dielectrophoretic microfluidic sensor integrated with SERS. The method demonstrated high sensitivity for *E. coli* O157:H7, but the method was complicated and lacked the applicability of bacterial detection in complicated food samples. Another research reported the off-chip labeling to separate and detect *Listeria monocytogenes* in pure culture. A detection limit of 10^5 CFU/mL was achieved in this study, which is higher than the infectious dose of *Listeria monocytogenes*.

CHAPTER 3

NANOFIBRILLAR CELLULOSE/AU@AG NANOPARTICLE NANOCOMPOSITE AS A SERS SUBSTRATE FOR DETECTION OF PARAQUAT AND THIRAM IN LETTUCE

3.1 Introduction

Pesticides are widely used in agriculture to protect fruits and vegetables against different types of pests. Despite the implementation of good agricultural practices, pesticide residues and their metabolites can still contaminate and impact foods at nearly all stages from production to consumption. These remaining residues in food products can be toxic to humans and may negatively impact consumers' health (Fenik et al. 2011). Safety issues associated with pesticide residues in fresh produce have become a hot topic recently. Consequently, various instrumental techniques have been devised for identification and quantification of the pesticide residues in fruits and vegetables.

High-performance liquid chromatography (HPLC), gas chromatography (GC), thin layer chromatography (TLC), electrochemical sensing, fluorescence, and SERS are important analytical methods that have been developed for detection of pesticides in agricultural and food products (Llorent-Martínez et al. 2011; López-Paz and Catalá-Icardo 2011; Mirceski and Gulaboski 2014; Chang et al. 2016; Pang et al. 2016). Among them, SERS is a powerful label-free and non-destructive analytical tool with ultrahigh sensitivity to the analytes. In SERS analysis, Raman cross-section scattering is significantly amplified owing to localized surface plasmon resonance (LSPR), providing molecular fingerprint-like information of analyte molecules (Aroca 2006).

SERS performance is highly dependent on the SERS-active substrate. Conventionally, roughened noble metal nanoparticles having been widely used as the SERS substrates, such as gold nanoparticles (Au NPs) or silver nanoparticles (Ag NPs)

(Bantz et al. 2011). However, single-element nanoparticles (Au NPs or Ag NPs) have restricted plasmonic absorptions (Ji et al. 2010). Tunable LSPR and richer plasmonic modes can be obtained by combining Au and Ag in a bimetallic nanoparticle (Cortie and McDonagh 2011). It is believed that Ag coating of Au NPs can continuously enhance Raman intensities (Jana 2003). In other words, gold-silver core-shell nanoparticles (Au@Ag NPs) take advantage of high SERS activity of Ag NPs and homogeneity and stability of Au NPs (Yang et al. 2014). Additionally, LSPR of a bimetallic nanoparticle can be tuned by varying the core size or the thickness of the coating layer (Raveendran et al. 2006). These features make Au@Ag NPs an attractive candidate as the SERS substrate.

However, for real-world applications, it is inconvenient to use metallic nanoparticle colloids (Wei et al. 2014). Besides that, these SERS substrates are not stable for long-term storage. Thus, depending on the type of the nanoparticle, fresh substrates should be prepared each time prior to the experiments, making it hard sometimes to get homogeneous results for the same analyte. To overcome this issue, cellulose-based composites, in which cellulose fibers are decorated with metallic nanoparticles, were introduced as SERS substrates. Cellulose, as a SERS substrate platform, has gained favor owing to its abundancy, inexpensiveness, flexibility, ease of functionalization, and biodegradability (Ogundare and van Zyl 2019). High sensitivity of these substrates is a result of natural wrinkles and high porosity of cellulose, leading to a large area for the creation of so-called plasmonic “hotspots” (Ngo et al. 2012). Having no or very little interference adds another advantage to cellulose-based nanocomposites as the SERS substrates (Ogundare and van Zyl 2019). Nonetheless, micro-sized fibers may restrain uniform distribution of nanoparticles, leading to poor reproducibility of cellulose-based SERS substrates (Xiong et al. 2017a). Using

nanofibrillar cellulose (NFC) is superior because the nanofibrils can hold more nanoparticles and form more homogeneous structures than regular cellulose (Wei et al. 2015). Previous studies showed satisfactory results for detection purposes using NFC-based nanocomposites. These nanocomposites were based on a combination of NFC, as a stabilizing and/or reducing agent, with unmodified Au NPs (Xiong et al. 2017b), modified Au NPs (Xiong et al. 2018), Au nanorods (Zhang et al. 2018), Ag NPs (Liou et al. 2017), and Ag nanospheres (Jiang and Hsieh 2014). Although these methods are usually straightforward, the nanomaterials previously used are not efficient enough to have an acceptable SERS substrate. Therefore, there remains a need for a more powerful and practical SERS substrate with higher SERS sensitivity for probing trace amounts of pesticides in fresh produce. The combination of NFC and core-shell NPs as a SERS nanocomposite has not been reported so far. Hypothetically, deposition of highly SERS-active Au@Ag NPs on NFC can result in ultrasensitive SERS measurement due to strong SERS activities of these bimetallic nanoparticles stabilized in a robust platform. Overall, the new nanocomposite would offer a more stable SERS substrate that can be usable for a longer period of time. Additionally, multiple numbers of these SERS substrates can be fabricated in one-time synthesis and the fabricated substrates can be stored for future use.

To take advantage of all these merits, this study aimed at the synthesis of NFC/Au@Ag NP nanocomposite. Characterization of both Au@Ag NPs and NFC/Au@Ag NP nanocomposite was conducted to indicate the successful fabrication of the SERS substrate. The new substrate was utilized to detect two widely used pesticides (thiram, a dithiocarbamate fungicide, and paraquat, a bipyridyl herbicide) either individually or as a mixture in lettuce samples. The as-prepared NFC/Au@Ag

NP nanocomposite was used in SERS analysis, which was analyzed by multivariate statistical tools.

3.2 Experiment section

3.2.1 Materials and reagents

Hydrogen tetrachloroaurate solution ($HAuCl_4$, 30 wt% in dilute HCl), silver nitrate (ACS reagent ≥99.9%), L-ascorbic acid, thiram and paraquat (Pestanal® analytical standard) were obtained from Sigma-Aldrich (St. Louis, MO, U.S.A.). Trisodium citrate dihydrate (Certified A.C.S), methanol (HPLC grade), and acetone (HPLC grade) were purchased from Fisher Scientific (Fair Lawn, New Jersey, U.S.A). The 4-mercaptobenzoic acid (4-MBA, 95%) was purchased from TCI (Tokyo, Japan). NFC was obtained from the University of Maine (Orono, ME, USA) in the form of a slurry of ~3 wt% cellulose nanofibers with 90% fines. Organic lettuce was purchased from a local grocery store. All chemicals were used as received without further purification and Millipore water was used throughout the experiments. Prior to use, all glassware was soaked in aqua regia (HCl/HNO_3 3:1, v/v) for 24 h and rinsed with Millipore water.

3.2.2 Synthesis of Au@Ag NPs

Au@Ag NPs were prepared by coating Au seeds with a layer of Ag through chemical reduction in the Au seed solution. First, ~26 nm-sized Au seed colloid was prepared according to a previous protocol (FRENS 1973) and the coating of Au NPs was conducted based on the method developed by Olson *et al*. (Olson et al. 2008) with minor modifications.

3.2.3 Preparation of NFC suspension

NFC suspension with different concentrations (1, 3, 5, and 7%, w/v) was prepared by mixing of 0.5, 1.5, 2.5, and 3.5 g of NFC slurry in 50 mL of Millipore water and allowed for stirring for 2 h. As-prepared NFC suspensions were stored at 4°C and the suspension were stirred for 5 min prior to each use.

3.2.4 Fabrication of NFC/Au@Ag NP nanocomposite

Varying concentrations of Au@Ag NPs were prepared as follows: 1 mL of the original solution was centrifuged in a micro-centrifuge tube at 10,000 rpm min^{-1} for 10 min. Then, different volumes (100, 300, 500, 700, and 900 µL) were removed from the supernatant. Various combinations of different concentrations of NFC suspension and Au@Ag NPs were used to synthesize and identify the optimum SERS substrate. Nanocomposites were prepared by mixing of NFC suspension and concentrated Au@Ag NP solution with a ratio of 1:1. The mixing time effect was also investigated at 5-min intervals over 30-min mixing. Subsequently, an aliquot of 2 µL of the mixture was dropped on a slide and air-dried at room temperature. The as-prepared nanocomposite was used as the SERS substrate.

3.2.5 Characterization of Au@Ag NPs and NFC/Au@Ag NP nanocomposite

UV–Vis spectroscopy and transmission electron microscopy (TEM) were used for characterization of Au@Ag NPs. The UV-vis spectrum of the nanoparticle solution was measured by a Varian UV–Vis spectrophotometer (Cary Bio 50, Agilent, CA, USA). TEM images were used to observe the distinguished boundary between the inner Au core and the thin Ag outer layer. TEM samples were prepared by air-drying of 5 µL of Au@Ag NP solution on a copper grid at room temperature. The as-prepared samples were scanned by a high-resolution FEI Tecnai F30 Twin TEM operating at 300 kV. Elemental distribution of Au@Ag NPs was also examined by high-angle annular dark-

field scanning transmission electron microscopy-energy dispersive X-ray spectroscopy (HAADF-STEM-EDS) mapping.

Zeta potential of NFC suspension, Au@Ag NP solution, and the mixture of NFC and Au@Ag NPs were measure by Zetasizer Nano ZS (Malvern Instruments Ltd., Worcestershire, UK) without any dilutions or concentrations. SEM micrographs were used for characterization of NFC/Au@Ag NP nanocomposite structures. Concurrent SEM and STEM imaging were performed using FEI Quanta 600 FEG in high vacuum mode. An aliquot of 5 µL of the nanocomposite mixture was placed on a copper grid and then air-dried prior to imaging. Grids were then loaded into the specialty STEM detector mount, allowing for simultaneous SEM and STEM collection (via an Everhart-Thornley detector).

3.2.6 Preparation of samples

In this study, different concentrations of 4-MBA in methanol solution were used as a probe molecule to investigate the SERS activity of NFC/Au@Ag NP nanocomposite. A 10^5 µg/L stock solution of pesticides was prepared by dissolving 5 mg of the pesticide powder into 50 mL of solvent and solutions of 1, 5, and 10 mg/L, and 10, 50, 100, and 500 µg/L were prepared by serial dilutions of the stock solution. Acetone and water were used as the solvents for thiram and paraquat, respectively.

Lettuce samples were thoroughly washed with and soaked for 30 min in distilled water. Then, lettuce samples (2 g) were cut into small pieces and spiked with different amount of pesticide solution, resulting in different final concentrations of pesticide (1, 5, and 10 mg/L, 10, 50, 100, and 500 µg/L) in the lettuce samples. For the mixture, the same volumes of each pesticide were first mixed in a conical tube and lettuce samples were then spiked by the mixture. Afterwards, the samples were air-dried in a fume hood

and placed in conical tubes, which contained 4 mL of mixed solvent (acetone/H_2O 1:1, v/v). After vigorously vortexed for 1 min, the mixture was sonicated using an ultrasonic bath for 5 min. Finally, the mixture was filtered using a filter paper Whatman #1 and the filtered mixture was then used for SERS detection. The solvent without pesticide was used as the control.

3.2.7 SERS detection

For SERS measurements, an aliquot (2 µL) of the sample was placed on the nanocomposite film and after air-drying, the film with dried sample was ready for SERS detection. In this study, a DXR2 Raman spectroscopy equipped with a 785-nm laser source (Thermo Fisher Scientific Inc., Madison, Wis., USA) was used. All data were collected in the range of 400-2000 cm^{-1} using a 10× objective through a 25 µm pinhole aperture with 1 s acquisition time and ~20 mW laser power. Ten scans were selected, and averaged spectra were obtained. Spectral data were collected by the OMNIC software (Thermo Fisher Scientific Inc., Waltham, MA, USA). The reproducibility of the nanocomposite was also monitored by SERS intensity map of 500 µg/L thiram and paraquat pure solutions through area and point-to-point mapping.

3.2.8 Data analysis

SERS spectral data were collected and analyzed by the software Delight version 3.2.1 (D-Squared Development Inc., LaGrande, OR, USA). The enhancement factor (EF) of the SERS method using NFC/Au@Ag NP nanocomposite as the SERS substrate was calculated by measuring SERS signals of 4 µL of 4-MBA solution with and without having NFC/Au@Ag NPs as the substrate. EF value was obtained as follows;

$$EF = \frac{I_{SERS} C_{nor}}{I_{nor} C_{SERS}} \quad (1)$$

where I_{SERS} and I_{nor} represent the peak intensities in SERS and normal Raman spectra, respectively and C_{SERS} and C_{nor} are the analyte concentrations in the SERS and normal Raman measurements, respectively.

In this study, first, preprocessing algorithms including smoothing at 2 cm^{-1} and second-derivative transformation with 12 cm^{-1} gap were employed to eliminate instrumental noises and separate overlapping peaks. Then, a partial least squares (PLS) model was established to predict pesticide concentrations in tested samples and to obtain the limit of detection (LOD) of each target pesticide. To avoid over-fitting of the spectral data, the PLS latent variable number with the lowest root-mean-square error of prediction (RMSEP) value was selected as the optimal number for PLS modeling. A model with higher R value and lower RMSEP value suggests better predictability.

LOD of the SERS method for each pesticide was calculated using equation 2, where σ is the standard error of predicted values (equals to RMSEP in PLS model) and m is the slope of PLS calibration plot. Calculated values were compared with maximum residue limits (MRLs) as set by United States Environmental Protection Agency (EPA).

$$LOD = 3\sigma/m \quad (2)$$

3.3 Results and discussion

3.3.1 Characterization of Au@Ag NPs and NFC/Au@Ag NP nanocomposite

Au@Ag NPs were fabricated through a two-step seed-growth procedure. In this method, Au cores were first synthesized by reducing $HAuCl_4$ with trisodium citrate in an aqueous solution. Subsequently, Ag shell gradually formed, grew and coated on the Au cores after mixing $AgNO_3$ and ascorbic acid (as a reducing agent and stabilizer)

solutions with Au NP colloid. Successful fabrication of Au@Ag NPs is confirmed by a blue shift in the UV-Vis absorption spectrum of Au NPs (Song et al. 2016) since optical properties of silver shell dominated the plasmon resonance of Au core. Figure 3.1a demonstrates a strong broad plasmon absorption range from ~340 to ~520 nm for Au@Ag NPs, representing the concurrence of dissimilar plasmon resonance frequencies of Au core and Ag shell in core-shell nanoparticles (Liu et al. 2012). This also confirms stronger SERS performance of Au@Ag NPs than Au or Ag NPs. TEM images clearly showed homogeneous core-shell structures for the as-prepared nanoparticles (Figure 3.1b) and the majority of synthesized Au@Ag NPs showed spherical shapes in a narrow size distribution with an average size of 34.83 ± 5.083 (Figure 3.1c). The core-shell structure of nanoparticles was further demonstrated by HAADF-STEM imaging. The difference between the atomic numbers resulted in the darker inner Au core and brighter Ag shell. EDS mapping analysis and TEM-EDS spectrum of the same Au@Ag NPs confirmed the dense Au core and consistent Ag outer shell.

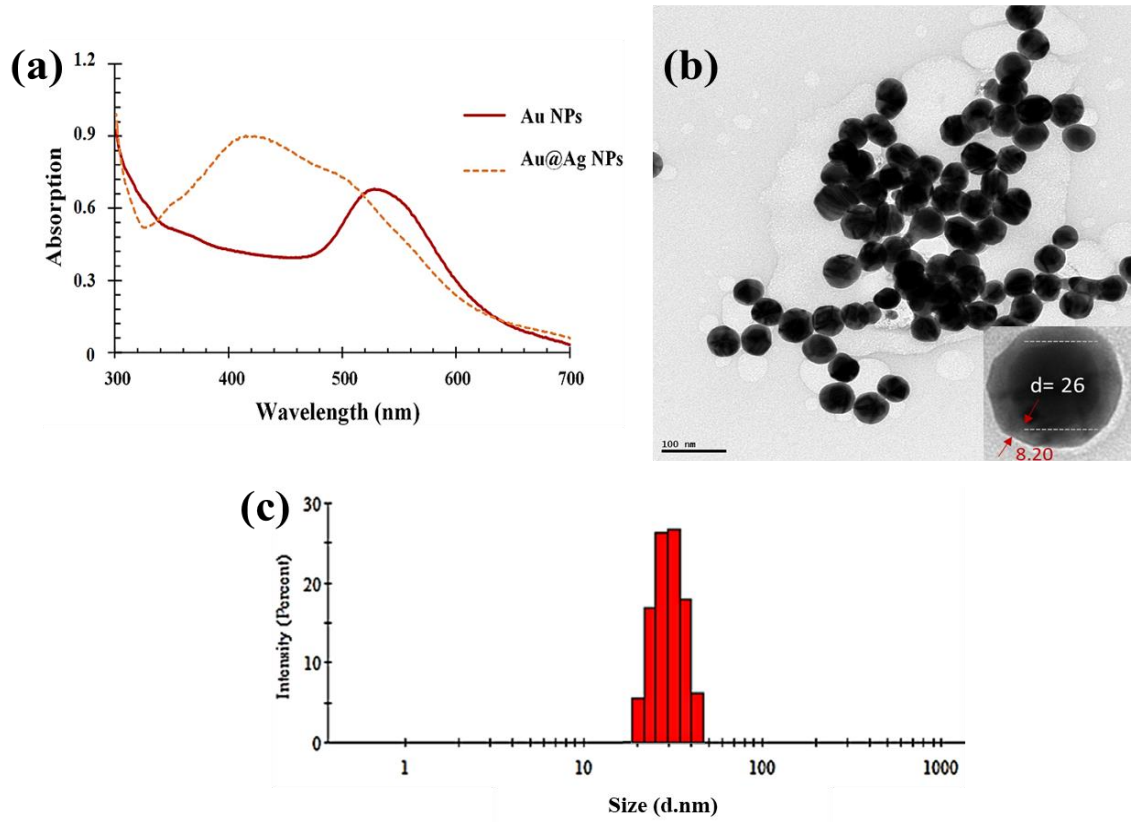

Figure 3.1 UV–Vis spectra of Au and Au@Ag NPs (a), TEM image of Au@Ag NPs (the inset: a typical Au@Ag NP with a core diameter of ~26 nm and shell thickness of 8.20 nm) (b), and particle size distribution of Au@Ag NPs (c).

This study synthesized a nanocomposite by a combination of Au@Ag NPs and NFC, which can be used as a powerful SERS substrate. NFC has a high aspect ratio (length/width) (Cheng et al. 2009) and contains fibers with a width of 2-120 nm and length of up to micrometer ranges (Jonoobi et al. 2015) that enable it to host a large number of tiny nanoparticles. After mixing Au@Ag NPs with NFC solution, nanoparticles were distributed along the nanofibers, attached to them and accommodated within the wrinkles, leading to a well-structured SERS nanocomposite. Zeta potential values show anionic surface properties of NFC, Au@Ag NPs, and their mixture. Therefore, gravity-assisted loading is supposed to be the main driving force for the alignment of nanoparticles within the NFC network. Drying out of the mixture

also helped nanoparticles to be kept by the NFC web-like network through elimination of water molecules (Wei et al. 2015) and grasping the nanoparticles especially between adjacent nanofibrils. Additionally, fibrillar structure of NFC allows nanoparticles (and their aggregates or clusters) to stably place within the wrinkles and distribute various hotspots along the fibers, which led to an efficient SERS substrate. Based on the preliminary tests, the combination of the most concentrated Au@Ag NP solution with 3% NFC solution and a 15-min mixing time showed the best SERS performance, so this composite was chosen and used for SERS analysis. The effectiveness of mixing and holding time on the SERS performance of NFC/Au@Ag NP nanocomposite indicates another possible phenomenon involving in the fabrication of the nanocomposite. As an assumption, Au@Ag NPs can also be chemically bonded on the NFC through the linkage of carboxylate groups on citrate-capped nanoparticles and hydroxyl groups on nanofibrils (Wei et al. 2015). SEM and TEM images of NFC/Au@Ag NP nanocomposite are displayed in Figure 3.2 that clearly show that fibers are entirely covered by individual nanoparticles and many aggregated/clustered nanoparticles are also observable on different spots of nanofibers, especially at the junctions. Roughness of NFC nanofibers also makes a contribution to more nanoparticle aggregation (Zhang et al. 2015). These aggregated nanoparticles are considered as potential hotspots (Liu et al. 2012).

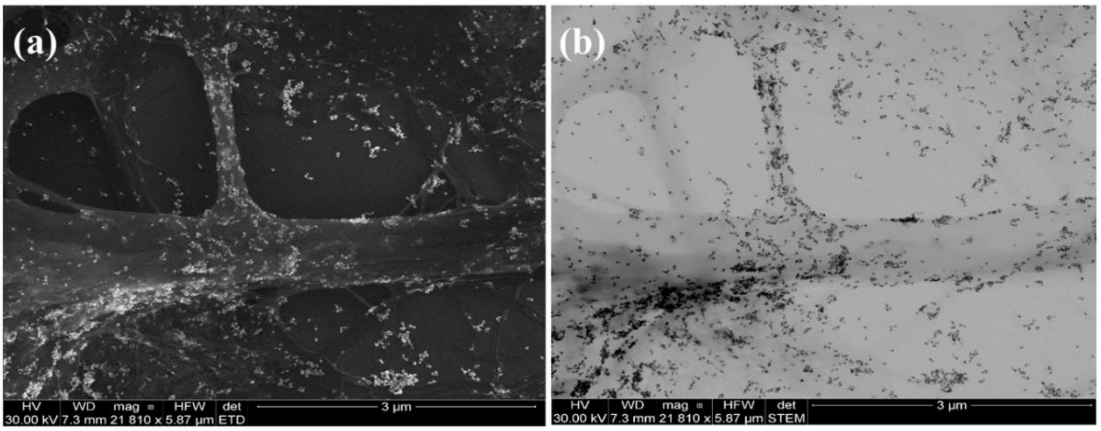

Figure 3.2 SEM (a) and TEM (b) images of NFC/Au@Ag NP nanocomposite.

3.3.2 SERS performance of NFC/Au@Ag NP nanocomposite

SERS enhancement is dominantly based on the electromagnetic mechanism. Amplification of Raman signals in SERS method is a result of the intensification of electromagnetic field due to LSPR when the analyte molecules locate in the proximity of roughened metal surfaces (Haynes et al. 2005). Significantly enhanced Raman scattering signals allow SERS to detect analytes even at diluted concentrations (Lu et al. 2013). Well-distribution of metallic nanoparticles facilitates the reaction of more analyte molecules with nanoparticles, increasing the efficiency of SERS substrate.

Large surface area and 3D nanofiber network structures of NFC/Au@Ag NP nanocomposite increased the likelihood for more analyte molecules to react with nanoparticles and enhanced the SERS detection efficiency (Liou et al. 2017). Excellent SERS performance of this nanocomposite was confirmed by the high intensity observed for different concentrations of 4-MBA. Figure 3.3 shows a set of Raman spectra (n = 8) obtained from different concentrations of 4-MBA. Observed SERS peaks were consistent with previous literature (Song et al. 2016) and the intensity of the major peaks were concomitant with 4-MBA concentrations. This is in contrast to a previous study in which poor SERS activity of Au@Ag NPs was reported for high concentrations (higher than 5 µM) of 4-MBA, saying that random aggregation of nanoparticles in

higher 4-MBA concentration resulted in lower SERS intensity (Song et al. 2016). This comparison again reveals that cellulose nanofibrillar architecture decorated with evenly distributed and stabilized Au@Ag NPs provided more available sites of interaction between more analyte molecules and nanoparticles within the substrate. An EF value of ~10^4 was obtained for NFC/Au@Ag NPs nanocomposite as the SERS substrate. Our findings indicate that NFC/Au@Ag NP nanocomposite is an appropriate SERS substrate for detection purposes with notably high functionality and sensitivity.

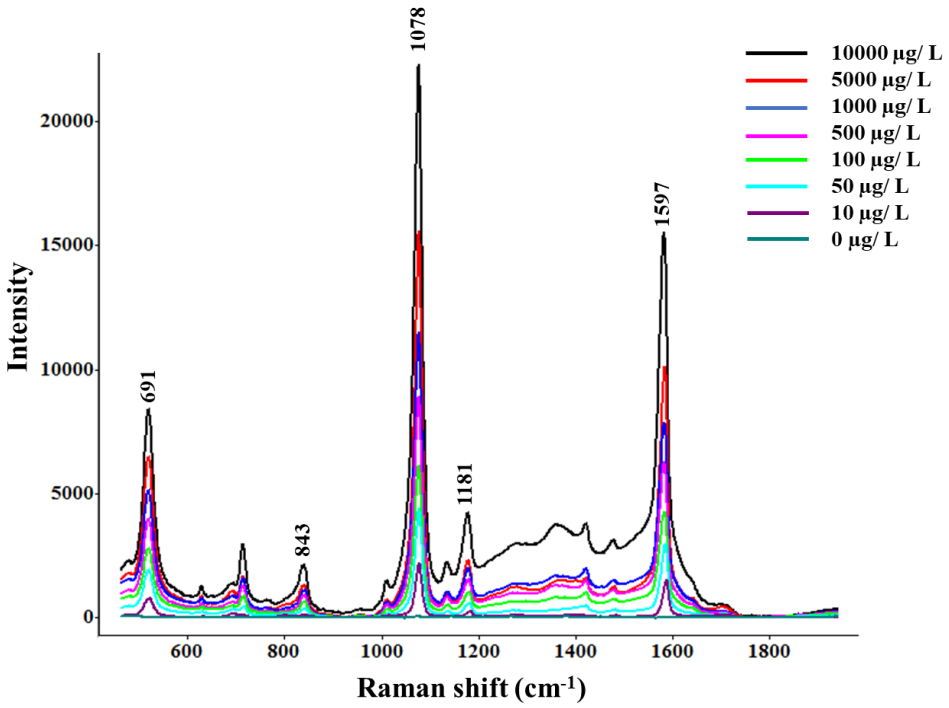

Figure 3.3 SERS measurements of 4-MBA by NFC/Au@Ag NP nanocomposite.

3.3.3 Detection of thiram and paraquat by SERS

To evaluate SERS performance for detection of pesticides, SERS spectra of different concentrations of thiram and paraquat on NFC/Au@Ag NP nanocomposite were measured and the acquired average SERS spectra (n = 8) are shown in Figure 3.4. Thiram was detected by the SERS method when the molecules were chemisorbed to the Ag shells via bidentate ligands. In other words, when thiram molecules interacted

with the Ag shells, they formed a resonated radical structure, which in turn caused the cleavage of a S-S bond in thiram molecules, leading to the formation of two dimethyl residues. The resultant dimethyl residues were adsorbed to the Ag shell via two strong Ag-S bonds (Zhang et al. 2014). The prominent peaks for thiram are 548 cm^{-1} (SS stretching mode), 930 cm^{-1} (CH_3N and C=S stretching), 1370 cm^{-1} (CH_3 deformation and CN stretching), 1138 cm^{-1}, and 1504 cm^{-1} (CN stretching and CH_3 rocking modes) (Saute and Narayanan 2011). The peak at 1370 cm^{-1} is the most characteristic in the thiram spectrum that should be probed as evidence for the presence of thiram in food samples. Nonetheless, Figure 3.4a shows that all peaks are clearly observed at all tested concentrations of thiram solution. An intensity of up to ~35,000 was obtained when the concentration of thiram increased from 0 to 10 mg/L. A comparison between NFC/Au@Ag NPs and NFC/Au NP nanocomposites (Xiong et al. 2018) demonstrates that the replacement of Au NPs by Au@Ag NPs yielded higher Raman intensity of thiram about 8 times, confirming the advantage of using Au@Ag NPs over regular Au NPs.

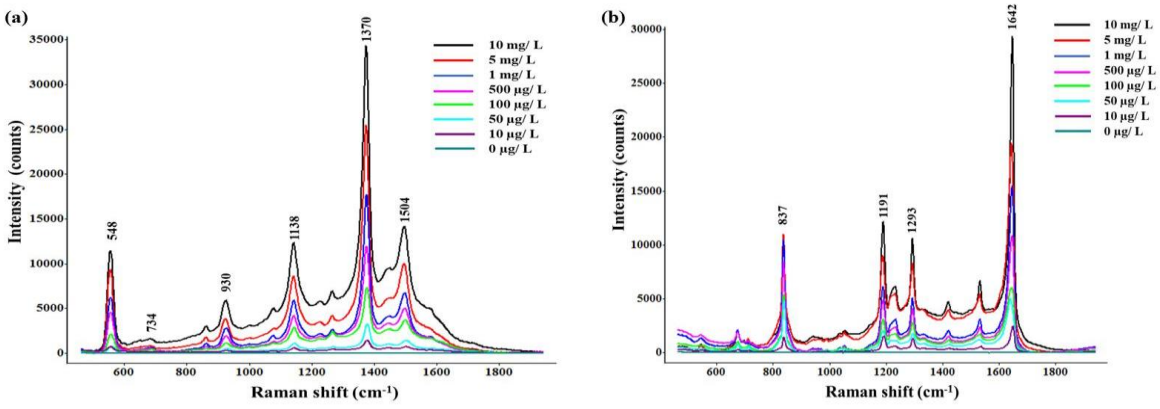

Figure 3.4 SERS measurements of thiram (a) and paraquat (b) solutions by NFC/Au@Ag NP nanocomposite.

Cationic paraquat was also efficiently detected by negatively charged NFC/Au@Ag NP nanocomposite (Figure 3.4b). High hydrophilicity and ionic nature of paraquat enable the molecules to be strongly adsorbed on the Ag shells via hydrogen, ionic, and π bonds (Luo et al. 2018). Major peaks of paraquat are located at 837 cm^{-1} (CN stretching), 1191 cm^{-1} (C=N bending vibration), 1293 cm^{-1} (structural distortion), and 1642 cm^{-1} (C=N stretching modes) (Fang et al. 2015). Among these peaks, the peak at 1642 cm^{-1} is the most distinctive peak. As shown in Figure 3.4b, major peaks are observable at all concentrations of paraquat even at 10 µg/L and very high intensities are observed for all concentrations of pesticide solutions. Increasing the concentration from 0 to 10 mg/L noticeably increased the intensity of Raman spectrum up to ~30,000 for paraquat molecules. Similarly, hybridization of Au@Ag NPs with an Au film also resulted in significantly higher SERS performance for detection of paraquat at very low concentrations of 10^{-8}-10^{-5} M with the intensity in the approximate range of 1000-15000 a.u. (Wang et al. 2016a).

Reproducibility of the SERS substrates over a large area is believed to be one of the challenges in SERS studies (Pang et al. 2016). Hence, better signal reproducibility in a SERS substrate should be credited as an advantage. Spectral homogeneity of NFC/Au@Ag NP nanocomposite was examined based on the optical images and related SERS spectra mappings of two 100 µm × 100 µm regions after the deposition of 500 µg/L thiram and paraquat pure solutions (Figure 3.5). SERS intensity maps of bands at 1370 and 1642 cm^{-1} illustrate a uniformity of the nanocomposite. As observed in the figures, the junctions of nanofibers, where nanoparticles accumulate more, are spots with higher intensity as shown by the red color. Blue colors on the optical image are regions with less nanoparticle clusters, in which pesticide spectra are observed but with the lowest intensities. The uniformity of our nanocomposite was

further supported by a point-to-point mapping on six distinct spots on the selected regions. Corresponding SERS spectra (n = 6) were shown, representing the same prominent peaks of each pesticide with different intensities. Data obtained from area and point-to-point mappings demonstrate the uniformity and as a result reproducibility of NFC/Au@Ag NP nanocomposite, indicating that this nanocomposite is a suitable SERS substrate that can be used to acquire reliable results.

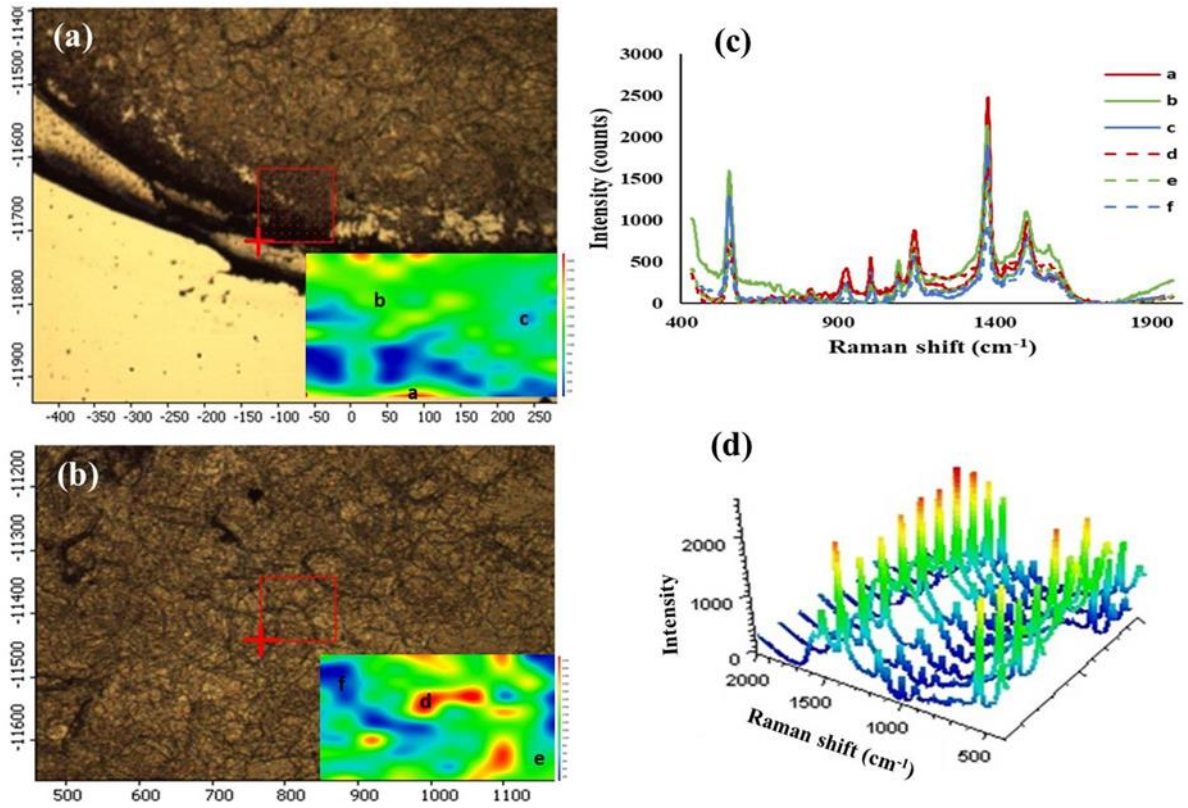

Figure 3.5 Optical images of NFC/Au@Ag NP nanocomposite with deposited 500 µg/L thiram (a and b) and its corresponding SERS intensity map (d) SERS spectra collected from point-to-point mapping of six points on NFC/Au@Ag NP nanocomposite (c).

Lettuce was listed as one of the "Dirty Dozen" fruits and vegetables, i.e. twelve fresh produce with the most pesticide contamination, in Shopper's Guide to Pesticides in Produce released by Environmental Working Group, and after 2013, lettuce was assorted to moderately contaminated vegetables (Group). But it is still important to control pesticide residues in lettuce as a daily consumed vegetable. Accordingly, in our

study, to further evaluate the detection performance and sensitivity of NFC/Au@Ag NP nanocomposite, lettuce samples were probed for the presentence of pesticides either individually (Figure 3.6a and c) or as a mixture (Figure 3.7). The samples were spiked by solutions of thiram and paraquat or their mixture, and their SERS spectra (n = 8) were collected from lettuce extract. Although different components in the lettuce extract (such as phenolic compounds, pigments, and amino acids) brought more noises to the acquired spectra, no interfering noise appeared in these spectra and all characteristic peaks of each pesticide were clearly observable even at very low concentrations. Besides that, relatively high intensities of the characteristic peaks mitigated any interference from noises in the detection scheme. Our SERS measurements show that the intensities of characteristic peaks were consistent with different concentrations of thiram and paraquat in lettuce and thus, can be usable for quantification of pesticide residues in real food samples. Detection of paraquat in a real food sample should be also considered as another advantage of NFC/Au@Ag NP nanocomposite for detection purposes. Technically, hydrophilic nature of paraquat makes it hard to be extracted and detected by multi-residue methods. Additionally, its high affinity to bind to different surfaces calls for special techniques for extraction of paraquat from the food samples (Kolberg et al. 2012). However, we demonstrated that SERS enabled by the NFC/Au@Ag NP nanocomposite could successfully detect paraquat with high sensitivity in complex food matrices.

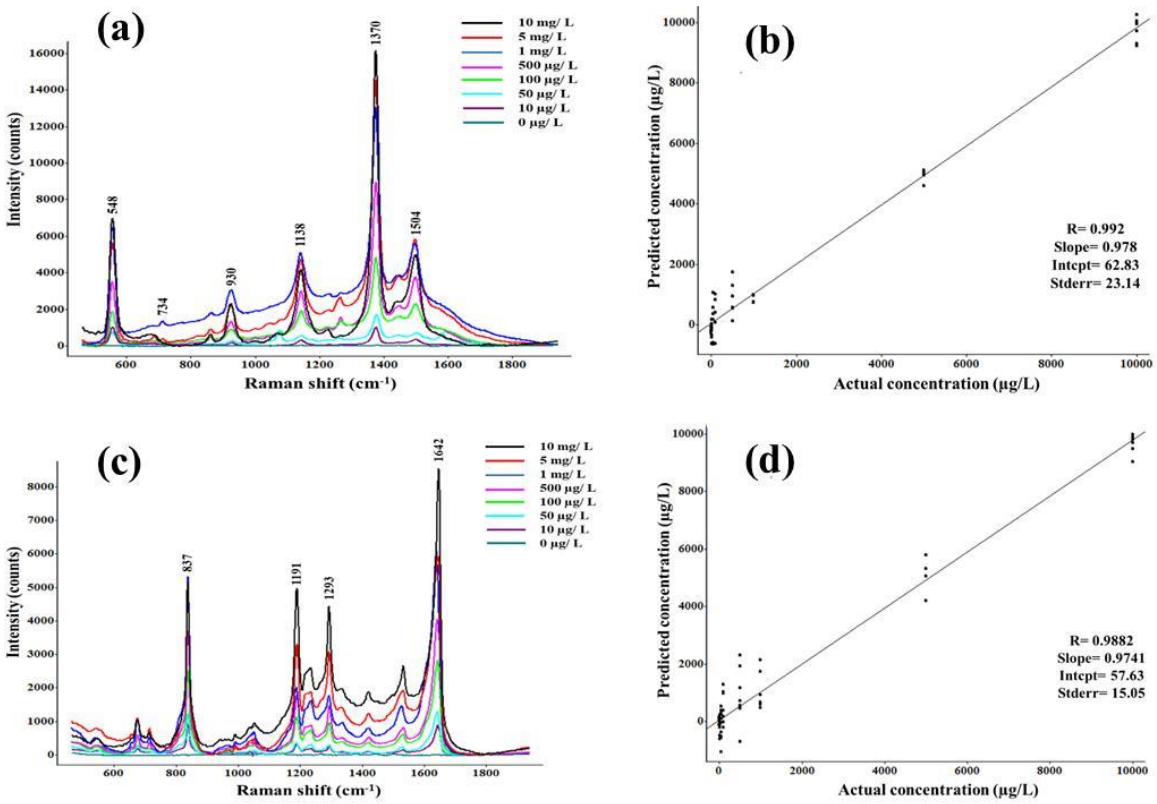

Figure 3.6 SERS measurement of thiram (a) and paraquat (c) detected in the lettuce extract; actual thiram (b) and paraquat (d) concentrations in lettuce extract vs. predicted concentrations using PLS model.

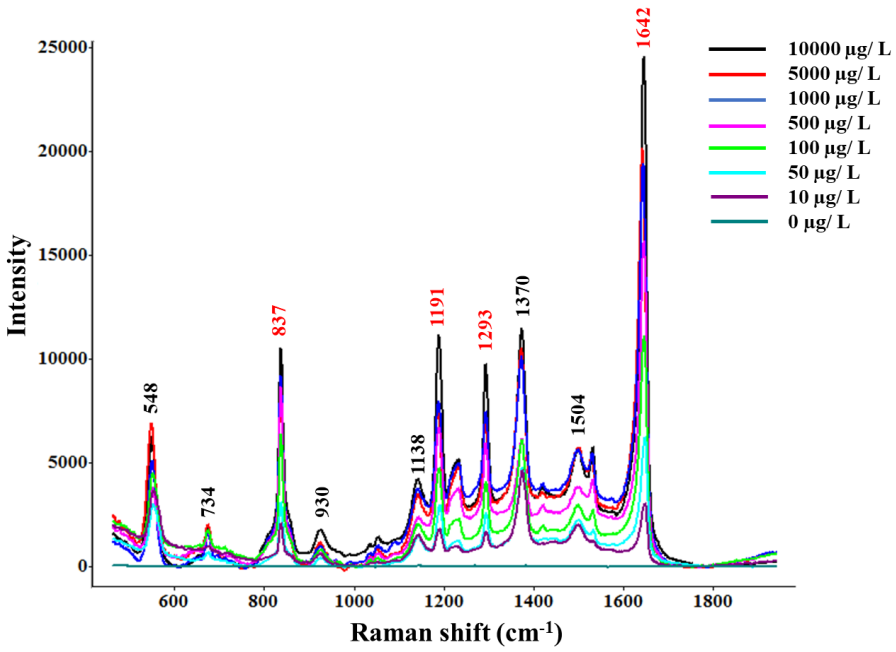

Figure 3.7 SERS measurements of the mixture of thiram and paraquat (black and red wavelengths show the significant peaks of thiram and paraquat, respectively).

In this work, a PLS model was developed to analyze SERS spectra of thiram and paraquat extracted from lettuce. PLS models for prediction of thiram and paraquat in the lettuce extract (n = 80) are depicted in Figure 3.6b and d based on the calibration plots of spiked and predicted concentrations of pesticides. The RMSEP and R values obtained from the PLS models for thiram and paraquat in lettuce were listed. Our results reflect the preciseness of PLS model to predict thiram and paraquat concentrations in the lettuce extract. High R values were found for both pesticides, indicating a very strong linear correlation between the predicted and actual concentrations of pesticides detected in lettuce extract. The good linear relationship can be explained by the well-structured and uniform nanocomposite substrate.

The practicality of NFC/Au@Ag NP nanocomposite in real-world analysis was assessed by calculation of LOD values of each pesticide. The LOD of thiram measured by NFC/Au@Ag NP nanocomposite was 71 μg/L. This LOD value was far below the LOD (240 μg/L) previously reported for thiram, which was monitored by a SERS film based on PMMA/Ag NPs/graphene (Sun et al. 2017). A LOD value of 46 μg/L was obtained for paraquat, which is well below the acceptable MRL value allowed for paraquat in lettuce, 50 μg/L (EPA 2019). Thiram usage is prohibited in lettuce cultivation. A comparison of our results with the results obtained by other studies using an NFC-based nanocomposite as the SERS substrate have been conducted. Accordingly, our substrate provided excellent results for determination of pesticides in complex food samples. These results verify an excellent sensitivity of our nanocomposite for precise detection and quantification of pesticides in fruits and vegetables. This substrate proves its superiority over previous NFC-based nanocomposites since it provides a robust, tunable SERS substrate (compared with single element-based nanocomposites), which can be fabricated in large scale at one-

time with less risk of degradation during the storage times (compared with AgNP-based nanocomposites) with reasonably high SERS performance (compared with AuNP-based nanocomposites).

Most current literature were focused on the detection of a single pesticide in food samples. However, multiple pesticides are usually used in real agricultural practices to hinder various pests and diseases. Besides the negative effects attributed to each individual pesticide, pesticide co-exposure is also regarded as a growing concern to the environment and human health (Bennett et al. 2019). This issue requires a sophisticated tool to be able to simultaneously detect multiple pesticides in a food sample. To address this demand, applicability of NFC/Au@Ag NP nanocomposite for detection of multiple pesticides was also evaluated in this study. Simultaneous detection of thiram and paraquat in lettuce was successfully performed by NFC/Au@Ag NP nanocomposite. All peaks in Figure 3.7 were clear and sharp enough to present a fingerprint-like spectrum for each pesticide in complex lettuce extract. The results of this study prove that multiple pesticides can be detected and distinguished from each other by SERS coupled with NFC/Au@Ag NP nanocomposite at very low concentrations, even at 10 μg/L within 1 s acquisition time without any sample prelabeling. Therefore, SERS method coupled with NFC/Au@Ag NP nanocomposite is a rapid and feasible method for detection of multiple chemical contaminants in complex food matrices with high intensity and reproducibility.

The advantages and disadvantages of some of the analytical techniques, which are commonly used for the detection of pesticides are listed. All analytical methods have their own advantages and limitations. However, among them, SERS provided advantages that are comparable to the other methods and the limitations of this method can be resolved by improving the SERS substrate and including the sample preparations

prior to the analysis, which are mostly straightforward like filtration or centrifugation. Portable Raman devices also substantially reduced the high costs of analysis that was a critical concern for using the bench-top analytical instruments. Fluorescence and SERS are usually considered as "rivals" (Etchegoin and Le Ru 2008). However, SERS also proved its superiority over fluorescence method by having narrower signals compared with broad signals usually obtained by fluorescence, resulting in distinct peaks and in turn, more accurate analysis using SERS method. Therefore, SERS is currently known as a powerful label-free and non-destructive analytical tool with ultrahigh sensitivity to the analytes. However, more research is needed to prove the applicability, accuracy and sensitivity of the proposed nanocomposite for more complicated samples that contain a mixture of target analytes. Moreover, gravity-based loading of NPs on NFC may result in nonuniformity of the nanocomposite, so approaches like electrostatic interaction-based methods should be also implemented for changing the Au@Ag NPs charges to improve the homogeneity of SERS substrate by enhancing the affinity of positively-charged nanoparticles towards the negatively-charged NFC, and as a result, to improve the reproducibility and sensitivity of the SERS analysis even more.

3.4 Summary

This study introduced a cost-effective and efficient SERS substrate based on a NFC platform coated with Au@Ag NPs. NFC is a robust platform in which bimetallic nanoparticles were thoroughly distributed and stabilized, which was used as a SERS substrate. Therefore, this nanocomposite overcomes the instability and weak SERS activity of common SERS substrates, i.e., AgNPs and AuNPs, respectively and the stabilized nanoparticles on NFC provides a stable SERS substrate that can be used for longer periods which was impossible with colloidal substrates. Abundant, cheap NFC and one-time fabrication of multiple substrates also offers an economical SERS

analysis. Different concentrations of 4-MBA were used to evaluate SERS performance of NFC/Au@Ag NP nanocomposite. The excellent detection performance of nanocomposite was also demonstrated by the detection of thiram and paraquat either individually or as a mixture in lettuce. Very low LODs were obtained for both pesticides. The synthesized NFC/Au@Ag NP nanocomposite can be readily used for real food analysis with reproducible SERS measurements and with little matrix interference. Satisfactory results indicate the capacity of this nanocomposite for detection, identification, and quantification of pesticides. Selectivity of the substrate for target molecules can be also extended for detection of other prohibited substances, such as antibiotics and adulterants in complex food matrices. Moreover, bonding NFC/Au@Ag NP nanocomposite NFC/Au@Ag NP nanocomposite NFC/Au@Ag NP nanocomposite NFC/Au@Ag NP nanocomposite NFC/Au@Ag NP nanocomposite on flexible analysis platforms is a promising approach for on-site analysis.

CHAPTER 4

OPTIMISATION USING THE FINITE ELEMENT METHOD OF A FILTER-BASED MICROFLUIDIC SERS SENSOR FOR DETECTION OF MULTIPLE PESTICIDES IN STRAWBERRY

4.1 Introduction

The need for onsite analysis of samples prompted the development of portable devices coupling microfluidic channels with SERS. This novel approach can build up an efficient manipulation and analysis technique that has been examined in various scenarios so far (Zhou and Kim 2016; Pu et al. 2017b). Lab-on-a-chip method is used to miniaturize and integrate multiple analytical methods in a single device, where all analytical steps, from sample preparation to final detection, are performed on a microfluidic platform (Jokerst et al. 2010). Miniaturization allows the analysis to be performed even with tiny amounts of the sample (McDonald et al. 2000; Aghvami et al. 2017). On the other hand, SERS, a highly sensitive method, is capable of selectively probing target analytes in low concentrations even at a single cell or molecule level (Pu et al. 2017a). Interestingly, highly reproducible SERS measurements can be achieved in flow conditions rather than in a static system due to the precisely controlled conditions, particularly if continuous flow and homogenous mixing are fulfilled (Wang and Yu 2015). Thus, integrating SERS in a microfluidic channel enables one to precisely monitor target analytes in a small amount of sample (Knauer et al. 2012). In a SERS chip detection protocol, the liquid sample is either well-mixed with nanoparticle colloid or interacts with a metal nanostructure (prefabricated in the channel) while flowing through the device where target analytes are traced by the SERS detector in a specific detection zone (Chen et al. 2014a). SERS microchips take the advantage of portability, low sample and reagent consumption, flexibility in design and

high process controllability adopted from microfluidic platform and high accurate measurement, sensitive detection, and fast sample screening from SERS method (Pu et al. 2017b). Consequently, the whole system provides highly reproducible, fast in-field detection with high efficiency and low fabrication costs compared with macroscopic methods. Therefore, this method has been widely studied for drug delivery monitoring (Ackermann et al. 2007), biochemical testing for distinguishing cancer cells (Pallaoro et al. 2015), immunoassays (Kamińska et al. 2015b), forensics for drugs of abuse testing (Andreou et al. 2013), and for detection and determination of environmental and food contaminants including heavy metals (Lin et al. 2016b), antibiotic residuals, pathogens, and pesticides (Pu et al. 2017a).

Although SERS microchip sensor features many improvements over the bench-top analytical devices, there are still some restrictions hindering its wide applications. Off-chip sample preparation has been always considered as one of the limitations of using this platform as a detection technique for food samples (Escarpa 2014). In fact, the absence of an on-chip preparation step undermines the true concept of lab-on-a-chip. Additionally, lack of such preparative step in SERS microchip platform prevents the use of the original food sample and even if the original sample is used, it leads to the fouling of the sensor or interfering with the SERS performance. Inclusion of a filtration step in the SERS microchip platform reduces the complexity of the initial sample and improves selective detection (Escarpa 2014). However, integrating a filter into the microfluidic device adds new functions to the fabrication process, such as increasing the possibility of leakage due to the improper attachment. Customized filters, like polydimethylsiloxane (PDMS) filters, have been promising for this purpose, however, the complexity of such filters requires more sophisticated fabrication methods, leading to an increase of the fabrication costs. Therefore, an appropriate chip

design with a proper bonding method assures impregnable attachment of the filter to the channel without leakage or increasing the production costs.

Filter-based microfluidic devices have been used as microdialyzers (Hsieh and Zahn 2005; Gu and Miki 2009; To et al. 2015) and biosensors (Floriano et al. 2005; Kurita et al. 2006) or to mimic human gut (Kim et al. 2012), cardiovascular (Chen et al. 2013) and olfactory systems (Lee et al. 2015).

To the best of our knowledge, there are no reports on using a filter-based SERS microchip as a sensor for analysis of food samples. In this study, a SERS microchip-coupled with filtration for detection of pesticides in fresh produce was established. The sensor contains two main channels, between which a filter membrane has been bonded at the inlet site. Food sample is filtered out from the unwanted parts while flowing from the upper to the lower channel. The filtrate is then mixed with nanoparticle colloid solution and analyzed by SERS in the detection zone while moving through the lower channel. Hypothetically, on-chip filtration at the sensor inlet removes interfering particulates, resulting in a more selective and accurate SERS detection of multiple analytes or mixed samples. Since real food samples usually contain different contaminants, a sensor should be able to detect multiple targets to be considered as a practicable detection technique. To address this requirement, strawberry was chosen as the food sample in this study. In 2020, according to the Shopper's Guide to Pesticides in Produce™ released by Environmental Working Group, strawberries have the highest pesticide residue score among fresh produce and ranked first in "Dirty Dozen" fruits and vegetables. Four pesticides, thiabendazole (fungicide), thiram (fungicide), endosulfan (insecticide), and malathion (insecticide), which are commonly used for cultivation of strawberries were selected for this purpose. Au@Ag nanoparticles have been used as the SERS substrate in our study since their multiple SERS detection ability

for pesticides has been demonstrated before (Asgari et al. 2020). Optimum features for the design geometry, efficient mixing of filtrate and nanoparticles in the mixing zone (at the lower channel) and highly sensitive detection in detection region were determined using the finite element method (FEM) and the obtained values were used for the whole analytical experiments.

4.2 Materials and methods

4.2.1 Chemicals

Silicon wafers were purchased from University Wafer (South Boston, MA, USA). SU-8 2075 negative photoresist (Kayaku Advanced Material, Inc Westborough, MA, USA) was used for patterning and masking the wafer. Sylgard™ 184 silicone elastomer kit was obtained from Dow Corning (Midland, MI, USA) to fabricate PDMS microfluidic channel. Hydrogen tetrachloroaurate solution ($HAuCl_4$, 30 wt% in dilute HCl), silver nitrate (ACS reagent ≥ 99.9%), L-ascorbic acid, polymethylmethacrylate (PMMA), toluene (Certified A.C.S), Pestanal® analytical grade standards of pesticides (thiabendazole, thiram, endosulfan, and malathion) were purchased from Sigma-Aldrich (St. Louis, MO, USA). Trisodium citrate dihydrate (Certified A.C.S), ethanol (Certified A.C.S), and isopropyl alcohol (IPA-70% v/v) were acquired from Fisher Scientific (Fair Lawn, NJ, USA). Polytetrafluoroethylene (PTFE) filter membrane with pore size of 5 µm and thickness of 265 µm was kindly provided by GE Healthcare Life Scientific (Marlborough, MA, USA). Organic strawberries were purchased from a local grocery store. Millipore water was used throughout the experiments and all chemicals were used without further purification. All glassware was soaked in aqua regia (HCl/HNO_3 3:1, v/v) for 24 h and rinsed with Millipore water prior to the experiments.

4.2.2 Finite element method simulation

In this work, simulation was conducted for modeling and optimization of the

sensor design. Since the main analysis is performed in the lower channel, the focus of the simulation was this part of the sensor. The fluid flow in the proposed design was simulated by FEM to optimize the microfluidic geometry, evaluate the mixing efficiency in the mixing zone and investigate the velocity field inside the channel to have thorough mixing and precise detection. The geometry was evaluated and optimized by slight changes of some important parameters including the angle between the two inlets, dimensions (length, width, and depth) of the upper and lower channels, length and width of the mixing zone and the flow rates of the sample and nanoparticle solution. Our designs are limited to fulfil the requirement for a laminar flow of the fluids, which is necessary for efficient SERS detection.

For simulation of the real flow condition, the following assumptions were made:

(1) both fluids (filtrate and nanoparticle solution) are incompressible;

(2) the fluids have Newtonian flow properties;

(3) the mixing is done in isotropic continuous flow condition;

(4) there is no-slip boundary condition in the channel;

(5) nanoparticles are chemically inert and naturally buoyant spheres.

For simulation, the architecture of the lower microfluidic channel was first created in two-dimensional (2D) models using AUTOCAD 2019 (Autodesk Inc., Mill Valley, CA, USA), assuming that there are no effects on the flow in the z-direction, and the generated designs were simulated by FEM. The simulation was started by defining the properties of strawberry extract and nanoparticle solution. To study the flow distribution within the channel, the velocity profile was modeled and shown by 2D surface plots and its fluctuations were analyzed at the cross-section of the channel and depicted by one-dimensional (1D) line graphs.

4.2.3 Device design and fabrication

The sensor consists of four layers: a capping PDMS layer, an upper PDMS channel, a lower PDMS channel, and a supporting glass surface. The capping layer contains three holes at the inlets and outlet positions. Upper and lower channels are identical, but mirror-inverted to facilitate their alignment and bonding. Each channel has two inlets and one outlet. The channels are also equipped with a winding mixing zone and the rectangular detection region. The filter membrane is located at the inlet of the lower channel. The whole device is mounted on a glass slide as a supporting layer.

4.2.4 Fabrication of the microfluidic channels

The two PDMS microfluidic channels were fabricated according to the techniques of standard photolithography and soft lithography. Specifically, silicon wafers were first cleaned by acetone and IPA and blown dry by nitrogen gas. SU-8 2075 was deposited on the cleaned Si substrates in two steps: first spin-coating was comprised of spreading (500 rpm for 10 s at an acceleration rate of 100 rpm/s), spinning (1000 rpm for 30 s at an acceleration rate of 300 rpm/s) and soft-baking (for 60 min at 100℃) to reach a ~220 μ thickness of the photoresist on the wafer. Second coating included spreading (500 rpm for 7 s at an acceleration rate of 100 rpm/s), spinning (3000 rpm for 30 s at an acceleration rate of 300 rpm/s) and soft-baking (for 12 min at 100℃) to a resultant thickness of ~70 μ, achieving the final thickness of ~300 μ of the photoresist. The SU-8 layer was then exposed to UV light at 300 mJ/cm^2 for 30 s. Post-exposure baking was conducted for 5 min at 65℃ followed by 15 min at 95℃. After cooling, the mold was developed in SU-8 developer for 18 min with gentle hand agitation. The developed pattern was then washed with fresh solution for 10 s, sprayed with IPA, and dried with nitrogen. Afterwards, the silicon substrate was spin-coated by PMMA2 solution and baked for 5 min at 180℃ for easier detachment of PDMS mold.

To fabricate the PDMS microchip, a degassed mixture of PDMS prepolymer and curing agent (10:1 w/w) was poured over the master mold and left to polymerize at 70℃ for 60 min. Finally, the solidified PDMS was peeled off from the mold and was ready to be assembled to the sensor platform.

4.2.5 Filter attachment

PTFE filter membrane was trimmed to be in the conforming shape and size of the inlet and was attached to the inlet of the lower channel by a previously described stamping method (Chueh et al. 2007). In this approach, an adhesive PDMS mortar was used as the glue for attaching the filter to the PDMS channel. The PDMS mortar is a 1:1 mixture of PDMS prepolymer and toluene. To ensure the robust attachment of the filter membrane, cement glue was carefully applied at the edges of the membrane where were in contact with the PDMS channel, ensuring that there is not any possibility of leakage.

4.2.6 Assembly of the filter-based microchip

The sensor assembling was conducted by the oxygen plasma treatment. For this purpose, the attaching surfaces were exposed by plasma streams for 30 s and the layers were subsequently attached together with special care to avoid the formation of bubbles. The assembled sensor was also bonded to the supporting glass slide by the same procedure and the assembled filter-based microchip was cured at 70℃ overnight. Puncturing inlets and outlets were done prior to the alignment and bonding.

4.2.7 Synthesis of Au@Ag NPs

Au@Ag nanoparticles were prepared as described in our previous paper (Asgari et al. 2020) in which Au cores are first fabricated by reduction of $HAuCl_4$ using trisodium citrate in an aqueous solution. The as-prepared Au nanoparticles are then used as seeds. Silver coating is gradually developed after adding $AgNO_3$ and ascorbic acid

solutions (as the reducing agent) to the colloidal Au nanoparticles.

4.2.8 Sample preparation

In this study, a 100 mg/Kg stock solution of each pesticide was prepared by dissolving 5 mg of the pesticide (thiabendazole, thiram, and endosulfan) powder or 4.06 μL of malathion into 50 mL of ethanol. A series of concentrations of each pesticide (5, 10, 50, 100, 300, and 500 μg/Kg) were prepared by diluting the stock solution. Pure solvent was also used as the control. Strawberry samples were thoroughly washed with and soaked for 30 min in distilled water. Then, strawberries (2 g) were cut into small pieces and spiked by different volumes of pesticide to a resultant concentration. The strawberry samples were spiked by the pesticide mixture, resulting in final concentrations of pesticides (50, 100, and 300 μg/Kg). After absorption of pesticides by fruit texture, the samples were placed in conical tubes, which contained 4 mL of ethanol. The mixture was vigorously vortexed for 1 min and ultrasonicated for 5 min to complete the extraction of pesticide from the fruit matrices. The mixture was then used for further analysis.

4.2.9 Detection

SERS experiments were performed by a Raman Spectrometer (Renishaw RM1000 System, Gloucestershire, UK) with an excitation wavelength of 785 nm and a 50× objective. The system is equipped with a microscope (Leica DMLB, Wetzlar, Germany) and a 388 × 578 pixel CCD array detector. The laser power of ~35 mW was used to focus laser beam on the detection zone and acquire SERS spectra over the range of 400-2000 cm^{-1} with 10 s integration time. Ten SERS signals were recorded for each experiment by WiRE 3.4 software (Gloucestershire, UK).

The performance of filter-based SERS microchip was investigated through detection of four pesticides in strawberry extract. Firstly, a mixture of acetone and water

(3:1 v/v) was used to wash off the channel and make the filter wet and ready for the operation. Analysis was initiated by injecting strawberry extract (5 μL) from inlet 1 of the upper channel. The injection of the strawberry extract was followed by the air flow to provide the pressure required for the filtration. The alternative injection of sample and air was continued during the analysis. At the same time, Au@Ag nanoparticle solution was injected to the chip through inlet 2 and was mixed with the flowing filtrate. To provide efficient mixing, nanoparticle solution was optimized to be injected with a higher flow rate compared to the flow rate of the sample. The filtrate and nanoparticles were mixed in the mixing zone and the mixture gradually penetrated the rectangular detection zone, which was exposed to Raman laser. The data was taken as the mixture filled up the detection zone. Finally, the waste was collected from the outlet. Optimum flow rates for efficient mixing and detection procedures were obtained by FEM and used throughout the detection process.

4.2.10 Data analysis

In this study, the software Delight version 3.2.1 (D-Squared Development Inc., LaGrande, OR, USA) was used for the data analysis. Two multivariate statistical regression models, partial least squares (PLS) and principal component analysis (PCA), were established for quantitative and qualitative analysis of the data, respectively. Prior to PLS and PCA modeling studies, the spectral data were preprocessed by smoothing at 4 cm^{-1} and secondary polynomial subtraction to reduce the noise and to adjust the baseline shift. Additionally, second-derivative transformation with a gap of 12 cm^{-1} was used for separating the overlapping peaks. Then, a PLS model was developed to predict analyte concentrations in strawberries and to compute the limit of detection (LOD) values of each pesticide in the tested samples. Generally, higher correlation coefficient and lower RMSEP values suggest better predictability of the model. The LOD values

of the sensor for each pesticide were determined based on PLS calibration curve using Equation 1, where σ is the standard error of predicted values (equivalent to RMSEP in the PLS model) and m is the slope of the calibration plot.

$$LOD = 3\sigma/m \quad (1)$$

To estimate recovery efficiency of our method, recovery percentage was calculated by dividing the average (n = 10) quantified pesticide concentration by the spiked concentration.

PCA clustering technique was used to assess the variability of the spectral data acquired from the measurements of the target pesticides and to construct a qualitative predictive model for our study. The PCA is a statistical approach that reduces a multidimensional data set to its most dominant features to remove random variations so that the principal components (PCs) can be retained and used to express the most variations between sample treatments (Goodacre et al. 1998). Therefore, PCA results explain the variance within a class and between different classes. Accordingly, if two classes do not overlap, it means that they are significantly different with 95% confidence level.

4.3 Results and discussion

4.3.1 Optimization of SERS-chip design

FEM is a widely used mathematical tool for solving complicated problems in applied science and engineering including solid-state mechanics, thermal transfer, electromagnetics and fluid dynamics (Arregui-Mena et al. 2016). To solve the problem, FEM splits the system, called computational domain, into smaller patches, or finite elements and finds the solution for the partial differential equation of each individual patch with numerous iterations. The individual solutions of each patch are finally assembled together, so that FEM is able to develop a global solution for that domain

and describe the characteristics of the system (Rapp 2017). Practically, FEM is implemented to numerically solve the complicated problems and reduce experimental efforts in a process design (Puri and Anantheswaran 1993; Rapp 2017; Sanjari Nia et al. 2020).

In this paper, FEM was used to optimize the geometry of our sensor and the design of our experiment for efficient mixing of the sample with nanoparticles and detection of analytes in the sample by the SERS method. In our proposed scenario, strawberry extract is loaded on the inlet 1 and is filtered out from the particulates on-site at the inlet as it flows through the upper channel to the lower channel. The filtrate is immediately mixed with Au@Ag nanoparticle solution, which is injected through the inlet 2, forming a continuous nanoparticle flow inside the channel. Further, efficient mixing of the sample and nanoparticles is achieved in the winding structure of the mixing zone as the flow velocity increases as well. The as-prepared mixture gradually flows toward the detection region, where the velocity drops and let the mixture gradually fill the rectangular detection zone. Here, the sample is exposed to the Raman laser and the Raman scattering signals of target analytes are detected by Raman spectrometer. Different designs were investigated by FEM (data are not shown) and the optimized geometry was selected based on our objectives and used for the rest of the study. Figure 4.1a shows different components of the sensor platform and the optimized parameters for upper and lower channels are shown in Figure 4.2a. Figure 4.1b and Figure 4.2b show modeled and experimentally assembled devices, respectively. Upper and lower channels have the same dimensions as they are 300 μm in width and 300 μm in depth. The filtered sample flows through the lower channel for 10 mm as it reaches the intersection of the two inlets. The passive micromixer is designed and optimized to mix the confluent streams in two steps. The first mixing occurs as the sample and

nanoparticle solution meet each other at the intersection point, where they leave the inlet channels and enter a single channel. Based on the simulations, it was found that if the nanoparticle solution is injected with a relatively higher velocity than the sample, the initial fusion can be achieved at this point. To find the optimum flow rates of the fluids, different flow velocities in the range of 5-40 µl/s were investigated for the sample and nanoparticle solution. A flow rate of 5 µl/s for the sample and a flow velocity of 10 µl/s for nanoparticle solution were found to be optimum for our objectives. Further efficient mixing would be accomplished in a winding structure where the velocity of the mixture (sample-nanoparticles) slightly increased, but it maintained the laminar flow. Other than the flow velocity, the mixing time and the geometry of a passive mixer determine the efficacy of mixing. Accordingly, a length of 21 mm was found optimum for the mixing zone. A winding structure was optimized to have 6 parts of ~ 2 mm for each to let the chaotic recirculation of the mixture enhance the mixing efficiency. In contrast to mixing zone, for an effective detection, it is ideal to have a more stable condition in the detection region. Hence, a larger area (10 mm × 6.3 mm) was designed as for the detection region, so that the flow velocity gradually lowers while flowing from the winding mixing zone to the detection region. This allows the laser to better focus on a single spot of the mixture and reduce the scattering lights which are generally interfering with the detection process.

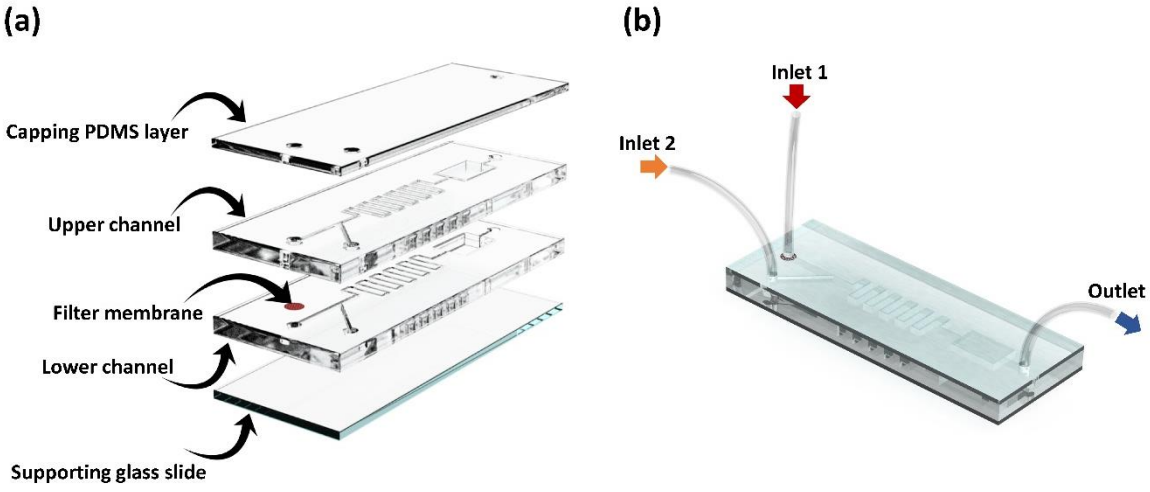

Figure 4.1 Different layers of filter-based SERS microchip platform (a) and the assembled filter-based SERS microchip (b).

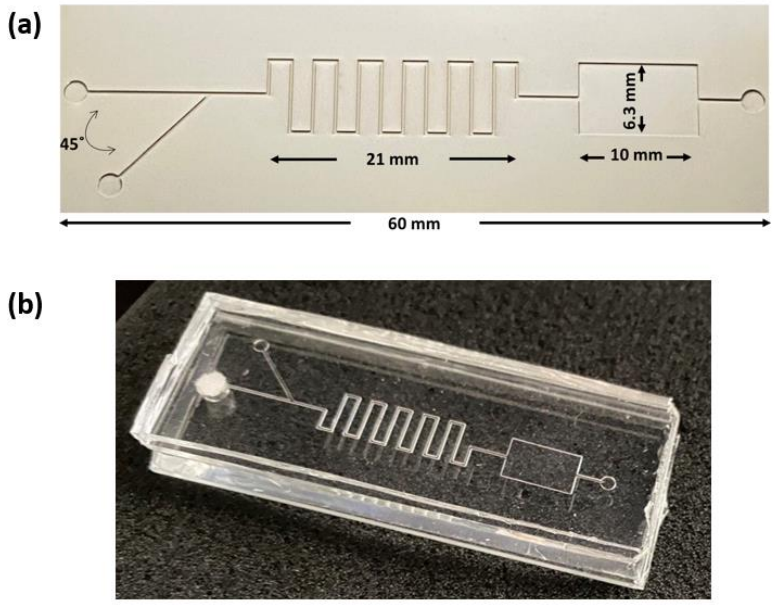

Figure 4.2 The optimized dimensions of the upper and lower microfluidic channels of the sensor (a) and the experimentally assembled filter-based SERS microchip (b).

Figure 4.3a demonstrates the changes of velocity field inside the lower channel. The flow rate of strawberry extract increases (transition from dark blue to red color) when it meets the high velocity nanoparticle solution at the intersection of the channel and the mixture gets higher velocities in the winding mixing zone. The velocity of the mixture drops at the detection zone (transition from red to dark blue color) as it flushes from the narrower channel to a wider one. Then, it flows out of the channel with a slightly increased flow rate (transition from dark blue to red color). The fluctuations of the velocity field of the sample were also evaluated at the cross-section of the channel, from inlet 1 to the outlet, as depicted in Figure 4.3b. The sample has a flow rate of 5 µl/s as loaded on the sensor. As the sample meets the more rapidly moving Au@Ag nanoparticle solution, the velocity of the mixture elevates to around 20 µl/s, leading to an impulsive merging of the two fluids. Further, as the mixture moves through the winding area, the velocity sequentially fluctuates between ~ 0-24 µl/s, reflecting the

microfluidic baker's transformation which is best described by a series of stretches, folds and rejoining to reduce the striation length and achieve a highly desirable mixing performance either theoretically (Wiggins and Ottino 2004) or practically (Ward and Fan 2015). The velocity, then, reaches to ~ 2 µl/s in the detection zone and goes up to 11 µl/s as flushing out of the outlet. The optimized design was fabricated and used for filtration and detection of pesticides of strawberry samples.

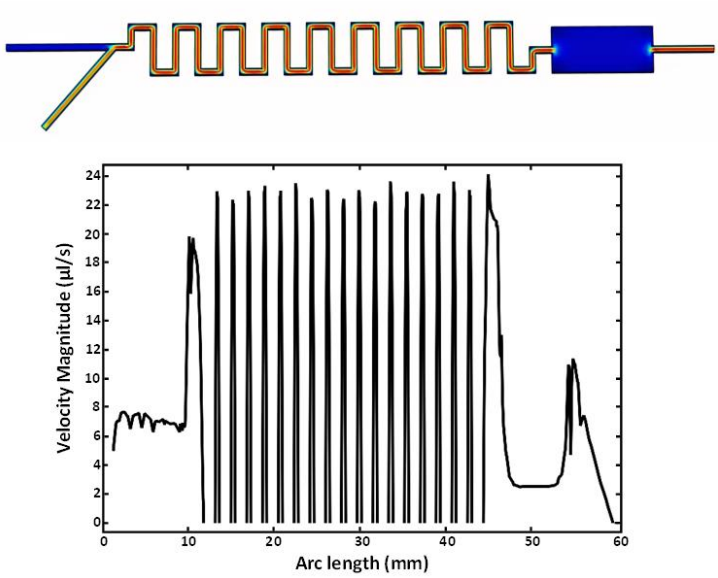

Figure 4.3 Velocity profile in the lower microfluidic channel (a) and the average velocity across the lower microfluidic channel (b).

4.3.2 On-site filtration and SERS sensing

The performance of the sensor was evaluated by measuring strawberry samples contaminated by four pesticides. Prior to the analysis, pesticides were first extracted from the fruit matrices into the solvent, and the extract was then used for analysis without further preparations. This device is designed to remove small particulates from the liquid sample and the resulting clear filtrate is used for analysis. The on-site filtration was successfully accomplished as the sample and subsequentially air were injected. The robust attachment of the filter was resistant to the employed flow velocity and pressure. Empirically, the sensor is reusable for maximum three runs depending on

the sample. Between each run, the sensor is washed off by flushing the pure solvent and flowing through the channel for 2-3 min. The sensor is then ready for the next analysis.

The typical Raman spectra of the four studied pesticides are displayed in Figure 4.4. Accordingly, the most prominent peaks for thiabendazole are located at 786 cm^{-1} (plane bending of CH), 1016 (plane bending of CH), 1282 cm^{-1} (ring stretching vibrations) and 1601 cm^{-1} (ring stretching vibrations of C=N group) (Kim et al. 2009). For thiram, the characteristic peaks are at 556 cm^{-1} (SS stretching), 1139 cm^{-1} (CN stretching and CH_3 rocking) and 1379 cm^{-1} (CH_3 deformation and CN stretching) (Saute and Narayanan 2011). Major bands of endosulfan are at 878 cm^{-1} (CH stretching), 1045 cm^{-1} (CH stretching)(Zhang et al. 2020) and 1659 cm^{-1} (stretching of the Cl−C=C−Cl moiety) (Kubackova et al. 2015). The most characteristic peak of malathion is at 1032 cm^{-1} attributed to the vibration of $POCH_3$ (Wong-ek et al. 2011).

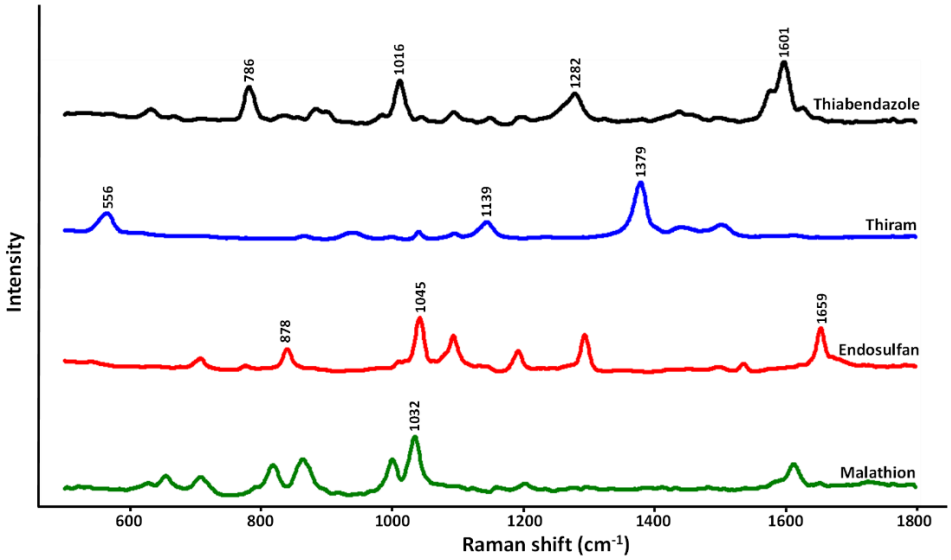

Figure 4.4 Raman spectra of the four studied pesticides.

Figure 4.5a-d demonstrate Raman spectra acquired from strawberry samples contaminated by the four pesticides at various concentrations. Each spectrum is associated with a concentration and represents the average of measurements from ten random spots. Although food matrices add interfering noises to the distinctive Raman

spectra, there are no significant undesirable peaks from strawberry visible in the recorded Raman signals. Although some of the main peaks were diminished by lowering the concentration, our sensor was still able to detect the pesticide by its fingerprint-like patterns, even in the presence of 5 µg/Kg of the pesticide. The most characteristic peaks of each pesticide are clearly seen at all concentration levels and their intensities were significantly enhanced as the concentration increased, reflecting

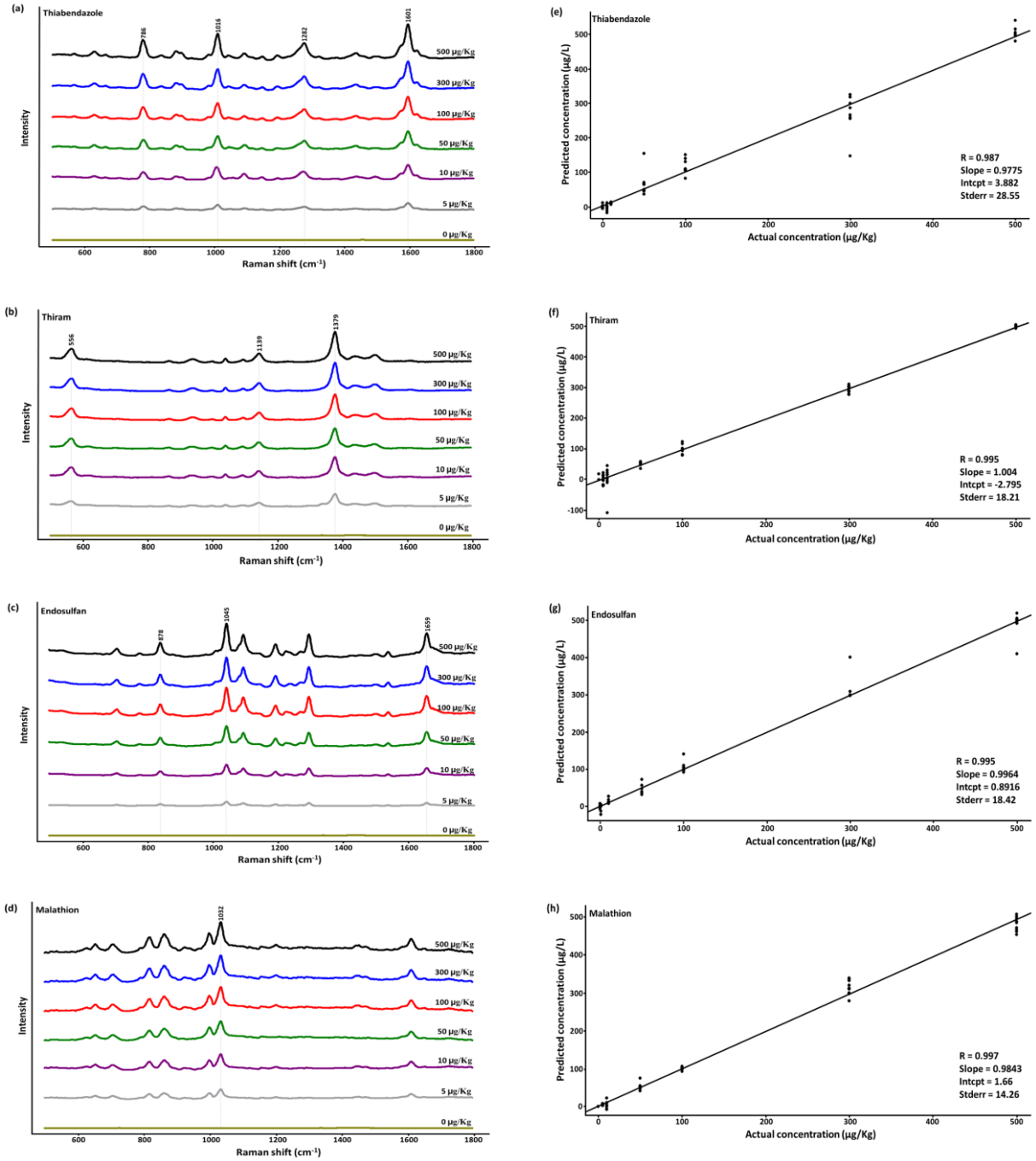

Figure 4.5 SERS measurements of the four studied pesticides detected in strawberry extract (a, b, c, d) and actual pesticides concentrations in the strawberry extract vs. predicted concentrations using PLS model (e, f, g, h).

the ability of our sensor to distinguish different concentrations of the analyte even in complex samples. PDMS has the main peaks at 488, 613, 708, 788, 862, 1266, and 1441 cm^{-1} as reported before (Chen et al. 2014b). However, these peaks were not observed or interfered with Raman spectra of the pesticides. It is believed that increasing the depth of the SERS microchip (to ~ 600 μm) allowed more nanoparticles and analytes to be flushed through the channel and the mixing performance was sufficient, so that relatively strong, accurate SERS signals from target molecules mitigated PDMS characteristic peaks. The PLS models were developed based on the calibration plots of predicted and spiked concentrations of the pesticides (Figure 5e-h).

Table 4.1 summarizes R and RMSEP values acquired from PLS models related to each pesticide. Our findings reveal the preciseness of our PLS model in predicting the concentration of thiabendazole, thiram, endosulfan and malathion in strawberry extract. The very high R values obtained for all four pesticides exhibit a strong linear correlation between the predicted and actual concentrations of the pesticides in strawberry extract, implying the validity of the PLS model used in this study.

Table 4.1 Prediction results derived from PLS models, LOD and MRL values of thiabendazole, thiram, endosulfan and malathion in strawberry

Pesticide	R value	Standard deviation	LOD (μg/Kg)	MRL (mg/Kg) *
Thiabendazole	0.987	28.55	55	5
Thiram	0.995	18.21	44	13
Endosulfan	0.995	18.42	88	2
Malathion	0.997	14.26	54	8

*Set by the United States Environmental Protection Agency (EPA)

The LOD values of each pesticide were calculated by equation 1 based on PLS

models. The LOD values were compared with the established maximum residue limits (MRLs) of each pesticide in strawberry as set by the United States Environmental Protection Agency (EPA) (Table 4.1). Accordingly, the LOD values of thiabendazole, thiram, endosulfan and malathion in strawberry extract were about 55, 44, 88, and 54 μg/Kg, respectively. These LOD values are far below the MRLs, which are 5, 13, 2, and 8 mg/Kg for thiabendazole, thiram, endosulfan and malathion, respectively. Therefore, this method meets EPA's requirement of the studied pesticides in strawberry. Furthermore, satisfactory recoveries were achieved by filter-based SERS microchip as shown in Table 4.2. The recovery values ranged from 90 to 122% for strawberry samples spiked by 50 and 500 μg/Kg of the four pesticides. Our results clarify that filter-based SERS microchip coupled with Au@Ag nanoparticles is a reliable, highly sensitive and precise detection and quantification technique for tracing thiabendazole, thiram, endosulfan and malathion in complex food samples.

Table 4.2 The recovery of thiabendazole, thiram, endosulfan and malathion in strawberry

Pesticide	Spiked value (μg/Kg)	Quantified value (μg/Kg)	Recovery (%)	Precision as RSD (%)*
Thiabendazole	50	61	122	5.3
	500	503	101	3.7
Malathion	50	50	99	2.5
	500	500	100	5.4
Endosulfan	50	49	98	4.5
	500	451	90	6.1
Thiram	50	58	116	2.2
	500	478	96	1.6

*RSD (%) = (standard deviation/mean) × 100 (n = 10)

Detection of multiple pesticides in fresh produce is challenging because there

exist many agrochemicals with very low concentrations in fruits and vegetables. Additionally, the presence of unwanted analytes can interfere with the target detection signals. Therefore, to rigorously determine the practicality of filter-based SERS microchip, simultaneous detection of thiabendazole, thiram, endosulfan and malathion was investigated in strawberry samples. Our sensor successfully detected multiple pesticides in the strawberry extract. As shown in Figure 4.6, some of the main peaks of each pesticide are missing in the Raman signals of the mixture. But the characteristic peaks of each pesticide are obviously observable at the three mixture concentrations and the intensities of the peaks are consistent with the concentration of the pesticides in the sample. Thiram shows the highest intensity that shows its highest affinity to the Au@Ag nanoparticles. The characteristic peak of endosulfan showed a slight shift from 1659 to 1647 cm^{-1} in the mixture signal. However, it is still within the range associated with the stretching vibration of the Cl−C=C−Cl (Kubackova et al. 2015). Hence, filter-based SERS microchip is able to simultaneously detect and differentiate SERS spectral patterns of multiple contaminants in complex food matrices.

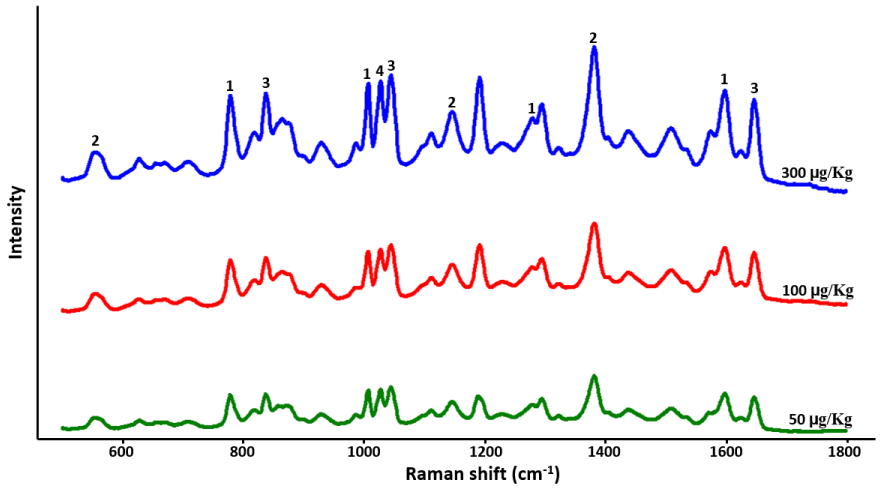

Figure 4.6 SERS measurements of the mixture of thiabendazole (denoted as 1), thiram (2), endosulfan (3) and malathion (4) in the strawberry extract.

Specificity of Raman analysis has been proved in previous literature. In fact, each chemical bond produces a specific vibrational mode, leading to a unique Raman

signal and even a slight change in the molecular structure, such as isomerization, represents itself by a shift in the position of Raman peaks. As a result, Raman analysis distinguishes analytes even with similar chemical structures (Halvorson and Vikesland 2010). Therefore, Raman analysis distinguishes High selectivity of the filter-based SERS microchip was confirmed by PCA analysis. According to Figure 4.7, the sensor is able to clearly discriminate the four pesticides as they are separated from each other. In addition, this method is able to distinguish thiabendazole, thiram, endosulfan and malathion from the SERS spectra of their mixtures, i.e., there is a statistically significant difference between the individual pesticides and their mixture. The data cluster of the mixture looks closer to the point cluster corresponding to thiram, confirming our finding of the more binding affinity of thiram to the Au@Ag nanoparticles compared with other studied pesticides.

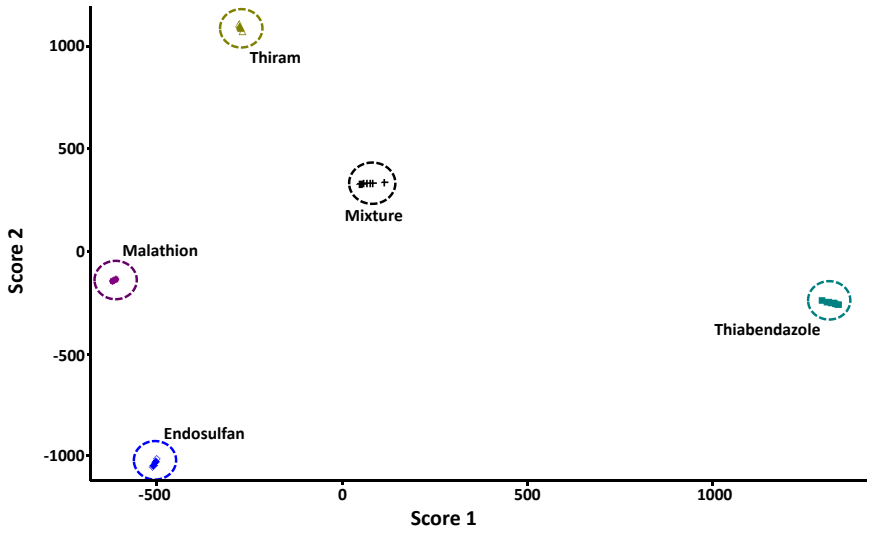

Figure 4.7 PCA plot of 300 µg/Kg of thiabendazole, thiram, endosulfan and malathion and their mixture at concentration of 300 µg/Kg in the strawberry extract.

4.4 Conclusion

We are first to report a SERS microchip equipped with filtration as a sensor for detection of chemical contaminants in real food samples. Filter-based SERS microchip eliminates the need for off-chip sample preparation, providing a fast and feasible on-

site analysis for food samples. The liquid, even original sample, can be directly injected to the channel while the filtration is conducted at the inlet. Therefore, the interfering particulates are removed prior to the blending of sample with SERS-active nanoparticles and the detection of target analytes, making both processes more effective. The channel was designed and optimized by FEM to provide an efficient mixing of the sample and nanoparticles solution at two points, the intersection of the inlets and at the winding mixing zone. The subsequent detection zone was designed to be a larger space to lower the flow velocity of the sample and facilitate the detection in a more stable condition. Highly sensitive and selective detection was accomplished by Au@Ag nanoparticles, so that four pesticides were detected in strawberry samples simultaneously while flowing through the microchip. Our results showed LOD values of less than 100 μg/Kg for the studied pesticides which are remarkably lower than established MRLs. This sensor can be used to detect multiple analytes and the method is transferable to other food and environmental samples. However, reusability of the sensor is limited to maximum three runs depending on the sample. Therefore, future studies are required for enhancing the reusability of the filter-based SERS microchips. Using a semipermeable membrane is also promising for concentration and detection of a specific analyte. Additionally, one could fabricate the filter-based SERS microchip with thermoplastics which has a suitable property for mass production. Thermoplastic microchips offer high-throughput production and low-price sensing devices resulting in disposable chips.

CHAPTER 5

SEPARATION AND DETECTION OF *E. COLI* O157:H7 USING A SERS-BASED MICROFLUIDIC IMMUNOSENSOR

5.1 Introduction

In the United States, the consumption of fresh fruits and vegetables is increasing among consumers. Since these products are mainly consumed raw and are minimally processed, the prevalence of multistate outbreaks of foodborne illnesses associated with raw fruits and vegetables has become an increasing concern recently (Yu et al. 2018). Among fresh produce, leafy greens are the most foreseeable implicated vehicles of pathogen hazards (FDA 1998). Among bacterial pathogens, Shiga toxin-producing *Escherichia coli* (STEC) are the main foodborne pathogens associated with these outbreaks (CDC 2021). Notably, more than half (54%) of the outbreaks were linked to a specific leafy vegetable (i.e., contaminated romaine lettuce), rather than mixed products (Marshall et al. 2020). The frequently occurring leafy green-associated outbreaks highlight the importance of early detection of *E. coli* O157:H7 in leafy greens for preventing further contamination over the production and processing chains.

Currently, conventional culture-based isolation and detection methods are used as gold standard methods for the detection of foodborne pathogens. Isolation and detection of *E. coli* O157:H7 in foods involve sample collection, serial dilution, plating, and culturing on selective media, such as sorbitol-MacConkey agar (SMAC) (March and Ratnam 1986). Despite being simple, inexpensive, and sensitive, these methods are laborious and time-consuming, taking up to one week to obtain results (Zhao et al. 2014). Likewise, if the number of bacteria in the food sample is low, these methods require enrichment of bacterial cells with an extra 8 to 24 h prior to the detection (Sharma and Mutharasan 2013). Currently, culture-independent methods, such as

nucleic acid-based methods and immunoassays have been widely used as alternative methods to overcome the drawbacks of conventional methods due to their higher sensitivity, specificity, and rapidity (Saravanan et al. 2020). Nucleic acid-based methods such as polymerase chain reaction (PCR) involve the detecting specific target genes or DNA sequences of target pathogens using a thermostable polymerase enzyme (Deisingh and Thompson 2004). These methods are considered sensitive and rapid methods as low concentrations of foodborne pathogens can be detected within hours. However, these techniques may bring other limitations to the detection procedure, such as high costs, the requirement for trained personnel and sophisticated devices and several technical issues, especially when used for complex matrices (López-Campos et al. 2012). Immunoassays such as enzyme linked immunosorbent assay (ELISA) are qualitative-quantitative tests that are based on the interaction of a specific antibody with a target antigen (Seiichi et al. 2018). Accordingly, there are commercial antibody-based kits developed for fast, on-site detection of *E. coli* O157:H7. However, their suitability for monitoring a low initial concentration level of bacteria is still questionable (D'Lima and Suslow 2009).

Surface-enhanced Raman spectroscopy (SERS)-based immunosensors have been recently recognized as a powerful clinical and biochemical diagnosis method. Generally, these methods are operated by (i) SERS-tags that include antibodies to anchor onto bacterial cells, (ii) SERS reporter molecules, and (iii) SERS active substrates (Xiao X. Han et al. 2008). The superiority of this technique over conventional immunoassay methods, such as ELISA and fluorescence-based assays, lies in the fact that (i) SERS has a relatively high sensitivity even at very low concentrations of the target analytes (Asgari et al. 2020, 2021), (ii) less susceptibility of Raman signals to photobleaching results in lower detection limits (Jun et al. 2007),

(iii) multiplexing is achievable using multiple complementary antibodies and different Raman reporters (Kamińska et al. 2015b), and (iv) narrow Raman signals facilitate the detection of multiple biomarkers and pathogens (Lee et al. 2012). Nonetheless, inconsistent and irreproducible SERS results cause difficulties in quantitative analysis (Rongke Gao et al. 2016). Therefore, the integration of SERS-based immunoassay into a microfluidic channel provides a homogeneous analysis condition, facilitating accurate quantitative evaluation of the target analytes (Rongke Gao et al. 2016). Additionally, this platform offers automatic sampling, continuous and multiplex analysis with low sample consumption (Bridle et al. 2014).

Various SERS-based microfluidic immunosensors have been evaluated to detect pathogens in recent years. Each research group developed a specific strategy to lower the limit of detection (LOD). Integration of SERS-tags into a microfluidic dielectrophoresis sensor led to a very low LOD of 70 $CFU.mL^{-1}$ (Lin et al. 2014). However, inefficient liquid from such sensors usually results in incompetent quantitative detection of bacteria in complex samples (Chen et al. 2020). A nano-dielectrophoretic microfluidic sensor coupled with SERS was employed for online enrichment, separation, and detection of *E. coli* O157:H7 in water (Wang et al. 2017). Although the method is highly sensitive and all steps were applicable in one step, the technique is too complicated and lacks applicability when bacteria exist in food samples (Weng et al. 2021). Off-chip labeling was another technique used to separate and detect *Listeria monocytogenes* in pure culture (Rodríguez-Lorenzo et al. 2019). This study achieved a very high LOD value of 10^5 $CFU.mL^{-1}$, which is too high for highly pathogenic bacteria. Therefore, it is necessary to develop an efficient, rapid, and feasible method to detect *E. coli* O157:H7 in complex food samples with high sensitivity and selectivity.

Herein, we developed a feasible and sensitive protocol to separate and detect pathogens in complex food samples. Our study targeted the detection of *E. coli* O157:H7 in romaine lettuce because of the importance of this pathogen in leafy greens, specifically lettuce. Our protocol consists of (1) an enrichment step; (2) off-chip separation and labeling of pathogens by fluorescent immune-nanoprobes in the food sample, and finally; (3) on-chip detection of the labeled bacterial cells by a sensitive SERS microchip which is capable of detecting individual cells in a thin layer of fluid flow. Remarkably, our protocol showed excellent separation and detection performance of the very low counts of pathogens in complex food samples. The detection time was much less than that of standard conventional methods. The results of this study are promising for the practical separation and detection of pathogens in food samples. To the best of our knowledge, there is no reported study on separation and detection of *E. coli* O157:H7 using SERS-based microfluidic immunosensors with a LOD value of less than 10^2 CFU.mL^{-1} in the food sample.

5.2 Materials and methods

5.2.1 Chemicals

Biotin anti-*E. coli* antibody (isotype: IgG) was purchased from Abcam (Cambridge, MA, USA, www.abcam.com) and three strains of *E. coli* O157:H7 (505B, 93-111 and EDL-933) were obtained from the culture collection in the Food Microbiology Laboratory at the University of Missouri (Columbia, MO, USA). Tryptic soy broth (TSB), tryptic soy agar (TSA), and MacConkey Agar were purchased from Difco Laboratories (Franklin Lakes, NJ, USA, www.bd.com). Silicon wafers were obtained from University Wafer (South Boston, MA, USA, www.universitywafer.com) and SU-8 2075 negative photoresist (Kayaku Advanced Material, Inc Westborough, MA, USA, www.kayakuam.com) was used for patterning and masking the wafer.

Sylgard™ 184 silicone elastomer kit was obtained from Dow Corning (Midland, MI, USA, www.dow.com) to fabricate the polydimethylsiloxane (PDMS) microfluidic channel. Hydrogen tetrachloroaurate solution ($HAuCl_4$, 30 wt% in dilute HCl), rhodamine 6G (R6G), thioctic acid, N-hydroxysuccinimide (NHS), streptavidin, and polymethylmethacrylate (PMMA) were purchased from Sigma-Aldrich (St. Louis, MO, USA, www.sigmaaldrich.com). Trisodium citrate dihydrate (Certified A.C.S), 1-ethyl-3-(3-dimethylaminopropyl) carbodiimide hydrochloride (EDC), phosphate buffered saline (PBS, 10X Solution), ethanol (Certified A.C.S), and isopropyl alcohol (IPA-70% v/v) were acquired from Fisher Scientific (Fair Lawn, NJ, USA, www.fishersci.com). Romaine lettuce was purchased from a local grocery store. Millipore water was used throughout the experiments and all chemicals were used without further purification. All glassware was soaked in aqua regia (HCl/HNO_3 3:1, v/v) for 24 h and rinsed with Millipore water prior to the experiments.

5.2.2 Gold (Au) nanoparticles synthesis

Au nanoparticles (AuNPs) were fabricated by the citrate reduction technique based on a previous method (Xiong et al. 2018). In brief, AuNPs were fabricated by reducing Au^{3+} ions using a mild reducing and stabilizing agent, trisodium citrate, in an aqueous medium.

5.2.3 SERS-nanoprobe synthesis

Citrate molecules on AuNPs were replaced by thioctic acid through a ligand exchange reaction. Accordingly, to ensure complete exchange of citrate molecules, thioctic acid solution was used in excess of the ligands, i.e., 50 mg thioctic acid powder was dissolved in 2 mL ethanol and added to 20 mL of the AuNP solution and allowed to stir for 5 h at room temperature. Then, 1.5 mL of R6G (3 mg. 15 mL-1) was added to thioctic acid conjugated AuNP solution and was left to stir at room temperature

overnight. Afterward, a mixture of 1 mL EDC (6 mM) and 1 mL NHS (0.03 M) was prepared and blended with the AuNP@R6G for 2 h at room temperature. The functionalized nanoparticles were then collected by centrifugation at 7513 ×g for 20 min and resuspended in PBS solution. To make streptavidin-capped AuNP@R6G, 20 µL of streptavidin solution (1 $mg.mL^{-1}$) was mixed and incubated with 1 mL AuNP@R6G for 1 h. Next, AuNP@R6G@SA were mixed and incubated with 20 µL of antibody to form AuNP@R6G@SA@Ab SERS-nanoprobe. Finally, AuNP@R6G@SA@Ab SERS-nanoprobe were collected by a series of washing and centrifugation steps. For this step, first, the original AuNP@R6G@SA@Ab SERS-nanoprobe solution was centrifuged at 9300 ×g for 15 min and afterwards, the supernatant was removed. Then, the tube was refilled with the same volume of PBS solution and the sample was centrifuged for the second time. Washing and centrifugation was repeated until when the supernatant became colorless. Finally, the collected SERS-nanoprobes were redispersed in PBS for further analysis.

5.2.4 Bacterial cocktail preparation

Three strains of STEC O157:H7 (Table 5.1) isolated from different sources were selected to prepare a cocktail for inoculation into the lettuce samples. First, each strain was separately grown overnight in fresh TSB broth at 37 °C. After incubation, the bacterial pellets were collected by centrifugation at 11200 ×g and suspended in sterile peptone water. Bacterial counts for each strain were obtained by performing serially diluting and pour plate counting colonies on TSA. Bacterial colonies for each strain were enumerated after incubation at 37 °C for 24 h. Based on the number of $CFU.mL^{-1}$ counts obtained for each strain, corresponding dilutions and volumes were determined to get a cocktail with a ratio of 1:1:1 for each strain. Finally, the cocktail was serially diluted to obtain spiking inoculums of 0.1, 0.5, 1, 10, and 100 $CFU.mL^{-1}$.

Table 5.1 *E. coli* O157:H7 strains used in this study.

O-serogroup	Strain	Source
E. coli O157:H7	505B	Beef (FRI)
E. coli O157:H7	93-111	Hamburger
E. coli O157:H7	EDL-933	Human (USA)

5.2.5 Lettuce examination for the absence of *E. coli* O157:H7

Prior to inoculation of the spiking cocktail into the lettuce samples, the purchased samples were evaluated for the presence of STEC O157:H7. For this purpose, 10 g lettuce was cut into roughly similar pieces and mixed with 90 ml of modified buffered peptone water (mBPW) supplemented with 8 $mg.L^{-1}$ vancomycin in a filter stomacher bag. The mixture was hand massaged for 2 min and then incubated at 42 ˚C for 15 min. The sample was serially diluted up to 10^{-6} dilutions. For the detection of *E. coli* O157:H7 in samples, two methods were used, as shown below.

Plating: Each dilution was spread-plated and incubated at 37 ˚C for 24 h on Sorbitol MacConkey agar (SMAC). After the incubation, the plates were evaluated for the presence of colorless *E. coli* O157:H7 on the agar plates due to their inability to ferment sorbitol.

Immunoassay kits: The Oxoid DrySpot *E. coli* O157 test (Thermo Scientific, Kalamazoo, MI), which is based on agglutination in the presence of serogroup O157, was used to test the presence of *E. coli* O157:H7 according to the instruction provided by the company.

5.2.6 Sample preparation

Lettuce samples were prepared by cutting lettuce leaves into pieces of roughly the same size. The prepared lettuce samples (200 g each) were placed in sterile

stomacher® bags and spiked with 1 mL of 0.1, 0.5, 1, 10, and 100 CFU.mL^{-1} of *E. coli* O157:H7 cocktail. After inoculation, the samples were left for 15 min to allow bacterial cells to attach to the leaves' surfaces. Then, 450 mL of sterile (1×) mBPW with vancomycin (8 mg.L^{-1}), prewarmed at 42 °C, was added to the samples and the bags were hand-massaged thoroughly for 1 min. *E. coli*-inoculated lettuce samples were incubated at 42 °C for 15, 30, 45, 60, and 120 min for enrichment, and sampling for SERS detection was performed (Singh and Mustapha 2015; FDA 2019). For sampling, 2 mL of the fluid was collected into the centrifuge tube and stored properly until further steps.

5.2.7 Labeling of the bacterial cells

First, 1 mL of glutaraldehyde solution (2.5%) was injected into 1 mL of the sample, followed by storing the samples at 4 °C for 30 min to allow bacterial cells to be fixed. Afterward, the cells were collected by twice washing and centrifugation at 9300 ×g for 15 min. The pellets were then mixed and homogenized with 1 mL of SERS-nanoprobe solution followed by incubation in a shaking incubator at 37 °C at a speed of 100 rpm.min^{-1} for 15, 30, 45, and 60 min. After incubation, free reagents and SERS-nanoprobes were withdrawn by twice washing and centrifugation at 9300 ×g for 15 min. The resulting labeled pellets were resuspended into 1 mL of sterile PBS and stored at 4 °C for further analysis.

5.2.8 Microfluidic channel fabrication

The microchip layout was designed using AUTOCAD 2021 (Autodesk Inc., Mill Valley, CA, USA) with desired dimensions, and PDMS microchip was fabricated according to the techniques of standard photolithography and soft lithography. Briefly, SU-8 2075 was deposited on cleaned silicon wafers in two sequential steps; (i) first spin-coating by spreading (500 rpm for 10 s at an acceleration rate of 100 rpm.s^{-1}),

spinning (1000 rpm for 30 s at an acceleration rate of 300 rpm.s^{-1}) and soft-baking (for 60 min at 100 °C); and (ii) second spin-coating by spreading (500 rpm for 7 s at an acceleration rate of 100 rpm.s^{-1}), spinning (3000 rpm for 30 s at an acceleration rate of 300 rpm.s^{-1}) and soft-baking (for 12 min at 100 °C) to reach to a ~220 μ and ~70 μ thickness of the photoresist on the wafer, respectively. UV exposure and development in SU-8 developer resulted in a channel with a depth of ~300 μ. For easier detachment of PDMS, PMMA2 solution was spin-coated and baked for 5 min at 180 °C on silicon wafer. To develop a PDMS microchip, a degassed PDMS mixture was cast on silicone-photoresist mold and left to polymerize at 70 °C for 1 h. The PDMS channel was finally peeled off from the mold and plasma-bonded to a cleaned glass slide.

5.2.9 Detection

To increase the efficiency of the detection performance, a flow-focusing microfluidic device was used in this study. For this purpose, the sample, labeled bacteria suspended in PBS, was injected from inlet B with the flow rate of 5 μL.min^{-1} and two lateral flows of PBS, as neutral flows, were injected from inlets A and C with flow rates of 10 μL.min^{-1} to surround the central sample flow. Raman signals were collected by focusing the Raman laser with a width of ~100 μm on the central stream and ten signals were continuously collected while the sample was flowing through the microchip.

Data collection was performed using a Raman Spectrometer (Renishaw RM1000 System, Gloucestershire, UK) with a 50× objective and an excitation wavelength of 785 nm at ~35 mW. The system is equipped with a microscope (Leica DMLB, Wetzlar, Germany) and a 388 × 578 pixel CCD array detector. SERS spectra were acquired over the range of 400-2000 cm^{-1} with 10 s integration time.

5.2.10 Characterization of SERS-nanoprobes

The SERS-nanoprobes were characterized by UV-Vis spectroscopy (Cary Bio

50, Agilent, CA, USA) and transmission electron microscopy (TEM) using high-resolution FEI Tecnai F30 Twin TEM operating at 300 kV at different stages of preparation. SEM images were acquired using a FEI Quanta 600 F SEM (FEI, Hillsboro, OR, USA) operated at 10 kV. Confocal microscopy of the labelled bacterial cells was performed with a Leica SP8 laser scanning confocal microscope equipped with a tunable supercontinuum white light laser and a 63×/NA1.20 water immersion objective.

5.2.11 Data Analysis

All experiments were repeated three times and in each run of SERS measurement, ten Raman signals were recorded by WiRE 3.4 software (Gloucestershire, UK).

5.3 Results and discussion

5.3.1 Principal of the separation and detection of *E. coli* O157:H7

Herein, a combination of immunoassay, SERS, and microfluidics was used to selectively separate and detect *E. coli* O157:H7 cells in romaine lettuce. The separation and detection are accomplished by fluorescent immune-nanoprobes that can selectively anchor onto *E. coli* O157:H7 cells and have high SERS activity which enables the detection of pathogenic bacteria, even with low counts, in complicated food matrixes. The nanoprobes consist of three important segments: (i) biotin anti-*E. coli* antibodies as the anchoring moiety to selectively capture *E. coli* O157:H7 cells, (ii) R6G molecules as the SERS reporter and as an indicator of the presence of the target bacteria in the sample, and (iii) AuNPs as the SERS active substrate to intensify the Raman signals from the captured bacterial cells. In our proposed protocol, when the food sample is incubated with SERS-nanoprobes, the probes are able to anchor and separate bacterial cells from the food matrix due to the avid interaction of antigen with antibody. In the

presence of the target pathogen, the separated bacterial cells are further collected and detected in a highly sensitive SERS microchip. However, detection of a single cell in a food sample faces challenges and is not generally straightforward, so having an enrichment step prior to the separation increases the likelihood of rapid detection of a single cell in food samples. Interestingly, our preliminary findings proved that long enrichment periods were not needed compared with traditional methods. Therefore, our proposed method is promising for fast, feasible, and practical applications in a large-scale context.

5.3.2 Fabrication of SERS-nanoprobes

The synthesis of the SERS-nanoprobe includes a series of reactions that couples AuNPs with the biotinylated antibodies. For this study, AuNPs of an average particle diameter of 40 nm were used. Commonly, nanoparticles are chemically bonded with antibodies in one of three ways: (i) chemisorption, (ii) via bifunctional molecules, or (iii) through adapter molecules like avidin or streptavidin (Ijeh 2011). The latter approach was used in this study. Streptavidin is a protein that is known and commonly used in immunoassays owing to the strongest non-covalent bond formed with biotin (Hyre et al. 2006). Streptavidin-functionalized nanoparticles have been used to attach to biotinylated proteins and antibodies (Bi et al. 2020).

For fabrication of SERS-nanoprobes, first, thioctic acid was bonded with AuNPs with its disulfide group at one end (Ghann et al. 2019). The mixture of EDC and NHS were employed to further activate the carboxyl groups on the other end of thioctic acid molecules (Wang et al. 2016b), enabling binding of thioctic acid to streptavidin upon the addition of streptavidin to thioctic acid-capped AuNPs. Finally, streptavidin was bonded with biotin moiety on the biotinylated antibody through eight hydrogen bonds and also a van der Waals interaction among non-polar groups (Hyre et

al. 2006). R6G, on the other hand, is directly conjugated with AuNP through a strong electrostatic bond (Akanny et al. 2019).

To verify the successful fabrication of SERS-nanoprobes, UV-Vis spectroscopy was performed at three points of synthesis. Figure 5.1(a) illustrates a UV–Vis absorption spectrum of SERS-nanoprobes at three different fabrication steps. AuNPs showed the maximum absorption at 531 nm, which is typical for AuNPs with a diameter of about 40 nm (Thacker et al. 2014). A slight redshift was observed in the spectral absorption upon capping AuNPs with thioctic acid and R6G, indicating the variation of the refractive index of AuNPs as the different functionalization layers occur on their surfaces (Ferhan et al. 2018). The surface plasmon band was again redshifted from 536 to 547 nm upon conjugating the particles with antibodies, proving the successful conjugation of antibodies to the nanoparticles (Kamińska et al. 2017). None of these steps significantly affected the size or morphology of AuNPs as shown in TEM images of AuNPs, AuNP@R6G and AuNP@R6G@SA@Ab (Figure 5.1(b) to (d)).

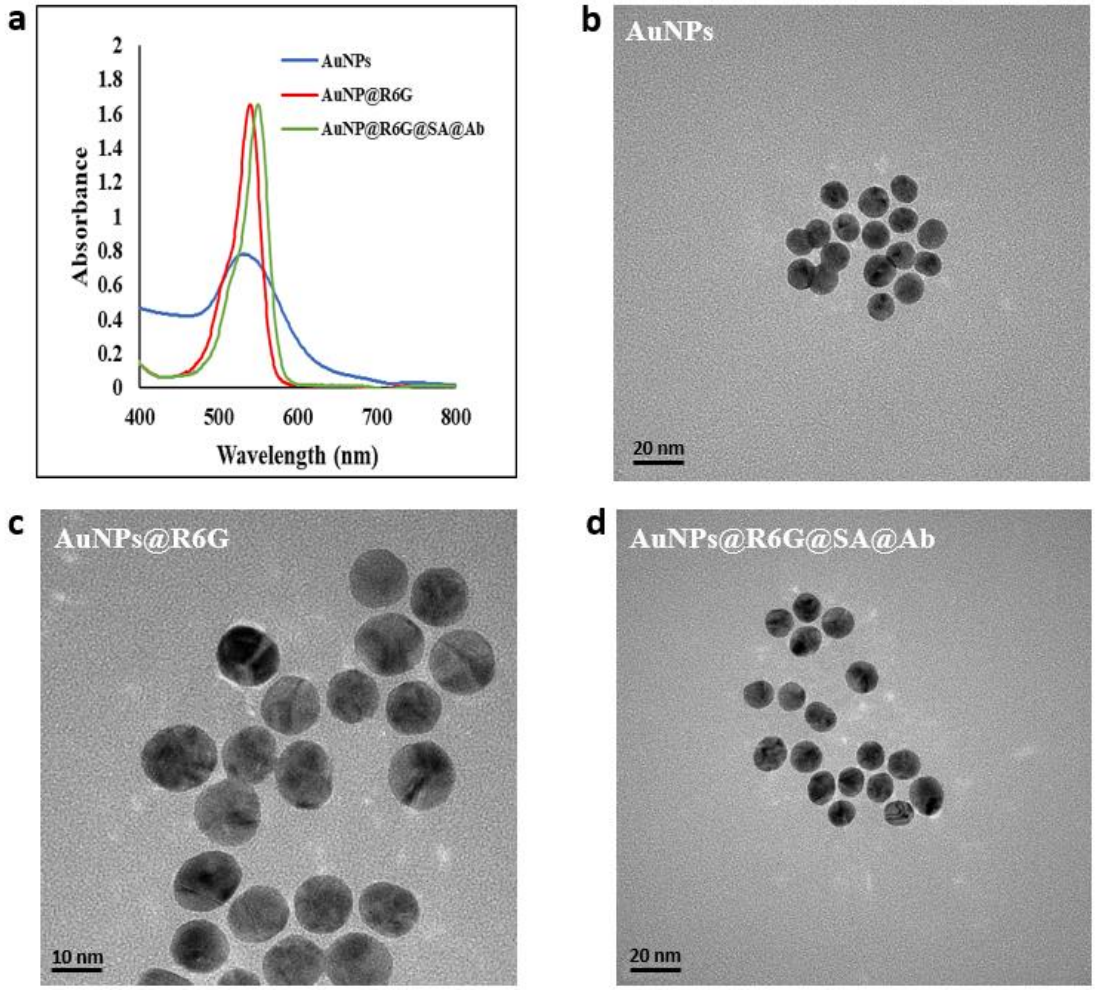

Figure 5.1 UV-Vis spectra (a) and TEM images (b-d) of SERS-nanoprobes at three different steps of preparation.

5.3.3 Anchoring and separation of *E. coli* O157:H7 cells

Bacterial cells collected in food samples were incubated with SERS-nanoprobes for different time periods. Based on our preliminary results, the best incubation condition was found to be 30 min at 37 °C with 100 rpm.min^{-1} shaking. TEM and SEM images were used to monitor the attachment of SERS-nanoprobes to *E. coli* O157:H7 cells (Figure 5.2(a) and (b)). These images clearly prove the successful self-assembly of SERS-nanoprobes on the bacterial cells. As it is observed, SERS-nanoprobes are attached to different regions around the *E. coli* O157:H7 cell. This is explained by the ability of polyclonal antibodies to attach various epitopes of the same antigenic site on the bacterial cell surface (Cho et al. 2015). Confocal fluorescent microscopy image

(Figure 5.2(c)) also confirmed that SERS-nanoprobes efficiently anchored onto the *E. coli* O157:H7 cell surface. Positioning SERS-nanoprobes on bacterial cells creates 'hotspots' between the probes on the bacterial cell surface and between the labeled bacteria, amplifying the Raman signals from separated target bacteria (Rodríguez-Lorenzo et al. 2019; Bai et al. 2020). This results in sharper

Raman signals with higher intensities, leading to a more efficient SERS detection performance.

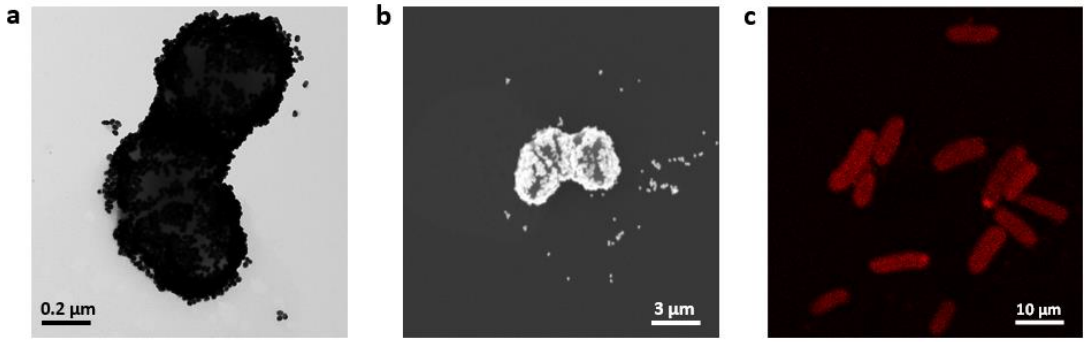

Figure 5.2 TEM (a), SEM (b) and confocal fluorescent microscopy (c) images of labeled *E. coli* O157:H7 cells by SERS nanoprobes.

5.3.4 Fabrication of hydrodynamic flow focusing SERS microchip

In this study, a hydrodynamic flow-focusing microfluidic channel with T-junction was designed for in-flow detection of incubated *E. coli* O157:H7 cells. The AutoCAD design and fabricated microchip are shown. The optimized channel was fabricated with a width and depth of 300 µm and a length of 3.5 cm. The microchip is devised and optimized in a hydrodynamic flow-focusing design, offering two advantages for more sensitive detection. The first benefit is that, in such a structure, the central fluid (separated and labeled bacterial cells) flows in a thin layer where a single cell, if present, is detectable (Pallaoro et al. 2015). Second, the chance that labeled cells are exposed to the Raman laser increases since bacterial cells are concentrated in the central stream where the Raman laser is focused at (Rodríguez-Lorenzo et al. 2019).

Our SERS microchip was successfully designed with the flow-focusing approach. The width of the central flow was measured to be about 15 μm.

5.3.5 Detection of *E. coli* O157:H7 cells by SERS-based microfluidic immunosensor

Typical Raman spectra of R6G and AuNP@R6G@SA@Ab SERS-nanoprobes are shown. As seen, the peaks in the SERS-nanoprobe signals represent main Raman peaks of R6G although a small shift is observed due to the presence of other components in the SERS-nanoprobes solution. The main peaks of R6G include 611 (C–C–C ring in-plane bending), 773 (C–H out-of-plane bending), 1197 (C–H out-of-plane bending), 1308 (aromatic C–C stretching), 1358 (aromatic C–C stretching), 1510 (aromatic C–C stretching), 1612 (aromatic C–C stretching) and 1650 cm^{-1} (aromatic C–C stretching) (Vosgröne and Meixner 2005). Among them, the peak at 1510 cm^{-1} is considered the characteristic peak of R6G which is equivalent to 1509 cm^{-1} in SERS-nanoprobes Raman peak. According to plating and immunoassay kits, the original romaine lettuce samples used in this study were not contaminated by *E. coli* O157:H7 prior to the experiments. Figure 5.3(a) to (e) display SERS signals collected from the detection of *E. coli* O157:H7 at different spiking levels, ranging from 0.1 to 10^2 $CFU.mL^{-1}$, and after various incubation times. The signals are in fact the fingerprint Raman signals of R6G, which have been enhanced by AuNPs present in the SERS-nanoprobes and indirectly represent *E. coli* O157:H7 in the sample. The images show that the obtained signals were clear and sharp. The changes of SERS signals were consistent with the changes of bacterial counts in lettuce samples, i.e., the SERS intensity concomitantly increased with the increase of in *E. coli* O157:H7 concentration. In this way, the intensity of the band 1509 cm^{-1} is the highest for samples spiked by 100 $CFU.mL^{-1}$, then it decreases as the spiking level decreases and reaches zero when bacterial concentration is very low. Likewise, increasing the

incubation time improved the sharpness of the peaks and intensity of the signals that were collected from the samples with the same spiking levels.

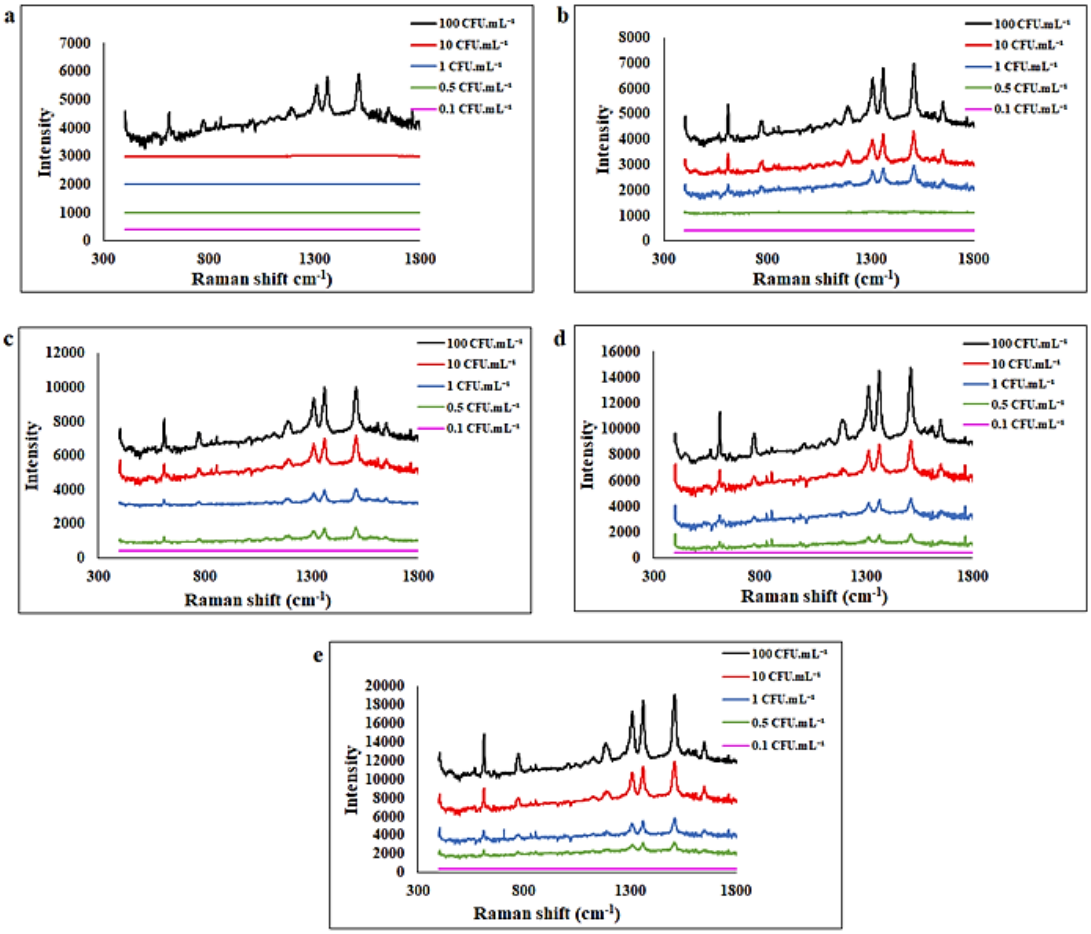

Figure 5.3 SERS signals obtained from lettuce samples spiked with *E. coli* O157:H7 at different spiking levels of 0.1, 0.5, 1, 10 and 10^2 CFU.mL^{-1} after 15 min (a), 30 min (b), 45 min (c), 60 min (d) and 120 min (e) of enrichment.

Table 5.2 summarizes the findings of this study and presents a better outlook of the capability of SERS-based microfluidic immunosensor to detect *E. coli* O157:H7 cells in lettuce. Accordingly, our protocol was able to detect *E. coli* O157:H7 cells at 100 CFU.mL^{-1} after 15 min enrichment. After only 30 min of enrichment, the protocol clearly detected the bacterial cells at the spiking level of 10 and 1 CFU.mL^{-1}. The results were the same after 45 min of enrichment although longer enrichment time resulted in stronger and clearer signals for all 10^2, 10, and 1 CFU.mL^{-1} counts. Further enrichment for 2 h provided even better results. The very low amount of 0.1 CFU.mL^{-1} of bacterial cells was not detectable by our protocol, which is considerably lower than the infectious

dose of less than 10^2 CFU.mL^{-1} for *E. coli* O157:H7 (Doyle 2013).

Table 5.2 Capability of SERS-based microfluidic immunosensor to detect *E. coli* O157:H7 cells in lettuce.

Spiked level	Enrichment time (min)				
(CFU.mL^{-1})	15	30	45	60	120
100	+	+	+	+	+
10	–	+	+	+	+
1	–	+	+	+	+
0.5	–	–	–	+	+
0.1	–	–	–	–	–

It is worth noting that, in this method, the total analysis time for detection of a single bacterium in a food sample is only 1 h considering the enrichment time that is significantly less than what is needed (days) in conventional methods. Interestingly, our protocol improved the results compared with the previously reported method (Bi et al. 2020) owing to the combination of enrichment, off-chip separation and in-flow detection in a highly efficient SERS microchip. Furthermore, the lowest concentration at which fingerprint-like SERS signals were obtained was 0.5 CFU.mL^{-1}. Therefore, our method achieved a very low LOD value of 0.5 CFU.mL^{-1} after only 60 min of enrichment which is an excellent proof of sensitivity and rapidity of our proposed method.

Intensity–concentration calibration curves for *E. coli* O157:H7 are plotted in Figure 5.4, showing obtained SERS intensity at 1509 cm^{-1} versus logarithmic (spiked) concentration of *E. coli* O157:H7 in lettuce after various enrichment times. Increasing the enrichment time after 15 min increased the linearity of the relationship between bacterial concentration and obtained signal (from R^2 of 0.72 to R^2 values of > 0.93), indicating more reliability of the results in enrichment times higher than 15 min.

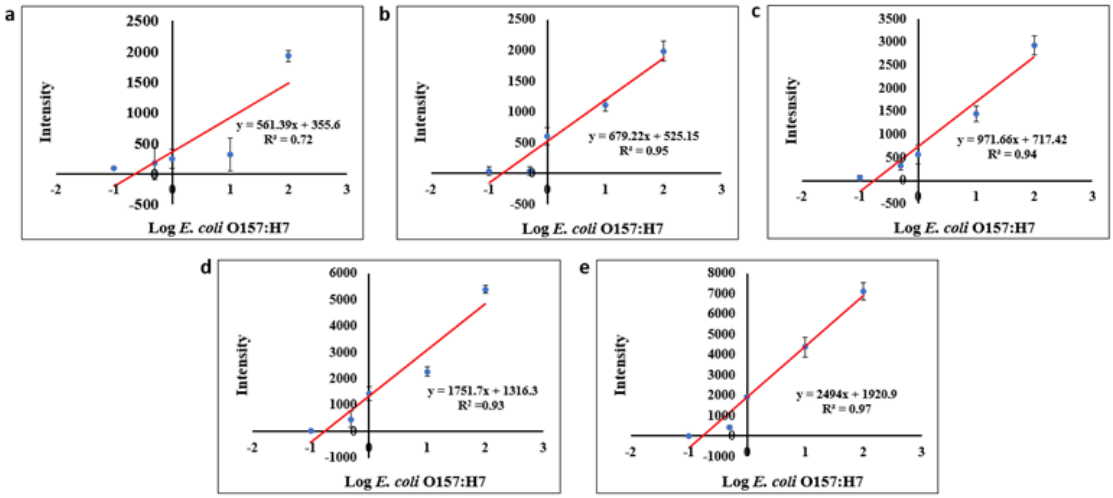

Figure 5.4 Calibration curves for *E. coli* O157:H7 at concentration levels of 0.1, 0.5, 1, 10 and 10^2 CFU.mL^{-1} in lettuce at SERS intensity of 1509 cm^{-1} after 15 min (a), 30 min (b), 45 min (c), 60 min (d) and 120 min (e) of enrichment. The signals were acquired by a Raman spectroscope with a 50× objective and an excitation laser of 785 nm at ~35 mW.

Raman spectra obtained from PDMS, non-labeled *E. coli* O157:H7 cells, and the mixture of *E. coli* O157:H7 cells and AuNPs were shown. The mixture of bacterial cells and AuNPs resulted in the enhanced signals of bacteria and did not include any other peaks. The peaks of PDMS and *E. coli* O157:H7 cells are not present in the signals obtained from labeled bacterial cells, which means that the signals received from the reporter are dominant and mask any other interfering noises or signals from PDMS, bacteria, and the food matrix.

The reproducibility of our technique was investigated by tracking the variations of SERS signals at the characteristic peak, 1509 cm^{-1}, obtained from samples inoculated with 100 CFU.mL^{-1} *E. coli* O157:H7 after 30 and 60 min of incubation at three repetitions. The obtained signals were almost consistent, proving the reproductivity of our technique for detection of *E. coli* O157:H7 in lettuce. Slight variations observed in the SERS intensities were expectable as the behavior of optical measurement systems. Depending on the sample, however, low-cost thermoplastic microchips offer the possibility for disposable sensors (Figure 5.5).

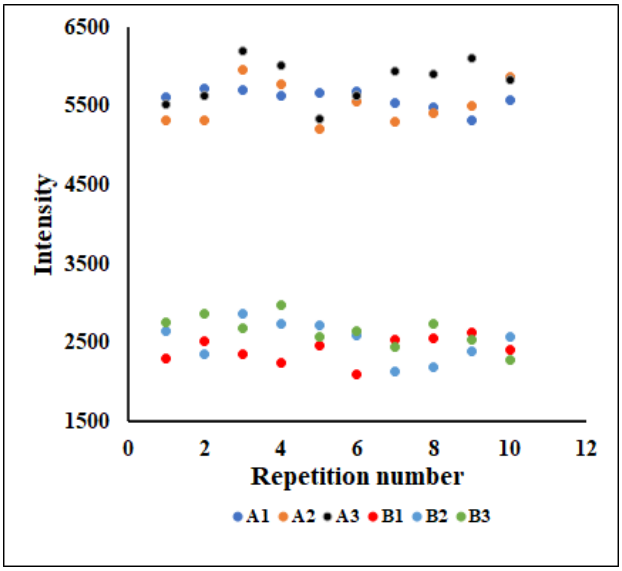

Figure 5.5 Variations of SERS intensity at 1510 cm^{-1} obtained from lettuce samples inoculated with *E. coli* O157:H7 (A1, A2, and A3= Repetitions 1, 2, and 3 of samples with 100 $CFU.mL^{-1}$ of bacteria after 60 min of incubation; B1, B2, and B3= Repetitions 1, 2, and 3 of samples with 100 $CFU.mL^{-1}$ of bacteria after 30 min of incubation).

The stability assessment of the SERS-nanoprobes showed that the SERS-nanotags were stable for 10 days (at 4 °C in the dark), showing their highest performance to attach to the target bacterial cells.

Table 5.3 summarizes the findings obtained from recent literature on the use of optical methods for the detection and determination of *E. coli*. Combined immunomagnetic separation and SERS detection methods are usually simpler; however, the uncontrolled analysis conditions may result in high background noises and less sensitivity. Fluorescent sensing is considered a very sensitive detection method, but the degradation of fluorescence may interfere with the accuracy of the results. Methods based on nano-dielectrophoretic microfluidic devices are usually complex and sometimes expensive to handle. The drawbacks associated with SERS-based sandwich immunoassay are the high possibility of cross-reactivity and inconsistent results of SERS measurements in an uncontrolled analysis condition. However, our method is not prone to degradation and is performed in a highly controlled hydrodynamic flow-focusing microfluidic device that was able to achieve a very low LOD value compared

to the other methods, proving the high sensitivity of our method against *E. coli* in lettuce and the potentiality of this protocol for detection of pathogens in complex food samples. Although the necessity of the enrichment time in our protocol may increase the total analysis time compared with some of the optical methods, it leads to very high sensitivity for detecting the target pathogen. Regarding the analysis costs, a very low number of antibodies is needed to conduct several analyses that neutralize the high costs of antibodies. Therefore, the cost per analysis is not considered high. This method consists of a series of simple chemical reactions, which can be done by a technician, and the detection step may be automatized for subsequent analyses, which makes this protocol easy to perform.

Table 5.3 An overview on recently reported nanomaterial-based optical methods for the determination of *E. coli*

Principal	Nanomaterial	LOD	Reference
Immunomagnetic separation + SERS	Magnetic nanoparticles + AuNPs	10 CFU.mL^{-1}	(IH et al. 2015)
Immunomagnetic separation + SERS	Magnetic gold nanorod	35 CFU.mL^{-1}	(Tamer et al. 2011)
Immunoseparation + Two-Photon Rayleigh Scattering	Gold nanorod	50 CFU.mL^{-1}	(Singh et al. 2009)
Fabry-Pérot interference	PSi-based Fabry-Pérot thin films	10^3 cells.mL^{-1}	(Massad-Ivanir et al. 2016)
Fluorescent sensing	Magnetic carbon dots	3.5×10^2 CFU.mL^{-1}	(Bhaisare et al. 2016)
Optofluidic + fluorescent sensing	Aptamer-conjugated fluorescent nanoparticles	10^2 CFU.S^{-1}	(Chung et al. 2015)
SERS-based sandwich immunoassay	AuNPs	10 CFU.mL^{-1}	(Bai et al. 2020)
SERS + nano-dielectrophoretic microfluidic device	Gold nanorods	10 CFU.mL^{-1}	(Wang et al. 2017)
Immunoseparation + SERS	Au@Ag core-shell nanorod	10^2 CFU.mL^{-1}	(Bi et al. 2020)
SERS-based microfluidic immunosensor	AuNPs	0.5 CFU.mL^{-1}	This study

5.3.6 Selectivity of SERS-based microfluidic immunosensor for *E. coli* O157:H7

Two sets of experiments were used to investigate the selectivity of our method for *E. coli* O157:H7. For the first control experiment, the control samples were inoculated with *Salmonella enteritis* (100 CFU.mL^{-1}), and the incubation, separation, and detection steps were followed as explained earlier under the same conditions by using the SERS-nanoprobes specific for *E. coli* O157:H7. No signals were observed after 30 and 60 min of incubation times, and there were only noises observed in the obtained spectra, proving that SERS-nanoprobes containing anti-*E. coli* antibodies did not interact with cells other than *E. coli* O157:H7, and therefore, our method is selective for a specific target. For the second control test, the selectivity of our method was evaluated in the presence of other common pathogens. Lettuce samples were spiked by 1 mL *E. coli* O157:H7 (100 CFU.mL^{-1}), 1 mL *S. Enteritis* (100 CFU.mL^{-1}), and 1 mL *S. Typhimurium* DT104 (100 CFU.mL^{-1}), and the separation and detection were conducted only by SERS-nanoprobes specific for *E. coli* O157:H7. The findings were consistent with the results obtained from lettuce samples inoculated by only *E. coli* O157:H7 after 30 and 60 min of incubation. No interfering noises were observed since the strong signals from labeled *E. coli* O157:H7 cells masked the weak noise signals from interfering bacterial cells or particulates. Thus, our method is selective for the separation and detection of the target pathogen even in the presence of the interfering species as the real world.

5.4 Summary

This study developed a novel protocol to selectively separate and sensitively detect *E. coli* O157:H7 in romaine lettuce. This technique combines three steps, an enrichment step, a selective separation with specific SERS-nanoprobes, and a sensitive

SERS microchip, resulting in a sensitive single-cell detection in food samples. Selective separation is accomplished by SERS-nanoprobes containing specific antibodies against the target pathogen. The hydrodynamic flow-focusing SERS microchip designed in this study not only facilitated a sensitive detection of the target bacteria, but also offered the controllability of the analysis conditions, automation, and better repeatability. Furthermore, a short enrichment time of 60 min resulted in the detection of 0.5 $CFU.mL^{-1}$ of bacterial concentration in romaine lettuce, which is much lower than *E. coli* O157:H7 infectious dose. Therefore, our findings prove the reliability and feasibility of the proposed SERS-based microfluidic immunosensor for the sensitive separation and detection of food-borne pathogens in food samples. The generic approach of this study may apply to other food-borne pathogens and other food types. This work can be improved further by using monoclonal antibodies to promote the selectivity of the SERS-nanoprobes. Multiplex detection of pathogens from a single food sample is also possible using multiple SERS-nanoprobes, each targeting a specific pathogen.

CHAPTER 6

MULTIPLEX DETECTION OF FOOD-BORNE PATHOGENS USING A SERS OPTOFLUIDIC SENSOR COUPLED WITH IMMUNOASSAY

6.1 Introduction

Microbial food safety is of utmost importance for consumers and the food industry because of its great impact on public health and economic growth (Akhtar et al. 2014). Under certain circumstances, pathogenic bacteria are able to enter, survive, grow, and multiply in foods and pose threats to public health by causing food poisoning, increasing foodborne disease outbreaks, and negatively affecting food security (Elkhishin et al. 2017). One of the challenges facing food safety is that, commonly, multiple bacterial pathogens coexist in the same food sample at different concentrations, some of which are life-threatening even at very low counts (Brecher and Hay 2005). Conventional methods for detecting a bacterial pathogen in foods involve culturing and biochemical tests (Cadnum et al. 2014). Although the methods are simple and accurate, there are some drawbacks ascribed to these techniques. The first limitation is that these detection methods are selective for only one specific pathogen (Liu et al. 2015), and therefore, for multiplex detection, multiple tests must be performed parallel on the same food sample. In addition, these methods are laborious and may take days to confirm the presence of the pathogens of interest (Sharma and Mutharasan 2013). Therefore, developing a rapid, sensitive, and accurate method to detect multiple pathogens simultaneously is necessary.

Lab-on-a-chip diagnostic sensors are emerging analytical tools developed as a promising approach for low-cost, portable, highly sensitive, and efficient sensing platforms to detect chemical, biochemical, and biological targets. Among these devices,

surface-enhanced Raman spectroscopy (SERS)-based optofluidic systems have gained great attention owing to their advantages for more efficient sensing and detecting assays (Gorjikhah et al. 2016). The benefits of such devices include high sensitivity and rapidity guaranteed by SERS, and reproducibility, controllability, and real-time monitoring provided by microfluidics (Pu et al. 2017a).

However, it has been argued that detecting multiple pathogens by SERS optofluidic devices is not a reliable approach since the SERS signals from different pathogens are almost similar. In other words, they are not easily distinguishable (Mungroo et al. 2015). Theoretically, by integrating immunoassays with SERS optofluidics, multiplex detection of target pathogens is achievable in a more controlled environment and the results are more selective and accurate (Bridle et al. 2014). The principle of such assays is that the target pathogens are anchored and separated from the original sample by selective labels, commonly known as SERS-nanotags. Then, the separated targets are detected by Raman on-line while the sample is flowing through the microfluidic chip. SERS-nanotags mainly consist of SERS-active substrates, specific antibodies against the target antigens, and Raman reporter molecules. Accordingly, target pathogens are probed and anchored by the specific antibodies on SERS-nanotags. Raman reporter molecules act as indicators of the presence of the targets and their Raman signals are enhanced by the active Raman substrates for a more efficient SERS measurement. This method has been investigated for the detection of *Salmonella enterica* (Lin et al. 2014), *Neisseria lactamica* (Lin et al. 2014), *Escherichia coli* O157:H7 (Wang et al. 2017), and *Listeria monocytogenes* (Rodríguez-Lorenzo et al. 2019). Although the methods proved the capability of SERS optofluidic sensor coupled with immunoassay to detect pathogens, there are some insufficiencies in the methods used in the previous studies. Primarily, the previous literature lacks the real

food studies and the limit of detection (LOD) values that these methods achieved were above the defined infection dose of these foodborne pathogens in foods, which is considered the main drawback of their techniques.

In this study, we developed a SERS optofluidic sensor coupled with an immunoassay to simultaneously detect multiple dangerous foodborne pathogens, *E. coli* O157:H7, *Salmonella Enteritidis,* and *Salmonella Typhimurium* DT104 in a flow-focusing hydrodynamic microfluidic chip. These strains were chosen because they are among the most dangerous pathogens associated with foodborne illnesses resulting in hospitalization in the U.S (CDC 2020). The detection was performed in the two commonly implicated vehicles for these pathogens: lettuce and a packed salad. In this protocol, a complex of multiple specific SERS-nanotags was used to simultaneously probe and detect multiple targets in the same sample. Hypothetically, adding an enrichment step prior to the detection and using flow-focusing hydrodynamic microfluidic chip results in a very low LOD value for both bacteria. To the best of our knowledge, there are no reports on the detection of multiple foodborne pathogens using SERS optofluidic sensor coupled with immunoassay using a flow-focusing hydrodynamic microfluidic chip.

6.2 2. Materials and methods

6.2.1 Media and chemicals

Bacterial culture and growth media (tryptic soy broth (TSB), tryptic soy agar (TSA), sorbitol MacConkey agar (SMAC) and Hektoen Enteric agar (HEA)) were purchased from Difco Laboratories (BD Diagnostics Systems, Sparks, MD, USA). Biotin anti-*E. coli* antibody (isotype: IgG) and biotin anti-*Salmonella* antibody (isotype: IgG) were bought from (Abcam, Cambridge, MA, USA). Silicon wafers were procured from University Wafer (South Boston, MA, USA) and SU-8 2075 negative

photoresist was obtained from Kayaku Advanced Material Inc (Westborough, MA, USA). Sylgard™ 184 silicone elastomer kit was purchased from Dow Corning (Midland, MI, USA). Hydrogen tetrachloroaurate solution ($HAuCl_4$, 30 wt% in dilute HCl), rhodamine 6G (R6G), fluorescein (FL), lipoic acid, N-hydroxysuccinimide (NHS), and streptavidin were acquired from Sigma-Aldrich (St. Louis, MO, USA). Trisodium citrate dihydrate (Certified A.C.S), ethanol (Certified A.C.S), 1-ethyl-3-(3-dimethylaminopropyl) carbodiimide hydrochloride (EDC), and phosphate buffered saline (PBS, 10× Solution) were obtained from Fisher Scientific (Fair Lawn, NJ, USA). Lettuce and packed salad (containing carrots, broccoli, green onions, lettuce, red and savoy cabbage) were purchased from a local grocery store.

6.2.2 Gold nanoparticles (GNPs) fabrication

The fabrication of GNPs with an average size of 40 nm in diameter was conducted based on the citrate method (Xiong et al. 2018). In this method, GNPs were synthesized via the reduction of $HAuCl_4$ by trisodium citrate in an aqueous medium at boiling temperature.

6.2.3 SERS-nanotags preparation

The synthesis of SERS-nanotags was based on a modified version of the previously reported method (Bi et al. 2020). Figure 6.1 demonstrates the schematic fabrication process of SERS-nanotags used in this study. To fabricate, first, lipoic acid solution (50 mg lipoic acid powder dissolved in 2 ml ethanol) was added to 20 ml of GNP colloid solution and was left to blend for 5 h at ambient temperature. To make GNPs capped with the fluorescent dye, either 1.5 ml of R6G (3 mg/ 15 ml) or FL (5 mg/ 10 ml) was added to the lipoic acid-conjugated GNPs and the mixture was allowed stirring overnight. Next, a mixture of NHS (0.03 M) and EDC (6 mM) was mixed with GNP@dye (GNP@R6G or GNP@FL) solution for 2 h. Then, the so-functionalized

GNPs were collected by centrifugation at 7513 ×g for 20 min and suspended in sterile PBS solution. Subsequently, 1 ml of GNP@dye was mixed and incubated with 20 µl of streptavidin solution (1 mg/ml) for 1 h. Immediately after 1 h, the mixture was incubated with 20 µl of biotinylated antibody solution to form GNP@R6G@SA@Ab or GNP@FL@SA@Ab SERS-nanotags. The SERS-nanotags were finally collected by a series of centrifugation and rinsing steps and the resulting SERS-nanotags were resuspended in PBS solution for further experiments.

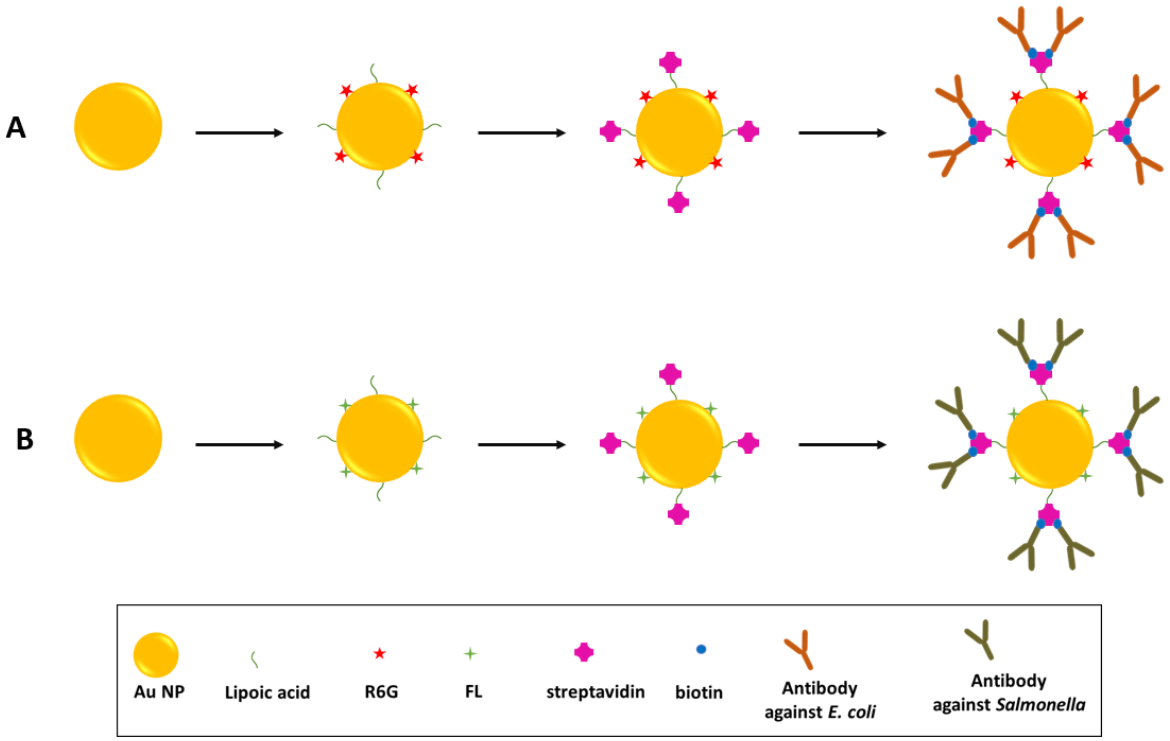

Figure 6.1 Fabrication process of GNP@R6G@SA@Ab and GNP@FL@SA@Ab SERS-nanotags.

6.2.4 Bacterial cocktail preparation

Bacterial samples were obtained from the frozen culture stocks of the Food Microbiology Laboratory culture collection, University of Missouri (Columbia, MO, USA). Two strains of Shiga toxin-producing *E. coli* (STEC) O157:H7 and two *Salmonella enterica* serotypes were used in our study (Table 1). The bacterial strains were grown overnight in TSB at 37 °C. The bacterial pellets were then harvested (11200 × g for 10 min) and re-suspended in sterile peptone water. The concentration of bacteria

was determined by serially diluting and pour plate counting on TSA after incubation at 37 °C for 24 h. A bacterial cocktail was prepared by mixing the appropriate volumes of each strain to get a cocktail with a ratio of 1:1:1:1 for each strain. For the experiments, the cocktail was serially diluted to make spiking inoculums of 10, 100, and 1000 CFU/ml.

Table 6.1 Bacterial strains used in this study.

O-serogroup	Strain	Source
E. coli O157:H7	505B	Beef
E. coli O157:H7	EDL-933	Human
S. Enteritidis	I4-2	Turkey feather
S. Typhimurium	700408	ATCC

6.2.5 Preparation of artificially spiked food samples

Prior to spiking, the lettuce and packed salad samples were evaluated for the presence of *E. coli* O157:H7 and *Salmonella* using culture-based protocols as mentioned by FDA's Bacteriological Analytical Manual (BAM) (FDA 2021a, b). Briefly, for detecting STEC O157:H7, 10 g lettuce sample was weighed in a filter stomacher® bag and enriched in 90 ml of modified buffered peptone water (mBPW) supplemented with 8 mg/l. The mixture was hand massaged for 2 min and then incubated at 42 °C for 24 h. The presence of *E. coli* O157:H7 in the lettuce sample was determined by spread-plating 100 µl of serially-diluted enriched sample on SMAC followed by incubation at 42 °C for 24 h. After incubation, the SMAC plates were evaluated for the presence of colorless colonies. Then, the suspected colorless colonies on SMAC agar plates were picked and confirmed using Oxoid DrySpot™ *E. coli* O157 Latex Agglutination test (Oxoid Diagnostic Reagents, Hampshire, England) according

to the manufacturer's instructions.

For detection of *Salmonella* in lettuce and packed salad samples, 10 g of food sample was enriched with 90 ml BPW and incubated at 37 ℃ for 24 h. The presence of *Salmonella* in the food sample by the purity of each strain was checked by streaking the enriched food sample on *Salmonella* selective HEA plates. Suspected *Salmonella* colonies from agar plates were picked and confirmed using a Remel Micro ID TM Identification system (Thermo Fisher, Scientific, Lenexa, KS, USA).

For artificial spiking, 200 g of lettuce and packed salad samples were weighed and placed in sterile filtered stomacher® bags. Then, the food samples were inoculated with 1 ml of 10, 100, and 1000 CFU/ ml of *E. coli* O157:H7 and *Salmonella* cocktail separately. After inoculation, the samples were left for 15 min to allow bacterial cells to attach to the surfaces of vegetable leaves and pieces. Then, 450 ml of sterile, prewarmed mBPW was added to spiked food samples and the samples were homogenized by hand massaging. Moreover, a negative control consisting of 450 ml sterilized enrichment media (mBPW) with 200 g food samples was used in our study. The inoculated and negative control lettuce samples were incubated at 42 °C for enrichment, and sampling for SERS detection was performed after 15, 30, and 45 min after enrichment. For sampling, 2 ml of the enriched broth was collected into the centrifuge tube and stored properly until further steps.

6.2.6 Separation and labelling bacterial cells

To separate and label pathogenic bacterial cells from food samples, first, 1 ml of fixative solution (2.5% glutaraldehyde) was injected into 1 ml of extracted samples from spiked lettuce and packed salad. The samples were left for 30 min to ensure the fixation of the cells. Fixed cells were then collected by centrifugation (9300 ×g for 15 min) and rinsed twice. Afterward, the pellets were resuspended in PBS and were mixed

with 1 ml of SERS-nanotags followed by incubation in a shaker incubator with a speed of 100 rpm/min at 37 °C for 30 min. The separation and labeling steps were finalized by twice centrifugation (9300 ×g for 15 min) and washing to withdraw free reagents. Labeled pellets were finally suspended in 1 ml of sterile PBS and kept at 4 °C for analysis.

6.2.7 Optofluidic device fabrication

The flow-focusing microfluidic device was made of polydimethylsiloxane (PDMS) and the dimensions of the channel were set to be 300 μm in depth, 300 μm in width, and 35 mm in the total device length. First, the master mold bearing the microfluidic device layout was fabricated by a two-step deposition of a 300 μm layer of SU-8 2075 on a cleaned silicon wafer and patterned by UV photolithography (at 300 mJ/cm^2 for 30 s) and developed in SU-8 developer for 20 min. Then, a degassed PDMS mixture (10:1 PDMS prepolymer: curing agent) was cast onto the master mold and cured for 1 h at 70 °C. The PDMS replica was finally peeled off from the mold and bonded onto a cleaned glass slide after oxygen plasma treatment for 30 s.

6.2.8 SERS measurement

For detection, PBS solutions, as neutral streams, were injected into the microfluidic channel at a flow rate of 10 μl/min from inlets 1 and 2 to make the lateral flows. Meanwhile, the sample, labeled bacterial cells resuspended in PBS, was induced into the channel with a flow rate of 5 μl/min. The central stream was exposed by Raman laser to collect SERS spectra of the labeled target pathogens. Spectral Raman data were collected while the sample was flowing through the optofluidic device. SERS measurement was performed by a Raman Spectrometer (Renishaw RM1000 System, Gloucestershire, UK) equipped with an excitation wavelength of 785 nm. The spectral data were collected by a microscope (Leica DMLB, Wetzlar, Germany) and a 388 ×

578 pixel CCD array detector at 35 mW over the range of 400-1800 cm^{-1} with 10 s integration time. A NE-300 syringe pump (Southpointe Surgical Supply, Coral Springs, FL, USA) was used to flush the reagents into the optofluidic device.

6.2.9 Characterization of SERS-nanotags

A successful synthesis of SERS-nanotags was monitored by measuring and comparing the UV-VIS absorbance of GNPs, GNP@R6G@SA@Ab, and GNP@FL@SA@Ab. The UV-VIS spectra of the samples were measured by a Varian UV–Vis spectrophotometer (Cary Bio 50, Agilent, CA, USA).

2.10 Labeling performance of SERS-nanotags

To monitor the labeling performance of SERS-nanotags, *E. coli* O157:H7 and *Salmonella* cells were separately treated with their specific SERS-nanotags and the successful attachment of SERS-nanotags to the bacterial cells was observed via SEM images. For SEM analysis, the samples were first fixed in a fixative (2% paraformaldehyde and 2% glutaraldehyde in 100 mM sodium cacodylate buffer; pH = 7.35). Next, the pellets were collected from each sample by centrifugation at 2500 ×g and the harvested pellets were suspended in HistoGel (Thermo Scientific, Kalamazoo, MI, USA). Fixed pellets were then rinsed with 100 mM sodium cacodylate buffer, pH = 7.35 (Sigma Aldrich, St. Louis, MO, USA) and 130 mM sucrose. Secondary fixation was conducted by using 1% osmium tetroxide (Ted Pella, Inc. Redding, CA, USA) in 2-ME buffer using a Pelco Biowave (Ted Pella) operated at 100 Watts for 1 min. After incubation at 4 °C for 1 h, specimens were rinsed with cacodylate buffer and further with distilled water. Afterward, En bloc staining was performed using 1% aqueous uranyl acetate and incubated at 4 °C overnight, then rinsed with distilled water. Using the Pelco Biowave, a graded dehydration series (per exchange, 100 Watts for 40 s) was performed using ethanol, transitioned into acetone, and dehydrated specimens were

then infiltrated with Epon resin (250 Watt for 3 min) and polymerized at 60 °C overnight. Sections were then cut to a thickness of 75 nm using an ultramicrotome (Ultracut UCT, Leica Microsystems, Germany) and a diamond knife (Diatome, Hatfield PA). A FEI Quanta 600 F SEM (FEI, Hillsboro, OR, USA), operated at 10 kV was used to acquire SEM images.

The bacterial suspension (6 µl) was placed on the glass slide and covered with a glass coverslip. Confocal microscopy was performed by a Leica SP8 laser scanning confocal microscope equipped with a tunable supercontinuum white light laser and a 63x/NA1.20 water immersion objective. RG6 was excited with the 525 nm wavelength while FL fluorescence was excited with the 495 nm wavelength and its emission was recorded using a 505-550 nm bandpath.

6.2.10 Data analysis

All experiments were conducted in triplicate and for each SERS measurement, ten spectral data were collected by WiRE 3.4 software (Gloucestershire, UK). The SERS spectra were plotted by Excel software 2016.

6.3 Results and discussion

6.3.1 Principle of separation and detection of multiple food-borne pathogens

In this study, a multiplex off-chip separation was combined with on-line simultaneous detection of *E. coli* O157:H7 and pathogenic *Salmonella* species in a SERS optofluidic device. In this method, bacterial cells were first enriched by incubating the food sample at 42 °C for different time intervals. The purpose of the enrichment step was to ensure the detection of very low counts of bacteria, even at a single-cell level, in the food sample. After enrichment, the target bacterial pathogens were anchored and separated from the food sample via their specific SERS-nanotags, and all unreacted reagents and molecules were removed by multiple centrifugations and

washing steps. The separated, tagged bacterial cells then flowed through the SERS optofluidic device, where Raman reporters (with different SERS signals) were detected under Raman laser exposure and the presence of target bacterial pathogens indicated the contamination of the food sample with the target pathogens. A hydrodynamic flow-focusing SERS optofluidic sensor enables one to detect bacterial cells even at very low concentration levels in the sample flow, facilitating highly sensitive and efficient detection of multiple bacterial pathogens in food samples.

6.3.2 Preparation of the specific SERS-nanotags

Each SERS-nanotag is composed of (1) a specific antibody against the target pathogen that helps the SERS-nanotag to anchor onto the bacterial cell, (2) either R6G or FL molecules as Raman reporters, which represent the presence of target pathogens in the sample, and (3) GNP which enhances the signals from the Raman reporter molecules.

To fabricate SERS-nanotags, a chain of reactions must be carried out to bond GNP to the antibody. First, GNP interacts with lipoic acid to replace citrate molecules on GNP with lipoic acid through a ligand exchange, i.e., GNP is bonded with lipoic acid via a disulfide bond (Ghann et al. 2019). Afterward, the EDC and NHS mixture is used to activate the carboxyl groups of the free end of a lipoic acid molecule (Wang et al., 2016). In the next step, the activated carboxyl groups are the spots where a lipoic acid molecule is bonded with a streptavidin molecule. Eventually, streptavidin is bonded with the biotin moiety on biotinylated antibody mediated by multiple hydrogen bonds and a conformational change in streptavidin subunit (Sedlak et al. 2020). Raman reporter molecules are directly attached to the nanoparticle via electrostatic interactions (Akanny et al. 2020).

Successful fabrication of SERS-nanotags was evaluated by UV-VIS

spectroscopy (Figure 6.2). Accordingly, the absorption spectrum of GNPs exhibited a broad peak with a maximum value at ~531 nm, which is in agreement with what would be anticipated for GNPs with a diameter of 40 nm (Xiong et al. 2017a). However, the spectral absorption of GNPs redshifted from 531 to 547 nm for GNP@R6G@SA@Ab, and to 541 nm for GNP@FL@SA@Ab. The redshifts observed in the absorption spectrum of GNPs indicate the variation of the refractive index of nanoparticles upon functionalization (Ferhan et al. 2018). Moreover, conjugation of antibodies onto the GNPs also resulted in a slight redshift of the plasmon absorption peak of the nanoparticles (Cheng et al. 2017; Kamińska et al. 2017). Based on these results, it is proven that the SERS-nanotags were successfully prepared in this work.

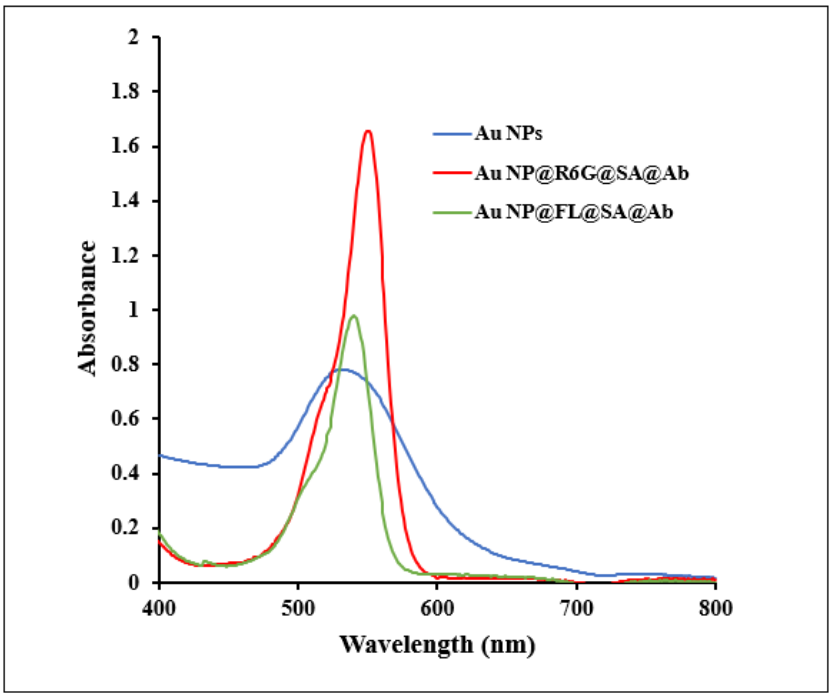

Figure 6.2 UV-VIS spectra of GNPs, GNP@R6G@SA@Ab and GNP@FL@SA@Ab SERS-nanotags.

6.3.3 Separation of pathogenic bacteria from food samples

SEM imaging and confocal microscopy were used to evaluate the efficiency of SERS-nanotags to anchor onto the bacterial cells separately or in the bacterial mixture,

respectively. As shown in Figure 6.3. *E. coli* O157:H7 and *Salmonella* cells have been successfully anchored by several specific SERS-nanotags via antigen-antibody interaction. It can be observed that SERS-nanotags were attached to different regions of bacterial cells because the polyclonal antibodies enabled SERS-nanotags to occupy different regions on the antigenic sites of the cell surface (Cho et al. 2015).

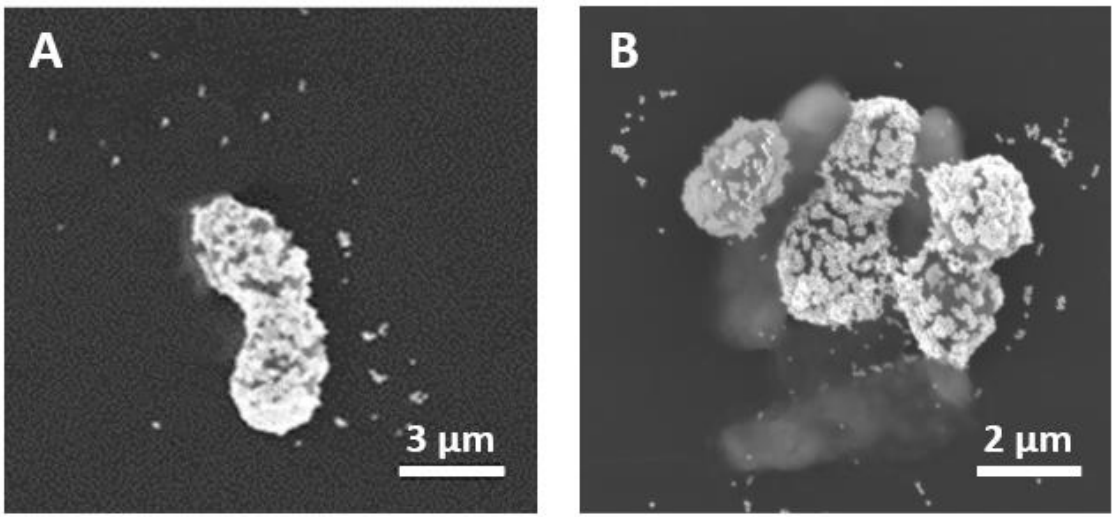

Figure 6.3 SEM images of *E. coli* O157:H7 (A) and Salmonella cells (B) anchored by SERS-nanotags.

Interestingly, in images obtained by confocal microscopy (Figure 6.4), SERS-nanotags were selectively attached to their specific targets, i.e., *E. coli* O157:H7 cells were anchored by GNP@R6G@SA@Ab SERS-nanotags that are exhibited as red rods, and *Salmonella* cells were anchored by GNP@FL@SA@Ab SERS-nanotags that are illustrated as green rods. These images confirm that selective separation of different pathogenic bacterial cells from food samples was successfully performed by the SERS-nanotags that have been synthesized in this study.

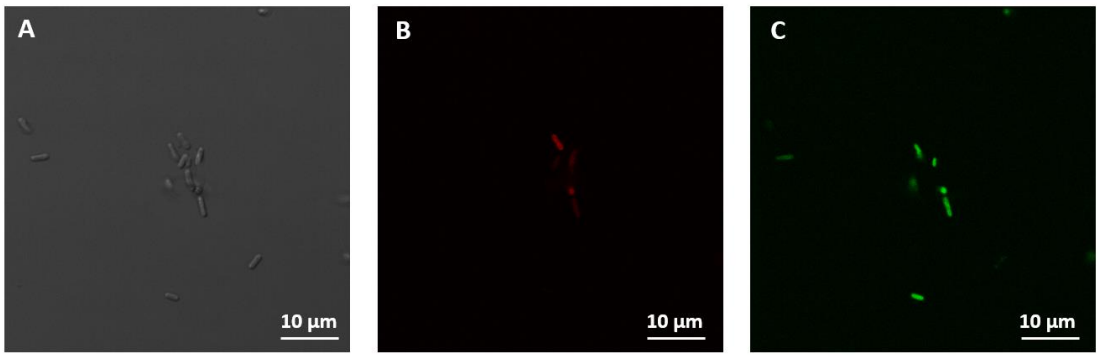

Figure 6.4 Confocal microscopy images of bacterial cocktail anchored by specific SERS-nanotags. Red rods represent *E. coli* O157:H7 cells captured by GNP@R6G@SA@Ab nanotags and green rods represent *Salmonella* cells captured by GNP@FL@SA@Ab nanotags.

6.3.4 Hydrodynamic flow-focusing SERS optofluidic sensor

In this study, a hydrodynamic flow-focusing SERS optofluidic device was devised and optimized to detect *E. coli* O157:H7 and *Salmonella* cells simultaneously in lettuce and packed salad. In this design, the sample flows through the central stream between two neutral lateral flows and was then exposed by Raman laser at a certain point after the T-junction zone, where target analytes were detected and identified. This pattern allowed the sample to flow through a narrow path, so that the target molecules were concentrated in the central thin stream, where they were more prone to the Raman laser exposure, resulting in enhanced SERS detectability of even sparse target molecules or trace amounts of target analytes. Figure 6.5 shows a schematic setup of the SERS optofluidic device used in this study. The device was optimized to have a channel width and depth of 300 μm, and the central flow width was adjusted to be 15 μm.

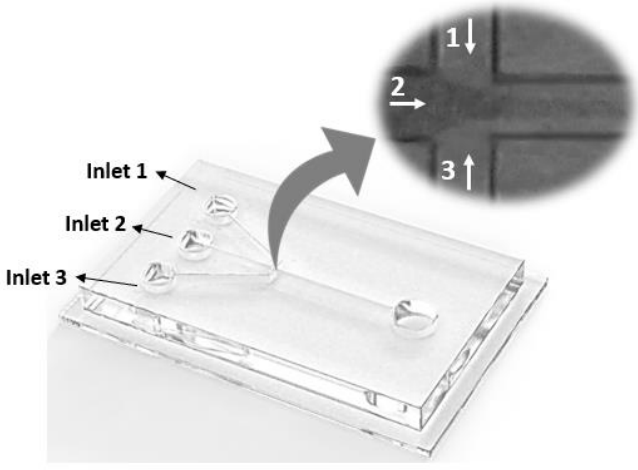

Figure 6.5 SERS optofluidic sensor. (inset) T-junction zone of the SERS optofluidic SERS device.

6.3.5 Detection of pathogenic bacteria in food samples

Figure 6.6 demonstrates characteristic Raman spectra of R6G,

GNP@R6G@SA@Ab, FL, and GNP@FL@SA@Ab. Clearly, the main peaks of each SERS-nanotag represent the fingerprint-like Raman spectra of its Raman reporter molecule, although slight shifts are observed at certain bands. The main Raman peaks of R6G and FL are listed in Table 6.2. Among them, the peaks at 1358 and 1510 cm^{-1} (1509 and 1361 cm^{-1} in GNP@R6G@SA@Ab) and 1183 and 1367 cm^{-1} (1368 and 1184 cm^{-1} in GNP@FL@SA@Ab) are considered as the most characteristic Raman bands of R6G and FL, respectively. Presumably, a successful separation and detection should display at least these four peaks from Raman signals obtained from bacterial mixtures of *E. coli* O157:H7 and pathogenic *Salmonella* in food samples.

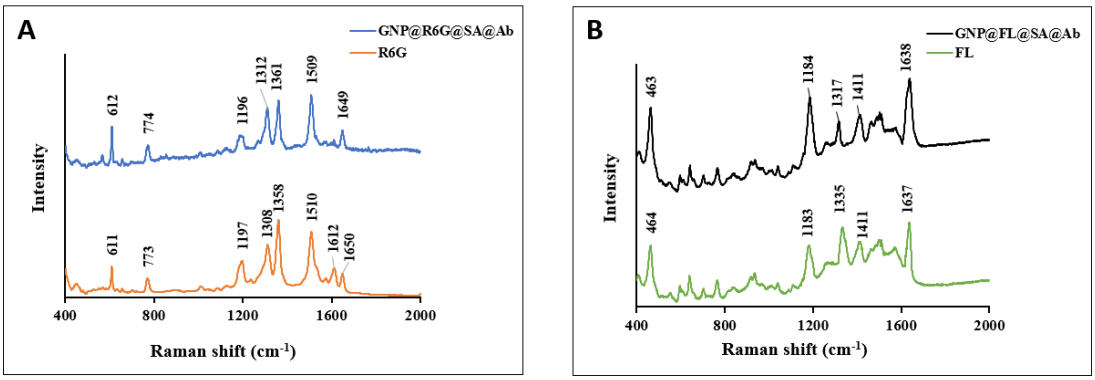

Figure 6.6 Raman spectra of R6G and GNP@R6G@SA@Ab SERS-nanotags (A) and FL and GNP@FL@SA@Ab SERS-nanotags (B).

Table 6.2 Characteristic Raman bands of R6G and FL.

	Raman shift (cm^{-1})	Band assignment
R6G	611	C–C–C ring in-plane bending
	773	C–H out-of-plane bending
	1179	C–H out-of-plane bending
	1308	Aromatic C–C stretching
	1358	Aromatic C–C stretching
	1510	Aromatic C–C stretching
	1612	Aromatic C–C stretching
	1650	Aromatic C–C stretching
	464	—

FL	1183	CCH and C–OH bends
	1335	Xanthene ring C–C stretch
	1411	CCH bend and C–C stretch
	1637	Xanthene ring C–C stretch

Figure 6.7 show the Raman spectra obtained from samples of lettuce and packed salad spiked by the pathogenic bacterial cocktail. Generally, the signals obtained from the samples contain various peaks. However, the four most prominent peaks that were our targets were clearly detectable in all signals. Some smaller peaks of the SERS-nanotags are not visible or might be merged by noises in the signals obtained from the samples. The signals collected from both food samples are clear and sharp. The intensity of the signals was directly dependent on the bacterial counts in lettuce and packed salad samples, i.e., the intensity of signals increased as the bacterial concentration increased from 10 to 1000 CFU/ml. Likewise, increasing the incubation time enhanced the intensity and sharpness of the Raman spectra obtained from samples with the same spiking levels.

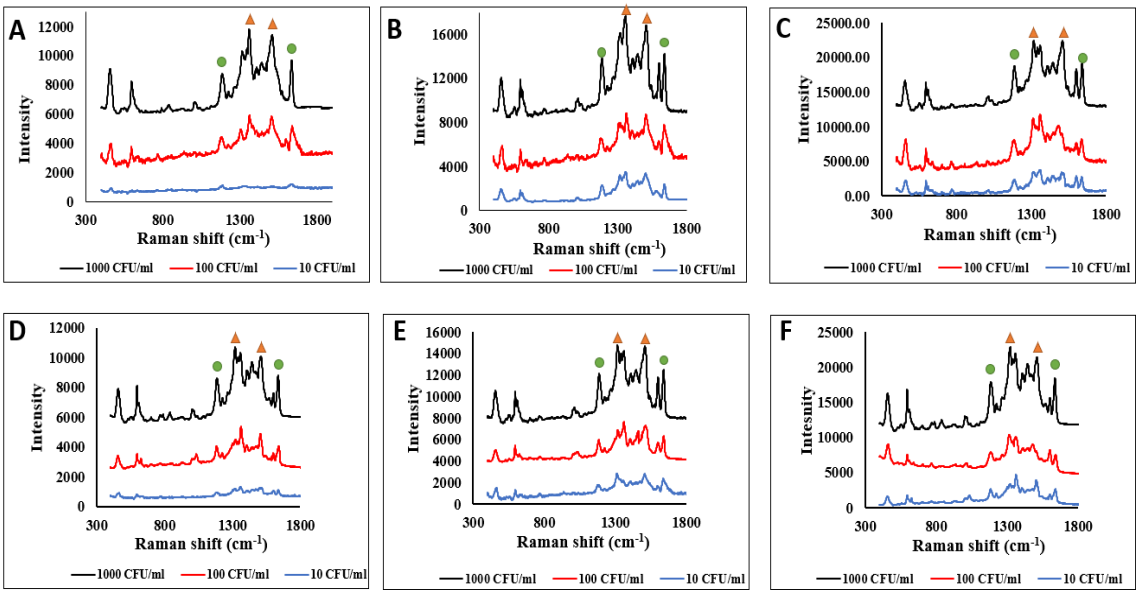

Figure 6.7 SERS spectra obtained from lettuce (A-C) and packed salad (D-F) samples spiked by the pathogenic bacterial cocktail.

To ensure that the peaks from the bacteria itself or the PDMS microfluidic

device do not interfere with our results, pure bacterial cultures and PDMS were examined by Raman (Figure 6.8). Clearly, the pattern or specific Raman peaks of bacteria and PDMS are not present in the Raman signals obtained from the samples, indicating that our results were not affected by the signals from bacterial cells themselves or PDMS. Therefore, the results obtained by our proposed protocol are accurate and reliable.

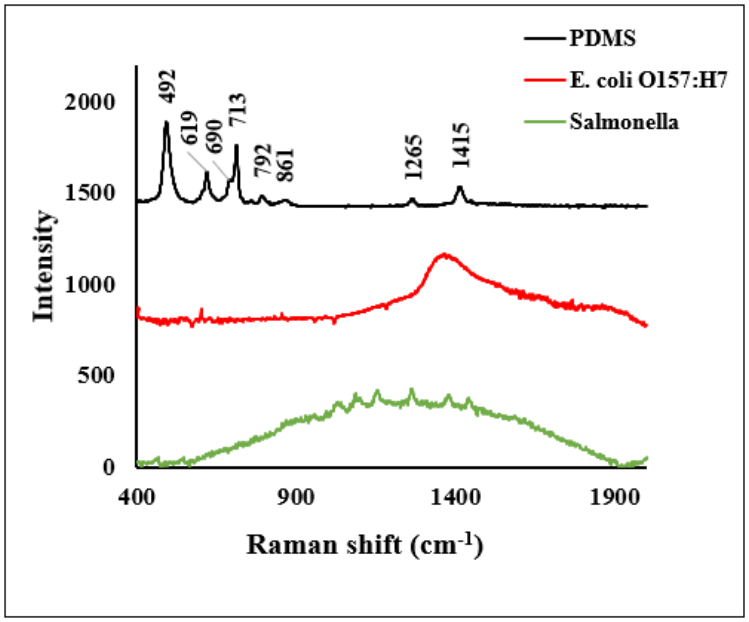

Figure 6.8 Raman spectra of PDMS, *E. coli* O157:H7, and Salmonella cells.

Table 6.3 Detectability performance of SERS optofluidic coupled with immunoassay for simultaneous detection of *E. coli* O157:H7 and pathogenic Salmonella in lettuce and packed salad. outlines the results obtained from the simultaneous detection of *E. coli* O157:H7 and pathogenic *Salmonella* in lettuce and packed salad after different incubation times. According to the findings, our method was able to detect all 1000, 100, and 10 CFU/ml of bacterial cocktails after 15 min of enrichment in both food samples. Although for the lettuce spiked by 10 CFU/ml of the bacterial cocktail, the peaks from *E. coli* O157:H7 are generally weaker than peaks from *Salmonella*, they are clearly recognizable. Therefore, our separation and detection

method achieved a very low LOD value of 10 CFU/ml for *E. coli* O157:H7 and pathogenic *Salmonella* cocktail in lettuce and packed salad after only 15 min of enrichment. This LOD value is notably lower than the infectious dose of *E. coli* O157:H7 (less than 10^2 CFU/ml) (Doyle 2013) and salmonellosis (~10^7 cells/g) (Jay et al. 2005), proving the high sensitivity of our method to detect multiple pathogens in food samples. Moreover, our results are also better improved compared with the findings from similar previously reported approaches (Rodríguez-Lorenzo et al. 2019; Bi et al. 2020) due to the combination of an enrichment step, off-chip separation and labeling and on-line detection within a hydrodynamic flow-focusing SERS optofluidic device.

Table 6.3 Detectability performance of SERS optofluidic coupled with immunoassay for simultaneous detection of *E. coli* O157:H7 and pathogenic *Salmonella* in lettuce and packed salad.

	Spiked level	Enrichment time (min)		
	(CFU/ml)	15	30	45
Lettuce	100	+	+	+
	100	+	+	+
	10	+ (weak)	+	+
Packed salad	100	+	+	+
	100	+	+	+
	10	+	+	+

The intensity of the acquired Raman peaks became stronger after increasing the enrichment time. Based on our findings, an enrichment time of 30 min was sufficient to give clear signals from both species under the study. Hence, the total assay time in our protocol is considered to be less than 2 h, including the 30 min of fixation, 30 min of separation and labeling, 10 s of data collection, and a few minutes for setup arrangement and centrifugation/washing steps. Hence, our protocol significantly reduced the analysis time compared with the days of experiments in conventional

techniques.

6.4 Conclusions

In this study, we integrated immunoprobes with a SERS optofluidic sensor to selectively separate and simultaneously detect pathogenic *E. coli* O157:H7, *S. Enteritidis,* and *S. Typhimurium* DT104 in lettuce and packed salad samples. The approach consists of three steps: (i) an enrichment step, (ii) off-chip, selective separation and labeling of target pathogens by the aid of specific SERS-nanotags for each target strain, and (iii) detection of target bacterial cells within a hydrodynamic flow-focusing SERS optofluidic device, where the detection of fingerprint-like Raman spectra of Raman reporters indicates the presence of target bacteria in the food sample. Our approach achieved a very low detection limit of 10 CFU/ml for the bacterial mixture in both food samples, which is significantly lower than the infectious dose of *E. coli* O157:H7 and non-typhoidal *Salmonella*. This method not only detects multiple target pathogens simultaneously, but also remarkably reduces the assay time to less than 2 h. The applicability of this method can be extended to other food pathogens and to the medical fields. It is suggested that future work can focus on using monoclonal antibodies, rather than polyclonal, to improve the specificity of SERS-nanotags against target bacterial cells. Furthermore, the one-step separation and detection of pathogenic bacterial cells on the same SERS optofluidic device is another interesting topic that can be studied.

CONCLUSIONS AND FUTURE DIRECTIONS

7.1 Conclusions

In this project, two protocols were developed to simultaneously detect multiple pesticides and food-borne pathogens in fruits and vegetables. In the first protocol, a filter-based SERS microchip was designed and utilized to detect multiple pesticides in fresh produce. The architecture of the channel was optimized by FEM for efficient SERS detection. In this method, the original sample was first filtered through the filter membrane, which was installed in the inlet of the microfluidic channel. Then, efficient mixing of the sample with nanoparticle solution was performed at two points within the channel. Finally, a reliable SERS detection was performed in the stable conditions of the detection zone. The online filter membrane eliminated the need for offline sample preparation, where the original sample can be analyzed directly in a single analysis platform. Using powerful SERS substrates, Au@Ag NPs, also facilitated multiplex detection of four pesticides in the strawberry extract. Our protocol successfully achieved fast, reliable detection of four pesticides in strawberries with very low LOD values of less than 100 μg/ Kg for all pesticides, which is significantly lower than their MRLs.

The second protocol was developed to detect food-borne pathogens either individually or collectively in fresh produce. The method included three steps; (a) enrichment, (b) separation and labeling of the bacterial cells by specific SERS-nanoprobes, and (c) detection of the target pathogens using fingerprint-like SERS signals associated with the SERS-nanoprobes. An enrichment step of about 30 min guaranteed the detection of bacterial cells even in very counts. Separation and labeling of bacterial cells were performed by SERS-nanoprobes that contained the specific antibody against the target pathogen. Eventually, the detection of pathogens was

successfully conducted in a controlled analysis condition within a hydrodynamic flow-focusing microfluidic channel, where even a single bacterial cell could be detected. The method achieved a very low LOD value of 0.5 CFU/mL for *E. coli* O157:H7 and 10 CFU/mL for the mixture of *E. coli* O157:H7, *S. enteritidis,* and *S. enteric* in lettuce and packed salad, which are significantly lower than the bacterial infectious doses. Moreover, the total analysis time was less than 2 hours, which is remarkably shorter than days required in conventional methods. The findings of this project demonstrated the great potentiality of our protocols to detect and determine pesticides and pathogens either individually or collectively in complex food samples, and the methods are transferable to other targets in the field of food and environmental analysis.

7.2 Future directions

The project presented two protocols for the detection of multiple pesticides and food-borne pathogens in fruits and vegetables that are promising for wide applications. This research can be improved by fabricating the sensors with thermoplastics or cellulose, which result in high throughput production and relatively low costs that are suitable for mass production. The protocol for detecting pesticides, the filter membrane, in the filter-based SERS microchip can be replaced by a semipermeable membrane to better concentrate the target analyte for more efficient detection and lower LOD values. For bacterial detection, the SERS nanoprobes can be synthesized by monoclonal antibodies, rather than polyclonal ones, to enhance the selectivity of the method for target strains. Moreover, on-site sample preparation and detection can be employed to further reduce the analysis time.

REFERENCES

Ackermann KR, Henkel T, Popp J (2007) Quantitative online detection of low-concentrated drugs via a SERS microfluidic system. ChemPhysChem 8:2665–2670. https://doi.org/10.1002/cphc.200700554

Aghvami SA, Opathalage A, Zhang ZK, et al (2017) Rapid prototyping of cyclic olefin copolymer (COC) microfluidic devices. Sensors Actuators, B Chem 247:940–949. https://doi.org/10.1016/j.snb.2017.03.023

Akanny E, Bonhommé A, Commun C, et al (2019) Development of uncoated near-spherical gold nanoparticles for the label-free quantification of Lactobacillus rhamnosus GG by surface-enhanced Raman spectroscopy. Anal Bioanal Chem 2019 41121 411:5563–5576. https://doi.org/10.1007/S00216-019-01938-4

Akanny E, Bonhommé A, Commun C, et al (2020) Surface-enhanced Raman spectroscopy using uncoated gold nanoparticles for bacteria discrimination. J Raman Spectrosc 51:619–629. https://doi.org/10.1002/JRS.5827

Akhtar S, Sarker MR, Hossain A (2014) Microbiological food safety: a dilemma of developing societies. Crit Rev Microbiol 40:348–359. https://doi.org/10.3109/1040841X.2012.742036

Andreou C, Hoonejani MR, Barmi MR, et al (2013) Rapid detection of drugs of abuse in saliva using surface enhanced raman spectroscopy and microfluidics. ACS Nano 7:7157–7164. https://doi.org/10.1021/nn402563f

Aroca R (2006) Surface-Enhanced Vibrational Spectroscopy. John Wiley & Sons, Ltd: Chicheste

Arregui-Mena JD, Margetts L, Mummery PM (2016) Practical Application of the Stochastic Finite Element Method. Arch Comput Methods Eng 23:171–190. https://doi.org/10.1007/s11831-014-9139-3

Asgari S, Sun L, Lin J, et al (2020) Nanofibrillar cellulose/Au@Ag nanoparticle nanocomposite as a SERS substrate for detection of paraquat and thiram in lettuce. Microchim Acta 187:1–11. https://doi.org/10.1007/s00604-020-04358-9

Asgari S, Wu G, Aghvami SA, et al (2021) Optimisation using the finite element method of a filter-based microfluidic SERS sensor for detection of multiple pesticides in strawberry. Food Addit Contam - Part A Chem Anal Control Expo Risk Assess 38:646–658. https://doi.org/10.1080/19440049.2021.1881624

Bai X, Shen A, Hu J (2020) A sensitive SERS-based sandwich immunoassay platform for simultaneous multiple detection of foodborne pathogens without interference. Anal Methods 12:4885–4891. https://doi.org/10.1039/D0AY01541E

Bantz KC, Meyer AF, Wittenberg NJ, et al (2011) Recent progress in SERS biosensing. Phys Chem Chem Phys 13:11551–11567

Bennett B, Workman T, Smith MN, et al (2019) Longitudinal, Seasonal, and Occupational Trends of Multiple Pesticides in House Dust. Environ Health Perspect 127:17003

Bhaisare ML, Gedda G, Khan MS, Wu HF (2016) Fluorimetric detection of pathogenic bacteria using magnetic carbon dots. Anal Chim Acta 920:63–71. https://doi.org/10.1016/J.ACA.2016.02.025

Bi L, Wang X, Cao X, et al (2020) SERS-active Au@Ag core-shell nanorod

(Au@AgNR) tags for ultrasensitive bacteria detection and antibiotic-susceptibility testing. Talanta 220:121397. https://doi.org/10.1016/J.TALANTA.2020.121397

Boehle KE, Carrell CS, Caraway J, Henry CS (2018) Paper-Based Enzyme Competition Assay for Detecting Falsified β-Lactam Antibiotics. ACS Sensors 3:1299–1307. https://doi.org/10.1021/acssensors.8b00163

Brecher ME, Hay SN (2005) Bacterial contamination of blood components. Clin Microbiol Rev 18:195–204. https://doi.org/10.1128/CMR.18.1.195-204.2005

Bridle H, Miller B, Desmulliez MPY (2014) Application of microfluidics in waterborne pathogen monitoring: A review. Water Res 55:256–271. https://doi.org/10.1016/J.WATRES.2014.01.061

Cadnum JL, Hurless KN, Deshpande A, et al (2014) Sensitive and selective culture medium for detection of environmental Clostridium difficile isolates without requirement for anaerobic culture conditions. J Clin Microbiol 52:3259–3263. https://doi.org/10.1128/JCM.00793-14

Cate DM, Adkins JA, Mettakoonpitak J, Henry CS (2015) Recent developments in paper-based microfluidic devices. Anal. Chem. 87:19–41

CDC (2021) Lettuce, Other Leafy Greens, and Food Safety | Food Safety | CDC. https://www.cdc.gov/foodsafety/communication/leafy-greens.html. Accessed 27 Aug 2021

CDC (2020) Foodborne Germs and Illnesses | CDC. https://www.cdc.gov/foodsafety/foodborne-germs.html. Accessed 7 Nov 2021

Chang PL, Hsieh MM, Chiu TC (2016) Recent advances in the determination of

pesticides in environmental samples by capillary electrophoresis. Int J Environ Res Public Health 13:409

Chen G, Wang Y, Wang H, et al (2014a) A highly sensitive microfluidics system for multiplexed surface-enhanced Raman scattering (SERS) detection based on Ag nanodot arrays. RSC Adv 4:54434–54440. https://doi.org/10.1039/C4RA09251A

Chen G, Wang Y, Wang H, et al (2014b) A highly sensitive microfluidics system for multiplexed surface-enhanced Raman scattering (SERS) detection based on Ag nanodot arrays. RSC Adv 4:54434–54440. https://doi.org/10.1039/c4ra09251a

Chen J, Zhou Y, Wang D, et al (2015) UV-nanoimprint lithography as a tool to develop flexible microfluidic devices for electrochemical detection. Lab Chip 15:3086–3094. https://doi.org/10.1039/c5lc00515a

Chen MB, Srigunapalan S, Wheeler AR, Simmons CA (2013) A 3D microfluidic platform incorporating methacrylated gelatin hydrogels to study physiological cardiovascular cell-cell interactions. Lab Chip 13:2591–2598. https://doi.org/10.1039/c3lc00051f

Chen Y-J, Chen Y-Y, Wang K-H, et al (2020) Integration of a Thermoelectric Heating Unit with Ionic Wind-Induced Droplet Centrifugation Chip to Develop Miniaturized Concentration Device for Rapid Determination of Salmonella on Food Samples Using Antibody-Functionalized SERS Tags. Sensors (Basel) 20:1–14. https://doi.org/10.3390/S20247177

Cheng Q, Wang S, Rials TG (2009) Poly(vinyl alcohol) nanocomposites reinforced with cellulose fibrils isolated by high intensity ultrasonication. Compos Part A Appl Sci Manuf 4:2387–2394

Cheng Z, Choi N, Wang R, et al (2017) Simultaneous Detection of Dual Prostate Specific Antigens Using Surface-Enhanced Raman Scattering-Based Immunoassay for Accurate Diagnosis of Prostate Cancer. ACS Nano 11:4926–4933. https://doi.org/10.1021/ACSNANO.7B01536

Cho IH, Bhandari P, Patel P, Irudayaraj J (2015) Membrane filter-assisted surface enhanced Raman spectroscopy for the rapid detection of E. coli O157:H7 in ground beef. Biosens Bioelectron 64:171–176. https://doi.org/10.1016/J.BIOS.2014.08.063

Chueh BH, Huh D, Kyrtsos CR, et al (2007) Leakage-free bonding of porous membranes into layered microfluidic array systems. Anal Chem 79:3504–3508. https://doi.org/10.1021/ac062118p

Chung J, Kang JS, Jurng JS, et al (2015) Fast and continuous microorganism detection using aptamer-conjugated fluorescent nanoparticles on an optofluidic platform. Biosens Bioelectron 67:303–308. https://doi.org/10.1016/J.BIOS.2014.08.039

Cortie MB, McDonagh AM (2011) Synthesis and Optical Properties of Hybrid and Alloy Plasmonic Nanoparticles. Chem Rev 111:3713–3735

D'Lima CB, Suslow T V (2009) Comparative evaluation of practical functionality of rapid test format kits for detection of Escherichia coli O157:H7 on lettuce and leafy greens. J Food Prot 72:2461–2470. https://doi.org/10.4315/0362-028X-72.12.2461

Deisingh AK, Thompson M (2004) Strategies for the detection of Escherichia coli O157:H7 in foods. J Appl Microbiol 96:419–429. https://doi.org/10.1111/J.1365-2672.2003.02170.X

Doyle MP (2013) Food Safety: Bacterial Contamination. Encycl Hum Nutr 2–4:322–330. https://doi.org/10.1016/B978-0-12-375083-9.00124-0

Elkhishin MT, Gooneratne R, Hussain MA (2017) Microbial Safety of Foods in the Supply Chain and Food Security. Adv Food Technol Nutr Sci - Open J 3:22–32. https://doi.org/10.17140/AFTNSOJ-3-141

EPA (2019) Electronic Code of Federal Regulations

Escarpa A (2014) Lights and shadows on Food Microfluidics. Lab Chip 14:3213–3224. https://doi.org/10.1039/c4lc00172a

Etchegoin PG, Le Ru EC (2008) A perspective on single molecule SERS: Current status and future challenges. Phys. Chem. Chem. Phys. 10:6079–6089

Fan M, Andrade GFS, Brolo AG (2011) A review on the fabrication of substrates for surface enhanced Raman spectroscopy and their applications in analytical chemistry. Anal Chim Acta 693:7–25. https://doi.org/10.1016/J.ACA.2011.03.002

Fang H, Zhang X, Zhang SJ, et al (2015) Ultrasensitive and quantitative detection of paraquat on fruits skins via surface-enhanced Raman spectroscopy. Sensors Actuators, B Chem 213:452–456

FDA (1998) Guidance for Industry: Guide to Minimize Microbial Food Safety Hazards for Fresh Fruits and Vegetables | FDA. https://www.fda.gov/regulatory-information/search-fda-guidance-documents/guidance-industry-guide-minimize-microbial-food-safety-hazards-fresh-fruits-and-vegetables. Accessed 19 May 2021

FDA (2019) Guidelines for the Validation of Microbiological Methods for the FDA

Foods Program, 3rd editio

FDA (2021a) BAM Chapter 4A: Diarrheagenic Escherichia coli | FDA. https://www.fda.gov/food/laboratory-methods-food/bam-chapter-4a-diarrheagenic-escherichia-coli. Accessed 22 Oct 2021

FDA (2021b) BAM Chapter 5: Salmonella | FDA. https://www.fda.gov/food/laboratory-methods-food/bam-chapter-5-salmonella. Accessed 22 Oct 2021

Fenik J, Tankiewicz M, Biziuk M (2011) Properties and determination of pesticides in fruits and vegetables. TrAC - Trends Anal Chem 30:814–826

Ferhan AR, Jackman JA, Sut TN, Cho N-J (2018) Quantitative Comparison of Protein Adsorption and Conformational Changes on Dielectric-Coated Nanoplasmonic Sensing Arrays. Sensors 2018, Vol 18, Page 1283 18:1283. https://doi.org/10.3390/S18041283

Floriano PN, Christodoulides N, Romanovicz D, et al (2005) Membrane-based on-line optical analysis system for rapid detection of bacteria and spores. In: Biosensors and Bioelectronics. Elsevier Ltd, pp 2079–2088

FRENS G (1973) Controlled Nucleation for the Regulation of the Particle Size in Monodisperse Gold Suspensions. Nat Phys Sci 241:20–22

Galarreta BC, Tabatabaei M, Guieu V, et al (2013) Microfluidic channel with embedded SERS 2D platform for the aptamer detection of ochratoxin A. Anal Bioanal Chem 405:1613–1621. https://doi.org/10.1007/s00216-012-6557-7

Ghann W, Harris T, Kabir D, et al (2019) Lipoic Acid Decorated Gold Nanoparticles

and Their Application in the Detection of Lead Ions. J Nanomed Nanotechnol 10:. https://doi.org/10.35248/2157-7439.19.10.539

Goodacre R, Timmins ÉM, Burton R, et al (1998) Rapid identification of urinary tract infection bacteria using hyperspectral whole-organism fingerprinting and artificial neural networks. Microbiology 144:1157–1170. https://doi.org/10.1099/00221287-144-5-1157

Gorjikhah F, Davaran S, Salehi R, et al (2016) Improving "lab-on-a-chip" techniques using biomedical nanotechnology: a review. http://dx.doi.org/103109/2169140120151129619 44:1609–1614. https://doi.org/10.3109/21691401.2015.1129619

Group EW EWG's 2019 Shopper's Guide to Pesticides in Produce™. https://www.ewg.org/foodnews/summary.php

Gu Y, Miki N (2009) Multilayered microfilter using a nanoporous PES membrane and applicable as the dialyzer of a wearable artificial kidney. J Micromechanics Microengineering 19:065031. https://doi.org/10.1088/0960-1317/19/6/065031

Gweon D-G, Lee D, Lee EK, et al (2006) Quantitative Analysis of Methyl Parathion Pesticides in a Polydimethylsiloxane Microfluidic Channel Using Confocal Surface-Enhanced Raman Spectroscopy. Appl Spectrosc Vol 60, Issue 4, pp 373-377 60:373–377

Halvorson RA, Vikesland PJ (2010) Surface-enhanced Raman spectroscopy (SERS) for environmental analyses. Environ. Sci. Technol. 44:7749–7755

Haynes CL, McFarland AD, Van Duyne RP (2005) Surface-Enhanced Raman

Spectroscopy. Anal Chem 77:338 A-346 A

Hsieh YC, Zahn JD (2005) Glucose recovery in a microfluidic microdialysis biochip. Sensors Actuators, B Chem 107:649–656. https://doi.org/10.1016/j.snb.2004.11.039

Hyre DE, Trong I Le, Merritt EA, et al (2006) Cooperative hydrogen bond interactions in the streptavidin–biotin system. Protein Sci 15:459. https://doi.org/10.1110/PS.051970306

IH C, P B, P P, J I (2015) Membrane filter-assisted surface enhanced Raman spectroscopy for the rapid detection of E. coli O157:H7 in ground beef. Biosens Bioelectron 64:171–176. https://doi.org/10.1016/J.BIOS.2014.08.063

Ijeh MO (2011) Covalent gold nanoparticle-antibody conjugates for sensivity improvement in LFIA. Doctoral dissertation, Staats-und Universitätsbibliothek Hamburg Carl von Ossietzky

Jana NR (2003) Silver coated gold nanoparticles as new surface enhanced Raman substrate at low analyte concentration. Analyst 128:954–956

Janasek D, Franzke J, Manz A (2006) Scaling and the design of miniaturized chemical-analysis systems. Nature 442:374–380. https://doi.org/10.1038/nature05059

Jay JM, Loessner MJ, Golden DA (2005) Modern Food Microbiology. Springer US

Ji Y, Yang S, Guo S, et al (2010) Bimetallic Ag/Au nanoparticles: A low temperature ripening strategy in aqueous solution. Colloids Surfaces A Physicochem Eng Asp 372:204–209

Jiang F, Hsieh Y-L (2014) Synthesis of Cellulose Nanofibril Bound Silver Nanoprism for Surface Enhanced Raman Scattering. Biomacromolecules 15:3608–3616

Jokerst J V, Jacobson JW, Bhagwandin BD, et al (2010) Programmable Nano-Bio-Chip Sensors: Analytical Meets Clinical - Analytical Chemistry (ACS Publications). Anal Chem 82:1571–9. https://doi.org/10.1021/ac901743u

Jonoobi M, Oladi R, Davoudpour Y, et al (2015) Different preparation methods and properties of nanostructured cellulose from various natural resources and residues: a review. Cellulose 22:935–969

Jun BH, Kim JH, Park H, et al (2007) Surface-enhanced Raman spectroscopic-encoded beads for multiplex immunoassay. J Comb Chem 9:237–244. https://doi.org/10.1021/cc0600831

Kamińska A, Sprynskyy M, Winkler K, Szymborski T (2017) Ultrasensitive SERS immunoassay based on diatom biosilica for detection of interleukins in blood plasma. Anal Bioanal Chem 2017 40927 409:6337–6347. https://doi.org/10.1007/S00216-017-0566-5

Kamińska A, Witkowska E, Winkler K, et al (2015a) Detection of Hepatitis B virus antigen from human blood: SERS immunoassay in a microfluidic system. Biosens Bioelectron 66:461–467. https://doi.org/10.1016/j.bios.2014.10.082

Kamińska A, Witkowska E, Winkler K, et al (2015b) Detection of Hepatitis B virus antigen from human blood: SERS immunoassay in a microfluidic system. Biosens Bioelectron 66:461–467. https://doi.org/10.1016/j.bios.2014.10.082

Kim HJ, Huh D, Hamilton G, Ingber DE (2012) Human gut-on-a-chip inhabited by

microbial flora that experiences intestinal peristalsis-like motions and flow. Lab Chip 12:2165–2174. https://doi.org/10.1039/c2lc40074j

Kim MS, Kim MK, Lee CJ, et al (2009) Surface-enhanced Raman spectroscopy of benzimidazolic fungicides: Benzimidazole and thiabendazole. Bull Korean Chem Soc 30:2930–2934. https://doi.org/10.5012/bkcs.2009.30.12.2930

Knauer M, Ivleva NP, Niessner R, Haisch C (2012) A flow-through microarray cell for the online SERS detection of antibody-captured E. coli bacteria. Anal Bioanal Chem 402:2663–2667. https://doi.org/10.1007/s00216-011-5398-0

Kolberg DIS, Mack D, Anastassiades M, et al (2012) Development and Independent Laboratory Validation of a Simplified. Sample Preparation Method for the Determination of Paraquat and Diquat in Food Comodities. Anal Chim Acta 404:2465–2474

Kubackova J, Fabriciova G, Miskovsky P, et al (2015) Sensitive surface-enhanced Raman spectroscopy (SERS) detection of organochlorine pesticides by alkyl dithiol-functionalized metal nanoparticles-induced plasmonic hot spots. Anal Chem 87:663–669. https://doi.org/10.1021/ac503672f

Kurita R, Yabumoto N, Niwa O (2006) Miniaturized one-chip electrochemical sensing device integrated with a dialysis membrane and double thin-layer flow channels for measuring blood samples. Biosens Bioelectron 21:1649–1653. https://doi.org/10.1016/j.bios.2005.07.016

Lee S, Chon H, Yoon SY, et al (2012) Fabrication of SERS-fluorescence dual modal nanoprobes and application to multiplex cancer cell imaging. Nanoscale 4:124–129. https://doi.org/10.1039/c1nr11243k

Lee SH, Oh EH, Park TH (2015) Cell-based microfluidic platform for mimicking human olfactory system. Biosens Bioelectron 74:554–561. https://doi.org/10.1016/j.bios.2015.06.072

Li X, Yang F, Wong JXH, Yu HZ (2017) Integrated Smartphone-App-Chip System for On-Site Parts-Per-Billion-Level Colorimetric Quantitation of Aflatoxins. Anal Chem 89:8908–8916. https://doi.org/10.1021/acs.analchem.7b01379

Lin H-Y, Huang C-H, Hsieh W-H, et al (2014) On-line SERS detection of single bacterium using novel SERS nanoprobes and a microfluidic dielectrophoresis device. Small 10:4700–4710. https://doi.org/10.1002/SMLL.201401526

Lin Y, Gritsenko D, Feng S, et al (2016a) Detection of heavy metal by paper-based microfluidics. Biosens. Bioelectron. 83:256–266

Lin Y, Gritsenko D, Feng S, et al (2016b) Detection of heavy metal by paper-based microfluidics. Biosens Bioelectron 83:256–266. https://doi.org/10.1016/J.BIOS.2016.04.061

Liou P, Nayigiziki FX, Kong F, et al (2017) Cellulose nanofibers coated with silver nanoparticles as a SERS platform for detection of pesticides in apples. Carbohydr Polym 157:643–650

Liu B, Han G, Zhang Z, et al (2012) Shell thickness-dependent Raman enhancement for rapid identification and detection of pesticide residues at fruit peels. Anal Chem 84:255–261

Liu B, Thielert B, Reutter A, et al (2019) Quantifying the Contribution of Chemical Enhancement to SERS: A Model Based on the Analysis of Light-Induced

Degradation Processes. J Phys Chem C 123:19119–19124. https://doi.org/10.1021/ACS.JPCC.9B04526/SUPPL_FILE/JP9B04526_SI_002.PDF

Liu F, Liu H, Liao Y, et al (2015) Multiplex detection and genotyping of pathogenic bacteria on paper-based biosensor with a novel universal primer mediated asymmetric PCR. Biosens Bioelectron 74:778–785. https://doi.org/10.1016/J.BIOS.2015.06.054

Llorent-Martínez EJ, Ortega-Barrales P, Fernández-de Córdova ML, Ruiz-Medina A (2011) Trends in flow-based analytical methods applied to pesticide detection: A review. Anal Chim Acta 684:30–39

López-Campos G, Martínez-Suárez J V., Aguado-Urda M, López-Alonso V (2012) Detection, Identification, and Analysis of Foodborne Pathogens. 13–32. https://doi.org/10.1007/978-1-4614-3250-0_2

López-Paz JL, Catalá-Icardo M (2011) Analysis of pesticides by flow injection coupled with chemiluminescent detection: A review. Anal Lett 44:146–175

Lu X, Samuelson DR, Xu Y, et al (2013) Detecting and tracking nosocomial methicillin-resistant Staphylococcus aureus using a microfluidic SERS biosensor. Anal Chem 85:2320–2327

Luo H, Wang X, Huang Y, et al (2018) Rapid and sensitive surface-enhanced Raman spectroscopy (SERS) method combined with gold nanoparticles for determination of paraquat in apple juice. J Sci Food Agric 98:3892–3898

March S, Ratnam S (1986) Sorbitol-MacConkey medium for detection of Escherichia

coli O157:H7 associated with hemorrhagic colitis. J Clin Microbiol 23:869–872. https://doi.org/10.1128/JCM.23.5.869-872.1986

Marshall KE, Hexemer A, Seelman SL, et al (2020) Lessons Learned from a Decade of Investigations of Shiga Toxin-Producing Escherichia coli Outbreaks Linked to Leafy Greens, United States and Canada. Emerg Infect Dis 26:2319–2328. https://doi.org/10.3201/eid2610.191418

Massad-Ivanir N, Shtenberg G, Raz N, et al (2016) Porous Silicon-Based Biosensors: Towards Real-Time Optical Detection of Target Bacteria in the Food Industry. Sci Reports 2016 61 6:1–12. https://doi.org/10.1038/srep38099

McDonald JC, Duffy DC, Anderson JR, et al (2000) Fabrication of microfluidic systems in poly(dimethylsiloxane). Electrophoresis 21:27–40

Mir SA, Shah MA, Mir MM, et al (2018) Microbiological contamination of ready-to-eat vegetable salads in developing countries and potential solutions in the supply chain to control microbial pathogens. Food Control 85:235–244. https://doi.org/10.1016/J.FOODCONT.2017.10.006

Mirceski V, Gulaboski R (2014) Recent achievements in square-wave voltammetry (a review). Maced J Chem Chem Eng 33:1–12

Mungroo NA, Oliveira G, Neethirajan S (2015) SERS based point-of-care detection of food-borne pathogens. Microchim Acta 2015 1832 183:697–707. https://doi.org/10.1007/S00604-015-1698-Y

Ngo YH, Li D, Simon GP, Garnier G (2012) Gold nanoparticle-paper as a three-dimensional surface enhanced raman scattering substrate. Langmuir 28:8782–

8790

Ogundare SA, van Zyl WE (2019) A review of cellulose-based substrates for SERS: fundamentals, design principles, applications. Cellulose 26:6489–6528

Olson TY, Schwartzberg AM, Orme CA, et al (2008) Hollow Gold−Silver Double-Shell Nanospheres: Structure, Optical Absorption, and Surface-Enhanced Raman Scattering. J Phys Chem C 112:6319–6329

Pallaoro A, Hoonejani MR, Braun GB, et al (2015) Rapid identification by surface-enhanced raman spectroscopy of cancer cells at low concentrations flowing in a microfluidic channel. ACS Nano 9:4328–4336. https://doi.org/10.1021/acsnano.5b00750

Pang S, Yang T, He L (2016) Review of surface enhanced Raman spectroscopic (SERS) detection of synthetic chemical pesticides. TrAC - Trends Anal Chem 85:73–82

Parab NDT, Tomar V (2012) Raman spectroscopy of algae: A review. J Nanomedicine Nanotechnol 3:. https://doi.org/10.4172/2157-7439.1000131

Philippe V, Neveen A, Marwa A, Ahmad Basel AY (2021) Occurrence of pesticide residues in fruits and vegetables for the Eastern Mediterranean Region and potential impact on public health. Food Control 119:107457. https://doi.org/10.1016/J.FOODCONT.2020.107457

Pu H, Xiao W, Sun D-W (2017a) SERS-microfluidic systems: A potential platform for rapid analysis of food contaminants. Trends Food Sci Technol 70:114–126. https://doi.org/10.1016/J.TIFS.2017.10.001

Pu H, Xiao W, Sun DW (2017b) SERS-microfluidic systems: A potential platform for

rapid analysis of food contaminants. Trends Food Sci. Technol. 70:114–126

Puri VM, Anantheswaran RC (1993) The finite-element method in food processing: A review. J. Food Eng. 19:247–274

Qi N, Li B, You H, et al (2014) Surface-enhanced Raman scattering on a zigzag microfluidic chip: towards high-sensitivity detection of As(III) ions. Anal Methods 6:4077–4082. https://doi.org/10.1039/C3AY42283F

Quang LX, Lim C, Seong GH, et al (2008) A portable surface-enhanced Raman scattering sensor integrated with a lab-on-a-chip for field analysis. Lab Chip 8:2214. https://doi.org/10.1039/b808835g

Rapp BE (2017) Finite Element Method. In: Rapp BE (ed) Microfluidics: Modelling, Mechanics and Mathematics. Elsevier, Kidlington, Oxford, United Kingdom, pp 655–678

Raveendran P, Fu J, Wallen SL (2006) A simple and "green" method for the synthesis of Au, Ag, and Au-Ag alloy nanoparticles. Green Chem 8:34–38

Roda A, Mirasoli M, Roda B, et al (2012) Recent developments in rapid multiplexed bioanalytical methods for foodborne pathogenic bacteria detection. Microchim Acta 178:7–28. https://doi.org/10.1007/s00604-012-0824-3

Rodríguez-Lorenzo L, Garrido-Maestu A, Bhunia AK, et al (2019) Gold Nanostars for the Detection of Foodborne Pathogens via Surface-Enhanced Raman Scattering Combined with Microfluidics. ACS Appl Nano Mater 2:6081–6086. https://doi.org/10.1021/ACSANM.9B01223

Rongke Gao, Ziyi Cheng, J. deMello A, Jaebum Choo (2016) Wash-free magnetic

immunoassay of the PSA cancer marker using SERS and droplet microfluidics. Lab Chip 16:1022–1029. https://doi.org/10.1039/C5LC01249J

Sanjari Nia MS, Shamsi P, Ferdowsi M (2020) Investigation of Various Transformer Topologies for HF Isolation Applications. IEEE Trans Plasma Sci 48:512–521. https://doi.org/10.1109/TPS.2020.2967412

Saravanan A, Kumar PS, Hemavathy R V., et al (2020) Methods of detection of food-borne pathogens: a review. Environ Chem Lett 2020 191 19:189–207. https://doi.org/10.1007/S10311-020-01072-Z

Saute B, Narayanan R (2011) Solution-based direct readout surface enhanced Raman spectroscopic (SERS) detection of ultra-low levels of thiram with dogbone shaped gold nanoparticles. Analyst 136:527–532

Sedlak SM, Schendel LC, Gaub HE, Bernardi RC (2020) Streptavidin/biotin: Tethering geometry defines unbinding mechanics. Sci Adv 6:. https://doi.org/10.1126/SCIADV.AAY5999

Seiichi S, Putalun W, Sornkanok V, et al (2018) Enzyme-linked immunosorbent assay for the quantitative/qualitative analysis of plant secondary metabolites. J Nat Med 72:32–42. https://doi.org/10.1007/S11418-017-1144-Z

Sharma H, Mutharasan R (2013) Review of biosensors for foodborne pathogens and toxins. Sensors Actuators B Chem 183:535–549. https://doi.org/10.1016/J.SNB.2013.03.137

She P, Chu Y, Liu C, et al (2016) A competitive immunoassay for ultrasensitive detection of Hg2+ in water, human serum and urine samples using

immunochromatographic test based on surface-enhanced Raman scattering. Anal Chim Acta 906:139–147. https://doi.org/10.1016/J.ACA.2015.12.021

Singh AK, Senapati D, Wang S, et al (2009) Gold Nanorod Based Selective Identification of Escherichia coli Bacteria Using Two-Photon Rayleigh Scattering Spectroscopy. ACS Nano 3:1906–1912. https://doi.org/10.1021/NN9005494

Singh P, Mustapha A (2015) Multiplex real-time PCR assays for detection of eight Shiga toxin-producing Escherichia coli in food samples by melting curve analysis. Int J Food Microbiol 215:101–108. https://doi.org/10.1016/J.IJFOODMICRO.2015.08.022

Song L, Mao K, Zhou X, Hu J (2016) A novel biosensor based on Au@Ag core–shell nanoparticles for SERS detection of arsenic (III). Talanta 146:285–290

Sun H, Liu H, Wu Y (2017) A green, reusable SERS film with high sensitivity for in-situ detection of thiram in apple juice. Appl Surf Sci 416:704–709

Tamer U, BoyacI IH, Temur E, et al (2011) Fabrication of magnetic gold nanorod particles for immunomagnetic separation and SERS application. J Nanoparticle Res 2011 138 13:3167–3176. https://doi.org/10.1007/S11051-010-0213-Y

Thacker V V., Herrmann LO, Sigle DO, et al (2014) DNA origami based assembly of gold nanoparticle dimers for surface-enhanced Raman scattering. Nat Commun 2014 51 5:1–7. https://doi.org/10.1038/ncomms4448

To N, Sanada I, Ito H, et al (2015) Water-Permeable Dialysis Membranes for Multi-Layered Microdialysis System. Front Bioeng Biotechnol 3:70. https://doi.org/10.3389/fbioe.2015.00070

Vosgröne T, Meixner AJ (2005) Surface- and Resonance-Enhanced Micro-Raman Spectroscopy of Xanthene Dyes: From the Ensemble to Single Molecules. ChemPhysChem 6:154–163. https://doi.org/10.1002/CPHC.200400395

Wang C, Madiyar F, Yu C, Li J (2017) Detection of extremely low concentration waterborne pathogen using a multiplexing self-referencing SERS microfluidic biosensor. J Biol Eng 2017 111 11:1–11. https://doi.org/10.1186/S13036-017-0051-X

Wang C, Wu X, Dong P, et al (2016a) Hotspots engineering by grafting Au@Ag core-shell nanoparticles on the Au film over slightly etched nanoparticles substrate for on-site paraquat sensing. Biosens Bioelectron 86:944–950

Wang C, Yu C (2015) Analytical characterization using surface-enhanced Raman scattering (SERS) and microfluidic sampling. Nanotechnology 26:092001

Wang G, Lim C, Chen L, et al (2009) Surface-enhanced Raman scattering in nanoliter droplets: towards high-sensitivity detection of mercury (II) ions. Anal Bioanal Chem 394:1827–1832. https://doi.org/10.1007/S00216-009-2832-7

Wang J, Wu X, Wang C, et al (2016b) Facile Synthesis of Au-Coated Magnetic Nanoparticles and Their Application in Bacteria Detection via a SERS Method. ACS Appl Mater Interfaces 8:19958–19967. https://doi.org/10.1021/ACSAMI.6B07528

Wang S, Liu C, Wang H, et al (2014) A Surface-Enhanced Raman Scattering Optrode Prepared by *in Situ* Photoinduced Reactions and Its Application for Highly Sensitive On-Chip Detection. ACS Appl Mater Interfaces 6:11706–11713. https://doi.org/10.1021/am503881h

Ward K, Fan ZH (2015) Mixing in microfluidic devices and enhancement methods. J Micromechanics Microengineering 25:. https://doi.org/10.1088/0960-1317/25/9/094001

Wei H, Rodriguez K, Renneckar S, et al (2015) Preparation and evaluation of nanocellulose-gold nanoparticle nanocomposites for SERS applications. Analyst 140:5640–5649

Wei H, Rodriguez K, Renneckar S, Vikesland PJ (2014) Environmental science and engineering applications of nanocellulose-based nanocomposites. Environ Sci Nano 1:302–316

Weng X, Zhang C, Jiang H (2021) Advances in microfluidic nanobiosensors for the detection of foodborne pathogens. LWT 151:112172. https://doi.org/10.1016/J.LWT.2021.112172

WHO (2018) World health statistics 2018: Monitoring health for the SDGs, sustainable development goals. Geneva: World Health Organization. https://www.who.int/docs/default-source/gho-documents/world-health-statistic-reports/6-june-18108-world-health-statistics-2018.pdf. Accessed 7 Jan 2022

WHO (2020) Report of the FAO/WHO Expert Consultation on Dietary risk assessment of chemical mixtures (pp. 16–18). Geneva: WHO. (April 2019)

Wiggins S, Ottino JM (2004) Foundations of chaotic mixing. Philos Trans R Soc A Math Phys Eng Sci 362:937–970. https://doi.org/10.1098/rsta.2003.1356

Wong-ek K, Horprathum M, Eiamchai P, et al (2011) Portable surface-enhanced Raman spectroscopy for insecticide detection using silver nanorod film fabricated by

magnetron sputtering. In: Vo-Dinh T, Lakowicz JR (eds) Plasmonics in Biology and Medicine VIII. SPIE, San Francisco, California, United States, p 791108

Xiao X. Han †, Lin J. Cai ‡, Jie Guo †, et al (2008) Fluorescein Isothiocyanate Linked Immunoabsorbent Assay Based on Surface-Enhanced Resonance Raman Scattering. Anal Chem 80:3020–3024. https://doi.org/10.1021/AC702497T

Xiong Z, Chen X, Liou P, Lin M (2017a) Development of nanofibrillated cellulose coated with gold nanoparticles for measurement of melamine by SERS. Cellulose 24:2801–2811

Xiong Z, Chen X, Liou P, Lin M (2017b) Development of nanofibrillated cellulose coated with gold nanoparticles for measurement of melamine by SERS. Cellulose 24:2801–2811

Xiong Z, Lin M, Lin H, Huang M (2018) Facile synthesis of cellulose nanofiber nanocomposite as a SERS substrate for detection of thiram in juice. Carbohydr Polym 189:79–86

Yang D, Ying Y (2011) Applications of Raman Spectroscopy in Agricultural Products and Food Analysis: A Review. http://dx.doi.org/101080/057049282011593216 46:539–560. https://doi.org/10.1080/05704928.2011.593216

Yang Y, Liu J, Fu Z-W, Qin D (2014) Galvanic Replacement-Free Deposition of Au on Ag for Core–Shell Nanocubes with Enhanced Chemical Stability and SERS Activity. J Am Chem Soc 136:8153–8156

Yazdi SH, White IM (2012a) A nanoporous optofluidic microsystem for highly sensitive and repeatable surface enhanced Raman spectroscopy detection.

Biomicrofluidics 6:. https://doi.org/10.1063/1.3677369

Yazdi SH, White IM (2012b) Multiplexed detection of aquaculture fungicides using a pump-free optofluidic SERS microsystem. Analyst 138:100–103. https://doi.org/10.1039/C2AN36232E

Yu H, Neal JA, Sirsat SA (2018) Consumers' food safety risk perceptions and willingness to pay for fresh-cut produce with lower risk of foodborne illness. Food Control 86:83–89. https://doi.org/10.1016/J.FOODCONT.2017.11.014

Zhang D, Liang P, Yu Z, et al (2020) Self-assembled "bridge" substance for organochlorine pesticides detection in solution based on Surface Enhanced Raman Scattering. J Hazard Mater 382:121023. https://doi.org/10.1016/j.jhazmat.2019.121023

Zhang L, Li X, Ong L, et al (2015) Cellulose nanofibre textured SERS substrate. Colloids Surfaces A Physicochem Eng Asp 468:309–314

Zhang L, Wang B, Zhu G, Zhou X (2014) Synthesis of silver nanowires as a SERS substrate for the detection of pesticide thiram. Spectrochim Acta - Part A Mol Biomol Spectrosc 133:411–416

Zhang S, Xiong R, Mahmoud MA, et al (2018) Dual-Excitation Nanocellulose Plasmonic Membranes for Molecular and Cellular SERS Detection. ACS Appl Mater Interfaces 10:18380–18389

Zhao X, Lin C-W, Oh JW and DH (2014) Advances in Rapid Detection Methods for Foodborne Pathogens. J Microbiol Biotechnol 24:297–312. https://doi.org/10.4014/JMB.1310.10013

Zhou Q, Kim T (2016) Review of microfluidic approaches for surface-enhanced Raman scattering. Sensors Actuators, B Chem. 227:504–514

Zhou Q, Meng G, Wu N, et al (2016) Dipping into a drink: Basil-seed supported silver nanoparticles as surface-enhanced Raman scattering substrates for toxic molecule detection. Sensors Actuators B Chem 223:447–452. https://doi.org/10.1016/J.SNB.2015.09.115

Zhu J, Chen Q, Kutsanedzie FYH, et al (2017) Highly sensitive and label-free determination of thiram residue using surface-enhanced Raman spectroscopy (SERS) coupled with paper-based microfluidics. Anal Methods 9:6186–6193

VITA

Sara Asgari earned her Bachelor's degree in Food Science and Technology from Sari Agricultural Sciences and Natural Resources University, Iran, in 2012. She received her master's degree in Food Science and Technology from Tarbiat Modares University, Iran, in 2015. After that, she joined Payame Noor University, where she served as an instructor for two years. She attended the Ph.D. program at the University of Missouri in January 2018 and focused on Food Safety, Nanotechnology, and Microfluidics. She received her doctoral degree in February 2022.